Precambrian tectonic evolution of Central Tianshan, NW China: constraints from U-Pb dating and in-situ Hf isotopic analysis of detrital zircons

Xuxuan Ma, Liangshu S. Shu, Bor-Ming Jahn, Wenbin Zhu, Michel Faure

Precambrian tectonic evolution of Central Tianshan, NW China: Constraints from U–Pb dating and in situ Hf isotopic analysis of detrital zircons

Xuxuan Ma[a], Liangshu Shu[a], Bor-Ming Jahn[b], Wenbin Zhu[a], Michel Faure[c]

[a] State Key Laboratory for Mineral Deposits Research, Nanjing University, Nanjing 210093, China

[b] Department of Geosciences, National Taiwan University, P.O. Box 13-318, Taipei 106, Taiwan

[c] Institut des Sciences de la Terre d'Orléans, UMR 6113 - CNRS/Université d'Orléans, 1A, rue de la Férollerie, 45071 Orléans Cedex 2, France

Abstract

The Tarim Block is an important geologic unit in the reconstruction of the tectonic evolution of the Central Asian Orogenic Belt and the Precambrian Columbia and Rodinia supercontinents. In order to examine the evolution and crustal generation of the Tarim Block, we performed detrital zircon U–Pb dating and in situ Hf isotopic analysis of Devonian sandstones of the Baluntai area in Central Tianshan, which is part of the Tarim Block. Most analyzed zircon grains show oscillatory zoning and have Th/U ratios >0.4, suggesting that they were mainly derived from igneous rocks. A total of about 400 detrital zircon analyses yielded five age populations, namely, early Paleoproterozoic (peak at 2470 Ma), middle Paleoproterozoic (peak at 1858 Ma), early Mesoproterozoic (peak at 1541 Ma), early Neoproterozoic (peak at 952 Ma), and late Neoproterozoic (820–750 Ma). These peak ages are remarkably consistent with the polyphase tectonothermal events that occurred in the Tarim Block. The peak at 2470 Ma indicates the presence of late Neoarchean to early Paleoproterozoic magmatism in the Tarim Block. The two peaks at 1858 Ma and 952 Ma coincide with the two periods of assembly of the Columbia and Rodinia supercontinents. This further suggests that the Tarim Block was part of these two supercontinents. In fact, the age peak of 1541 Ma correlates with the breakup of Columbia, and the age range of 820–750 Ma is interpreted to represent the time of the breakup of Rodinia.

The zircon Hf model ages suggest three major stages of crustal evolution at 1.0–1.4 Ga, 1.8–3.3 Ga, and 3.4–3.8 Ga. The zircons exhibit a huge range of $\varepsilon_{Hf}(t)$ values from −33 to +51, suggesting that they were derived from highly diverse protoliths. However, since most detrital zircons show negative $\varepsilon_{Hf}(t)$ values, the protoliths of the Baluntai sandstones of Central Tianshan probably comprise rocks of Archean to Proterozoic crust. Owing to the similar Precambrian basement, lithology and age spectra between Central Tianshan and Tarim, it is argued that Central Tianshan belonged to the Tarim Block in the Precambrian time. Furthermore, euhedral zircons with high Th/U ratios (>0.4) yielded a prominent peak of 447 Ma. This can be correlated with an early Paleozoic arc development in Central Tianshan.

Keywords: Detrital zircon; U–Pb dating; Hf isotope composition; Precambrian tectonic evolution; Baluntai; Tarim Block

1. Introduction

The Central Asian Orogenic Belt (CAOB) was formed by amalgamation of a variety of terranes including Precambrian microcontinental fragments, Paleozoic to Mesozoic magmatic arcs, accretionary complexes, ophiolites and passive continental margins. These terranes have undergone subsequent polyphase tectonic evolution ([Coleman, 1989] , [Sengör et al., 1993] , [Windley et al., 1990] , [Windley et al., 2007] , [Allen et al., 1993a] , [Allen et al., 1993b] , [Shu et al., 2002] , [Jahn, 2004] , [Jahn et al., 2004] , [Kroner et al., 2005] , [Charvet et al., 2007] , [Xiao et al., 2002] , [Xiao et al., 2003] , [Xiao et al., 2008] and [Xiao and Kusky, 2009]). The nearly E-W-trending Tianshan Range (Fig. 1) is a gigantic Paleozoic orogenic belt in the southern margin of the CAOB. It connects the Tarim Block to the south and the Siberian Block to the north ([Carroll et al., 1995] , [Gao et al., 1998] , [Shu et al., 2004] and [Shu et al., 2010]).

The crustal evolution of the Tianshan belt has not been well understood. Controversy exists on the tectonic affinity of Central Tianshan and its position in the Precambrian tectonic framework. Tectonic models abound, including the Central Tianshan as a rifting terrane from the Tarim Precambrian basement (Luo, 1989), as the eastern part of the Yili-Central Tianshan plate ([Allen et al., 1993a] and [Qian et al., 2009]), as a late Paleozoic volcanic arc (Chen et al., 1999a), a mantle-derived block at 2.0–1.8 Ga (Hu et al., 2000) and an independent continental block (Li et al., 2001). More recently, some workers suggested that the Central Tianshan terrane is a rifted part of the Tarim Block during the Precambrian period ([Li, 1981] , [Zhu et al., 2004] and [Lei et al., 2011]).

Recently, major advancements in reconstructing the history of crustal growth and evolution for Central Tianshan have been achieved owing to plenty of precise zircon U–Pb dating data. The Weiya granodioritic gneiss from the eastern segment of Central Tianshan yielded a zircon U–Pb discordia upper intercept age of 1218 ± 17 Ma, which was interpreted as the emplacement age of the protolith granite (Liu et al., 2004). Two SHRIMP zircon U–Pb ages of 942 ± 7 Ma and 919 ± 6 Ma have been obtained from granitic gneisses in the Xingxingxia and Wenquan areas, respectively (Hu et al., 2010). Besides, Hu et al. (2006) determined an age of ca. 1.4 Ga for granodiorite in Xingxingxia. Later on, a zircon U–Pb dating age of 1.4 Ga from the Bingdaban granite was reported by Chen et al. (2009). And Yang et al. (2007) demonstrated that the granitic plutons were developed at about 956 Ma, which intruded the Precambrian basement of Central Tianshan. More recently, three populations of inherited zircons trapped in the Xingxingxia granodiorite indicate that Neoproterozoic (809 ± 41 Ma), Mesoproterozoic (ca. 1400 Ma) and Paleoproterozoic (ca. 1750 Ma) tectonomagmatic events in Central Tianshan (Lei et al., 2011).

Although Precambrian ages have been obtained for rocks from Central Tianshan, the available age data still cannot resolve the issue of the crustal evolution of the whole Central Tianshan. In order to better understand the Precambrian evolution of Central Tianshan, we chose to perform a comprehensive U–Pb dating of detrital zircons as well as Hf isotopic analyses of the dated zircon grains. We hope that the results would shed much light to identification of major tectonothermal or magmatic-metamorphic events in the protoliths of the sandstones. Recently, the age data histogram of detrital zircons has been frequently employed to infer the provenance characteristics of the protolith and tectonic events in the source regions ([Bruguier et al., 1997] , [Iizuka et al., 2005] , [Rino et al., 2008] , [Condie et al., 2009] , [Yu et al., 2008] , [Yu et al., 2010] , [Xiang and Shu, 2010] and [Yao et al., 2011]).

2. Geological background

The Chinese Tianshan belt is divided into three parts (Fig. 1), namely, the Northern Tianshan, Central Tianshan and Southern Tianshan. The Northern Tianshan is composed mainly of Carboniferous volcanic rocks, volcaniclastic rocks intercalated with sandy–muddy rocks. The Northern Tianshan belt is a late Paleozoic arc terrane ([Gao et al., 1998] and [Wang et al., 2008]).

The Central Tianshan belt consists of Precambrian basement rocks (Fig. 2) and is considered as part of the proto-Tarim block during Precambrian time ([Gao et al., 1998] , [Charvet et al., 2007] , [Shu et al., 2010] and [Shu et al., 2011]). Recent works ([Shu et al., 2002] , [Charvet et al., 2007] and [Wang et al., 2007]) suggested that Central Tianshan drifted away from the Tarim Block during middle Cambrian time, leading to the occurrence of the South Tianshan ocean. In the late Cambrian-Silurian, due to the southward subduction of the Tianshan ccean beneath the Tarim Block, an early Paleozoic Central Tianshan arc was formed on the Precambrian basement, and a Southern Tianshan back-arc basin developed to the south of the Central Tianshan arc. Central Tianshan was finally rewelded to the Tarim Block with the closure of the South Tianshan ocean during Silurian time.

The Southern Tianshan belt (Fig. 3) is situated in the southern margin of the CAOB. It has almost the same early Cambrian carbonate assemblages as those of Central Tianshan. However, Southern Tianshan comprises late Cambrian to Ordovician sedimentary rocks (sandstone, greywacke, mudstone and limestone) intercalated with volcanic rocks. This lithological assemblage is quite different from the arc-related volcanic rocks of Central Tianshan. Southern Tianshan is separated from the Tarim Block to the south by the Xingdi fault and from the Central Tianshan belt to the north by the Hongliuhe-Baluntai-Heiyingshan fault. Southern Tianshan was considered as a back-arc basin ([Shu et al., 2002] , [Charvet et al., 2007] and [Charvet et al., 2011]) or South Tianshan ocean during early Paleozoic time ([Windley et al., 1990] , [Xiao et al., 2008] , [Gao et al., 1998] and [Gao et al., 2009]). The closure of the South Tianshan ocean might be a scissor-like process, starting from the east and ending in the west (Chen et al., 1999a). The South Tianshan ocean was completely closed in the late Carboniferous ([Gao et al., 2009] and [Konopelko et al., 2009]) as inferred from the age of ca. 320 Ma of the Atbashi eclogites (Biske and Seltmann, 2010) and the post-collisional Permian magmatism ([Konopelko et al., 2007] , [Ren et al., 2011] and [Wang et al., 2011]).

After the closure of the South Tianshan ocean, Central Tianshan was accreted to the Tarim Block, and the Southern Tianshan region received middle Devonian deposits from both the Tarim Block and Central Tianshan.

The South China, North China and Tarim Blocks compose the tectonic framework of China (Fig. 1a) ([Zhao and Cawood, 1999] , [Qiu et al., 2000] , [Zhao, 2001] , [Zhao et al., 2001] , [Zhao et al., 2005] , [Zhao et al., 2010] , [Wilde and Zhao, 2005] , [Faure et al., 2007] , [Lu et al., 2008a] , [Lu et al., 2008b] , [Sun et al., 2009] , [Wang et al., 2010a] , [Yu et al., 2010] , [Jahn, 2011] and [Shu et al., 2011]). The Tarim Block occupies an area about 550,000 km^2 and its major part (more than 80%) is covered by Cenozoic desert. This block was affected by a Permian rift-type bimodal volcanism (mafic dykes, granites and syenites). A-type rapakivi granites crop out in the northern margin of Tarim ([Carroll et al., 1995] , [Pirajno et al., 2008] , [Shu et al., 2010] , [Zhang et al., 2010a] and [Zhang et al., 2010b]).

Paleoproterozoic and Neoarchean schist, gneiss and TTG suite (tonalite, trondhjemite and granodiorite) are scattered in the Altyn Tagh and Tieklik areas ([Zhang et al., 2007b] and [Lu et al., 2008a]), and in the Kuruqtagh area ([Shu et al., 2010] , [Shu et al., 2011] , [Long et al., 2010] , [Long et al., 2011a] , [Cao et al., 2011] and [Zhu et al., 2011a]) (Fig. 2). Voluminous Neoproterozoic weakly metamorphosed rocks (slate-phyllite, meta-igneous rocks), and Mesoproterozoic or locally Paleoproterozoic-Archean schists, gneisses and amphibolites are exposed in the E-W-trending Kuruqtagh domain located in the NE margin of Tarim. These rocks form the Precambrian basement of Tarim ([Gao et al., 1993] , [Guo et al., 2003] and [Zhu et al., 2010]).

A diorite core of 35 m thick was recovered from a drilling at a depth of >7000 m beneath the central Tarim desert. The rock was considered as part of the Precambrian basement, and was dated at 790 ± 22 Ma by the Ar–Ar method on hornblende grains (Guo et al., 2005).

Previous geochronological data from the TTG gneisses and other rocks in the Kuruqtagh, Altyn Tagh and Tieklik areas suggest that the basement of the Tarim Block formed in several periods at 2.65–2.45 Ga, 2.0–1.8 Ga, 1.1–0.9 Ga and 0.83–0.63 Ga ([Hu et al., 2000] , [Lu and Yuan, 2003] , [Zhu et al., 2008] , [Lu et al., 2008a] , [Shu et al., 2010] and [Long et al., 2011b]).

Four diamictite deposits related to the Neoproterozoic glaciations ([Xu et al., 2003] , [Xu et al., 2005] and [Xu et al., 2009]) are well preserved. A continental rift environment in the Neoproterozoic is documented by various 830–630 Ma magmatic rocks in the northern Tarim Block, probably resulting from the break-up of Rodinia ([Chen et al., 2004] , [Huang et al., 2005] , [Zhang et al., 2006] , [Zhang et al., 2007a] , [Zhu et al., 2008] , [Zhu et al., 2011a] and [Zhu et al., 2011b]).

Though much is known about the Precambrian tectonic evolution of the Tarim Block owing to the abundant precise geochronological data, the situation in Central Tianshan is poorly known due to the lack of precise isotopic age data.

In this work, five samples collected from the Devonian sandstones and greywackes from Baluntai (northern margin of Southern Tianshan) have been used for zircon U–Pb dating and in situ Hf isotopic analysis. The locations of these samples are shown in Fig. 3 and their petrographic features are shown in Fig. 4 and Table 1.

3. Analytical methods

Separation of zircon grains was performed using the conventional techniques including heavy liquids, magnetic separator and hand-picking under a binocular microscope fitted with a UV light. Zircon grains were mounted in epoxy disks, polished to expose the half-sections of zircon grains, and then coated with gold. Prior to analytical work, polished surfaces were photographed in transmitted and reflected lights to reveal internal structures.

3.1. Scanning electron microprobe

Cathodoluminescence (CL) images of the zircons were obtained with a Mono CL3+ (Gatan, USA) attached to an electron microscope (Quanta 400 FEG) at the State Key Laboratory of Continental Dynamics at Northwest University, Xi’an. These images were used to select the positions for LA-ICPMS analyses.

3.2. U–Pb dating

Zircon U–Pb isotopic analysis was carried out at the State Key Laboratory for Mineral Deposits Research, Nanjing University (NJU), using an Agilent 7500a ICP-MS attached to a New Wave 213 nm laser ablation system with an in-house sample cell. He carrier gas was used to transport the ablated sample from the standard laser-ablation cell, and then mixed with Ar gas via a mixing chamber before entering into the ICP-MS torch. All analyses were carried out using a beam spot size of 24 μm and a laser frequency of 5 Hz and 60% energy, which produce an energy density of 0.121 J/cm^2. Isotope mass fractionation was normalized using an external standard GEMOC GJ-1 (^{207}Pb/^{206}Pb age of 608.5 ± 1.5 Ma; Jackson et al., 2004) and analytical accuracy was monitored using zircon standards Mud Tank (intercept age of 732 ± 5 Ma; Black and Gulson, 1978).

Zircon samples were analyzed in runs of 15 analyses which included 5 zircon standards and up to 10 sample points. U–Pb ages were calculated from the raw signal data using the on-line software package GLITTER (ver. 4.4) (www.mq.edu.au/GEMOC). Because ^{204}Pb could not be measured due to low signal and interference from ^{204}Hg in the gas supply, common lead correction was carried out using the EXCEL program ComPbCorr#3–15G (Andersen, 2002). However, no analysis has been corrected effectively because of the concordance between different U–Th–Pb isotopic ratios and the very low common lead. A total of 400 groups of LA-ICPMS U–Pb isotopic ages from five samples are listed in Table 2. The spots of the age concordance lower than 90% such as spots 681-38, 681-51, 681-72 and 685-50 are deleted due to inadequate precision. Data requiring >2% correction was excluded in the following discussion.

As ^{235}U is of minor abundance in the U–Pb isotopic system of zircon, much less ^{207}Pb is produced in young zircon, so the ^{207}Pb/^{235}U and ^{207}Pb/^{206}Pb ages have lower precision than ^{206}Pb/^{238}U ages. Commonly, only ^{206}Pb/^{238}U ages were used, especially for young zircon. However, for discordant zircon, the ^{206}Pb/^{238}U age commonly underestimates actual age due to Pb loss, while ^{207}Pb/^{206}Pb age is closer to the primary crystallization age. Therefore the ^{207}Pb/^{206}Pb age is adopted for old zircon. In this study, ^{206}Pb/^{238}U ages are used for zircons with ^{207}Pb/^{206}Pb ages <1000 Ma, and ^{207}Pb/^{206}Pb ages for the older ones. Zircons with discordance >10% were discarded.

Th and U concentrations of zircons were calculated according to the comparison of relative signal intensity between the standard zircon GJ-1 (Th = 8 ppm, U = 330 ppm) and zircon samples using the EXCEL program Data Templatev2b from GEMOC. All of the U–Th–Pb age calculations and plotting of concordia diagrams were made using the ISOPLOT/Ex program (ver. 2.49) (Ludwig, 2001). Detailed analytical procedures are similar to those described by Griffin et al. (2004), Wang et al. (2010b) and Shu et al. (2010).

3.3. Hf-isotope analyses

Zircon Hf isotope analyses were carried out in situ using a Nu Plasma HR MC-ICP-MS (Nu Instruments Ltd, HK) coupled with Geolas 2005 laser ablation system equipped with a 193 nm ArF-excimer laser, with a spot size of 44 μm and a repetition rate of 10 Hz, at the State Key Laboratory of Continental Dynamics, Northwest University, Xi'an. The analytical procedures are similar to those described by Yuan et al. (2008). Zircon 91500 was used as the reference standard, with a recommended ^{176}Hf/^{177}Hf ratio of 0.282295 ± 0.000027 (n = 14, 2σ). The model ages were computed under the assumption that the ^{176}Lu/^{177}Hf of average

crust is 0.015, and the $^{176}Hf/^{177}Hf$ and $^{176}Lu/^{177}Hf$ ratios of chondrite and depleted mantle at the present are 0.282772 and 0.0332, 0.28325 and 0.0384 ([Blichert-Toft and Albarede, 1997] , [Vervoort et al., 1999] and [Griffin et al., 2004]). ^{176}Lu decay constant of 1.865E−11 (Scherer et al., 2001) was used for the model age calculation.

The model age (T_{DM}) provides only a minimum age for the source material of the magma from which the zircon crystallized. Therefore we have also calculated the crustal model age (T_{DM2}), in which we assume that the parental magma was produced from an average continental crust ($^{176}Lu/^{177}Hf = 0.015$) which was originally derived from the depleted mantle. The U–Pb age and REE data on zircons used for Hf isotope analysis were also collected. U, Th and Pb concentrations were calibrated by using ^{29}Si as the internal calibrant.

4. Analysis results

4.1. Zircon CL images

The representative CL images of the studied zircons together with spot ages are shown in Fig. 5. Four types of zircons are recognized. Type-I zircons are characterized by euhedral shape (681-25, 684-31), implying a near-source region; Type-II zircons are subhedral, exhibiting clear oscillatory zoning (682-54, 685-48); Type-III zircons show rounded grain morphology (682-72, 683-09), indicating that they have experienced long-distance transportation and abrasion; and Type-IV zircons show rounded-to-subrounded morphology, simultaneously featured by an anhedral inherited core with a narrow rim (681-01, 683-84). Generally, the structures of zircons with ages of <650 Ma are nearly euhedral, whereas the zircons with ages of >650 Ma are mainly subhedral to rounded, particularly the inherited cores (e.g. spots 682-18 and 683-61 in Fig. 5).

4.2. U–Pb dating

About 80 detrital zircon grains from each of the five samples (#681, 682, 683, 684 and 685) were analyzed. The results yielded a wide range of ages from 369 to 3663 Ma (Fig. 6), indicating multiple sources for the zircons and a great variety of rocks in the source areas. However, the data seem to fall in six major age populations: 2530–2380 Ma, 1900–1790 Ma, 1600–1500 Ma, 1000–900 Ma, 820–750 Ma and 480–410 Ma (Fig. 7), with peaks at ~2470 Ma, ~1858 Ma, ~1541 Ma, ~952 Ma, ~820–750 Ma, and ~447 Ma (Fig. 8), respectively.

On the frequency diagram of concordant ages, the largest age peak appears at 447 Ma, and the others occur at 952 Ma, 820–750 Ma and 2470 Ma. The age peaks at about 1541 Ma and 1858 Ma are also visible.

Of the 400 analyses, 37 spots gave concordant ages of >2500 Ma, of which 7 are >3000 Ma, with one at 3663 ± 38 Ma. Consequently, the presence of an Eoarchean source is evident.

4.3. Th/U ratios of zircons

The Th/U ratios of zircons have been commonly used to assess their origins (Maas et al., 1992). Generally, zircons with high Th/U ratios (>0.4) are considered to be magmatic, whereas those with low Th/U ratios (<0.1) are likely metamorphic ([Kinny et al., 1990] , [Zhao et al., 2002a] , [Zhao et al., 2008] and [Corfu et al., 2003]). In this study, most detrital zircons have Th/U ratios >0.4 (Table 2). Of about 400 zircon grains, 343 have Th/U ratios

>0.4, and 54 <0.4, and only 10 <0.1 (Fig. 9). Because the majority of the zircons (ca. 86%) appear to be magmatic, the zircon ages obtained offer a valuable constraints on the crustal evolution of the study region.

4.4. REE geochemistry of zircons

The REE patterns of zircons are useful to study the origins of zircons. It has been found that zircons of magmatic origin have remarkable positive Ce anomalies, negative Eu anomalies, HREE enrichment relative to LREE, and steep-rising REE patterns. By contrast, metamorphic zircons show marked depletion of HREE, characterized by flat MREE-HREE patterns without negative Eu anomaly, particularly when garnet is present in the rocks ([Schaltegger et al., 1999] , [Hoskin and Ireland, 2000] , [Hoskin et al., 2000] , [Belousova et al., 2002] , [Rubatto, 2002] , [Whitehouse and Platt, 2003] and [Hoskin and Schaltegger, 2003]).

Furthermore, the abundance and ratios of REE have been shown to be related to source rock types and crystallization environments ([Heaman et al., 1990] and [Belousova et al., 2002]). Hinton and Upton (1991) and [Belousova et al., 1998] and [Belousova et al., 2002] reported that mantle-derived zircons have a flat REE pattern and lower REE abundances (<50 ppm) than crustal zircons.

Variations in Ce and Eu anomalies have also been used to interpret specific crystallization conditions of zircons. Zircons that lack a positive Ce anomaly are known only from lunar samples forming under highly reducing conditions (Ireland and Wlotzka, 1992), whereas zircons that lack a negative Eu anomaly have been interpreted as having formed in plagioclase-absent assemblages, including kimberlite, syenite and eclogite ([Belousova et al., 1998] , [Rubatto, 2002] and [Bingen et al., 2004]).

In this study, REE compositions of 31 zircons have been determined (Table 3), all of which are enriched in heavy REE (HREE), and show negative Eu anomalies. As illustrated in Fig. 10, two types of zircon REE patterns can be recognized. Type I zircons display remarkable positive Ce anomalies, negative Eu anomalies and HREE enrichment relative to LREE, which are typical of magmatic zircons. Type II zircons show little or no positive Ce anomalies, suggesting their metamorphic origin.

Based on the Eu/Eu* and Ce/Ce* ratios of zircons (Fig. 11), we conclude that these zircons were derived from different source rock types and crystallization environments. Moreover, two zircons of mafic rocks have been found, and there are only few examples in the literature ([Belyatsky et al., 2008] and [Kostitsyn et al., 2009]).

4.5. Hf isotopic composition

Zircon Hf isotopic data are shown in Table 4 and illustrated in Fig. 12. The initial $^{176}Hf/^{177}Hf$ ratios, expressed in $\varepsilon_{Hf}(t)$ values, show a wide range even within a single age populations. Most zircons have negative $\varepsilon_{Hf}(t)$ values (85 out of 120), and only 35 grains have positive $\varepsilon_{Hf}(t)$ values, suggesting that most of them were derived from reworked Precambrian crust. However, even within single age populations, the zircons show positive and negative $\varepsilon_{Hf}(t)$ values (Fig. 12A). For example, zircons with ages about 2.5 Ga have $\varepsilon_{Hf}(t)$ of +42 to −16, and those of ~0.95 Ga have $\varepsilon_{Hf}(t)$ of +11 to −33 (Table 4). This suggests that these zircons have diverse origins or different magmatic protoliths of similar age. Based on the distribution of the Hf model ages, three major stages of crustal evolution may be revealed at 1.0–1.4 Ga, 1.8–3.3

Ga and 3.4–3.8 Ga (Fig. 12B). In addition, one analysis yielded a crustal model age (T_{DM2}) of 4230 Ma.

5. Discussion

5.1. Provenance of the Devonian sandstones

The age spectra of detrital zircons from the Devonian sandstones in Baluntai reveal that zircons of Precambrian ages came mainly from magmatic rocks of the three periods: 2530–2380 Ma, 1900–1790 Ma, and 1000–900 Ma (Fig. 7 and Fig. 8). The first period (2530–2380 Ma) corresponds to the Paleoproterozoic-Archean schists, gneisses, amphibolites and TTG rocks in the Kuruqtagh, Altyn Tagh and Tieklik massives of Tarim ([Gao et al., 1993] , [Guo et al., 2003] , [Zhang et al., 2007b] , [Shu et al., 2010] , [Long et al., 2010] , [Long et al., 2011a] and [Long et al., 2011b]). Shu et al. (2010) reported two concordant $^{207}Pb/^{206}Pb$ ages of crystallization of magmatic zircons: 2469 ± 12 Ma (gneissic granite, n = 17) and 2470 ± 24 Ma (diorite, n = 17) in the Kuruqtagh area.

The rounded Archean zircons suggest a long-distance transport. Moreover, no Archean tectonic activity has been recorded in Central Tianshan, thus we consider that zircons of 2530–2380 Ma ages in Baluntai were likely derived from the Tarim Block.

Regarding the second population of ca. 1900–1790 Ma, Paleoproterozoic magmatic rocks have been reported from the Tarim Block, thus the period is considered as an important time of crustal growth in Central Tianshan (Hu et al., 2000). In addition, Shu et al. (2010) determined an age peak of 1870 Ma for magmatic zircons in the Kuruqtagh massif in NE Tarim. These suggest that the analyzed zircons with middle Paleoproterozoic ages were sourced from both Tarim and Central Tianshan.

Detrital zircons with ages of ca. 1600–1500 Ma are markedly subrounded or rounded. We infer that both Central Tianshan and Tarim were the provenances of these detrital zircons. The direct evidence for synchronous magmatic rocks or contemporaneous deformational events have not yet been found in the two areas, and a possible interpretation is that the source rocks have now been eroded and reworked, or were deeply buried.

A prominent period from 1000 to 900 Ma can be singled out in the age spectra. The population of 1000–900 Ma is considered to mark an important tectonic episode for Tarim and Central Tianshan ([Lu et al., 2008a] , [Zhang et al., 2009a] and [Shu et al., 2010]). As reported by Hu et al. (2010), two zircon U–Pb ages of 942 ± 7 Ma and 919 ± 6 Ma have been determined for gneissic granites from Central Tianshan. In fact, magmatic and metamorphic ages of ca. 1.1–0.9 Ga are abundantly recorded in the Tarim Block. The 0.9–1.0 Ga metamorphic event recognized in the northern Kunlun Orogen (SW Tarim) has been interpreted as a result of the response of the Tarim Block to the assembly of Rodinia (Zhang et al., 2007c). Guo et al. (2005) obtained zircon ages of 890–932 Ma for a granodiorite drilled core (7200 m depth) from the desert of the central Tarim Block. Therefore, we conclude that Central Tianshan and the Tarim Block were the sources for the zircons with ages around 0.95 Ga.

The Tarim Block has been regarded as a component of Rodinia, and its break-up from Rodinia is considered to have occurred during the Meso-Neoproterozoic time ([Li et al., 2003a] and [Huang et al., 2005]). The zircons with U–Pb ages of 821 ± 11 Ma, 798 ± 8 Ma

and 707 ± 7 Ma have been obtained for the gneisses of Central Tianshan (Chen et al., 1999b). This age range is similar to that of the widely exposed Kuruqtagh diabase dyke swarms, which were dated at 824 ± 9 Ma, 777 ± 9 Ma and 760 ± 6 Ma (SHRIMP U–Pb zircon ages) ([Zhang et al., 2009a] , [Zhang et al., 2009b] and [Zhang et al., 2011]). Similar ages 806 ± 8 Ma and 798 ± 7 Ma for granites (LA-ICPMS zircon ages) were reported by Shu et al. (2010).

The age spectra shown in Fig. 8 revealed a prominent age peak at 447 Ma. These zircons have euhedral shape (Fig. 5), so they were likely derived from a nearby source. We argue that the provenance of these zircons was Central Tianshan based on the two facts: (1) no early Paleozoic magmatism occurred in the Tarim Block, and (2) Central Tianshan was an Ordovician island arc, as evidenced by the 432 ± 1 Ma and 435 ± 2 Ma Weiya granulite ([Shu et al., 2004] and [Charvet et al., 2007]) and ∼430 Ma Jingbulake mafic-ultramafic intrusion in Western Tianshan (Yang and Zhou, 2009), and zircon with age of 456.2 ± 0.6 Ma from the Baluntai granite (Han et al., 2004). Hopson et al. (1989) also reported a 435 Ma Silurian granite from Central Tianshan.

In summary, except the age peaks of 447 Ma (Central Tianshan) and 2470 Ma (Tarim), other populations of detrital zircons from the Baluntai sandstones were sourced from both Central Tianshan and Tarim Block.

5.2. Evolution of the provenance of the Southern Tianshan belt

As mentioned above, Central Tianshan was a member of the proto-Tarim block in the Precambrian, and was rifted away from Tarim during middle Cambrian time. In the Silurian, collision between the Central Tianshan arc and the Tarim Block occurred due to the closure of the South Tianshan ocean, forming the Central-Southern Tianshan orogen. U–Pb dating of detrital zircons from Baluntai provides a broad view of the Precambrian geodynamic history and crustal evolution of the study area.

Archean to Paleoproterozoic igneous rocks sporadically occurred in the Tarim Block ([Hu and Rogers, 1992] and [XBGMR, 1999]). The available age data indicate that the Tarim Block underwent an intense Neoarchean to Paleoproterozoic magmatic event, represented by 2.5–2.7 Ga TTG suites and TIMS U–Pb ages of zircons of ∼2.5 Ga for lasurquarz-bearing gneiss (Lu, 1992), and 2492 ± 19 Ma for amphibolite in the Kuruqtagh area (Guo et al., 2003). The magmatic zircons derived from the TTG rocks in Western Kunlun (SW Tarim) yielded concordant $^{207}Pb/^{206}Pb$ ages of 2534 ± 19 Ma (potassic granite) and 2602 ± 27 Ma (tonalite), indicating that these rocks were mainly emplaced at 2.6–2.5 Ga (Zhang et al., 2007b). More recently, Long et al. (2010) obtained a U–Pb age of 2516 ± 6 Ma from TTG suite in Kuruqtagh, which display typical geochemical features of an island arc tectonic setting. Furthermore, Shu et al. (2010) reported the U–Pb ages of 2469 ± 12 Ma for gneissic granite and 2470 ± 24 Ma for meta-diorite from Kuruqtagh, reflecting that a marked tectonomagmatic event took place in the early Paleoproterozoic.

Considering the negative $\varepsilon_{Hf}(t)$ values for most zircons with ages of 2530–2380 Ma, the early Paleoproterozoic rocks in Tarim were likely derived from reworking of the Archean crust. A minor amount of zircons with positive $\varepsilon_{Hf}(t)$ values suggest the presence of some juvenile crust.

The 1.9–1.8 Ga tectonomagmatic event in the proto-Tarim block is inferred from the age population of 1900–1790 Ma (peak at 1858 Ma) (Fig. 8). In both northeastern (Kuruqtagh)

and southeastern (Altyn) parts of Tarim, Mesoproterozoic greenschist facies strata unconformably overlie the Paleoproterozoic amphibolite facies khondalites ([XBGMR, 1993] and [Feng et al., 1995]). In the Altyn Tagh and Tieklik areas of the Tarim Block, metamorphic zircons yielded SHRIMP U–Pb ages of 2.0–1.8 Ga (Zhang et al., 2007b). Most recently, Shu et al. (2010) obtained an age peak of 1870 Ma for magmatic zircons from the rocks in Kuruqtagh. All these suggest that like Laurentia, North China, Baltica, Antarctica, Amazonia, India, West Africa, South Africa and Australia ([Daly et al., 2001] , [Hanski et al., 2001] , [Wilde et al., 2002] , [Kroner et al., 2005] , [Santosh et al., 2004] , [Santosh et al., 2006] , [Zhao et al., 2002b] , [Zhao et al., 2003] , [Zhao et al., 2004] , [Zhao et al., 2009] , [Rogers and Santosh, 2002] , [Rogers and Santosh, 2009] , [Hou et al., 2008] , [Kusky and Santosh, 2009] and [Santosh, 2010]), the Tarim Block also underwent a tectonothermal event at 1900–1790 Ma, broadly coincident with the global collisional events that led to the assembly of the Columbia supercontinent ([Zhao et al., 2002b] , [Zhao et al., 2002c] and [Zhao et al., 2004]). Therefore, the argument for the Tarim Block as a component of the Columbia supercontinent is further supported.

The most characteristic feature of the global Mesoproterozoic geology is the widespread continental rifting and occurrence of anorogenic magmatism ([Green, 1992] , [Tarney, 1992] , [Windley, 1993] and [Zhao et al., 2006]). This could be related to mantle plume or asthenospheric upwelling. The Mesoproterozoic rifting event is considered to be equal to the breakup of Columbia ([Rogers and Santosh, 2002] , [Zhao et al., 2002b] and [Zhao et al., 2004]). As a response to the breakup of Columbia, a Mesoproterozoic tectonomagmatic event took place, and it is likely represented by the zircon population of 1600–1500 Ma as revealed in the studied area (Fig. 8). However, direct evidence has not been found in Tarim or Central Tianshan.

The age population of 1000–900 Ma (peak at 952 Ma; Fig. 8) might indicate an event related to the Grenville orogeny in Central Tianshan and Tarim. The Grenville Orogeny (ca. 1300–900 Ma) was widely known in Laurentia and East Antarctica (Hoffman, 1991), forming a global-scale orogenic belt that welded together the older continental blocks to form the Rodinia supercontinent (Li et al., 2008).

Neoproterozoic gneisses occur in Tianshan of Kyrgyzstan (Brookfield, 2000). It could be a fragment of Tarim. Two zircon U–Pb ages of 942 ± 7 Ma and 919 ± 6 Ma from gneissic granites have been reported in Central Tianshan (Hu et al., 2010). Zhang et al. (2007c) reported a metamorphic zircon age of 0.9–1.0 Ga for paragneisses from the northern Kunlun Orogen, SW Tarim. The authors interpreted the age as a result of the response of the Tarim Block to the convergence of Rodinia. Ages of 890–932 Ma were reported for granodiorites from the central Tarim Block beneath the desert about 7200 m by Guo et al. (2005). Relevant dating data also include (1) the late Mesoproterozoic to early Neoproterozoic amphibolite facies metamorphic rocks with ^{40}Ar–^{39}Ar ages at 1050–1020 Ma, (2) the tightly folded metamorphic rocks with metamorphic zircon U–Pb ages of 1000–900 Ma along the southwestern margin of the Tarim (Zhang et al., 2009a), and (3) the magmatic zircons with an age of 933 ± 11 Ma in the Kuruqtagh foliated granite (Shu et al., 2010). Most recently, Cao et al. (2011) recognized Neoproterozoic granites in the Kuruqtagh area. Therefore, the age peak of 952 Ma may represent the record of the assembly of Rodinia in the Tarim Block.

The break-up of Rodinia seems to have been taken place in the middle Neoproterozoic (Rogers and Santosh, 2003), initiated by a mantle plume upwelling ([Park et al., 1995] , [Wingate et al., 1998] , [Li et al., 2003a] and [Li et al., 2003b]). The most typical

characteristics of the breakup of supercontinent are the emplacement of continental flood basalt, mafic dyke swarms and rift sequences, as well as large igneous provinces (LIPs) ([Cox, 1978] , [Richards et al., 1989] , [Campbell and Griffiths, 1990] and [Ernst et al., 2008]). Our detrital zircon dating shows a cluster of middle Neoproterozoic ages (820–750 Ma). This result might be a fingerprint of the breakup event in the Tarim Block.

Diabase dyke swarms, alkaline igneous complexes and bimodal volcanic rocks crop out widely around the Tarim Block (Liou et al., 1996). Mafic-ultramafic and felsic intrusions (bimodal igneous complex) at 825–800 Ma have also been reported, including a 825 Ma bimodal igneous complex in Kuruqtagh (NE Tarim) (Zhang et al., 2007a), a late Neoproterozoic rift-basin in the northwest Tarim (Turner, 2010), a 807 ± 12 Ma dyke swarm in Aksu (NW Tarim) ([Chen et al., 2004] and [Liou et al., 1996]) and a 783 ± 10 Ma bimodal intrusion in Kudi (SW Tarim) (Zhang et al., 2006).

The present geochronological data and available geological information allow us to conclude that the breakup of the Tarim Block from Rodinia was a protracted tectonic process.

5.3. Position of the Tarim Block in the Precambrian supercontinents

For a better understanding of the affinity of the Tarim Block with other major continents, the Precambrian age distributions of ancient blocks around the world are compared and shown in Fig. 13. The tectonic event of ca. 450 Ma is not discussed here as it is not relevant to the Precambrian reconstruction of Tarim.

5. Discussion

5.1. Provenance of the Devonian sandstones

The age spectra of detrital zircons from the Devonian sandstones in Baluntai reveal that zircons of Precambrian ages came mainly from magmatic rocks of the three periods: 2530–2380 Ma, 1900–1790 Ma, and 1000–900 Ma (Fig. 7 and Fig. 8). The first period (2530–2380 Ma) corresponds to the Paleoproterozoic-Archean schists, gneisses, amphibolites and TTG rocks in the Kuruqtagh, Altyn Tagh and Tieklik massives of Tarim ([Gao et al., 1993] , [Guo et al., 2003] , [Zhang et al., 2007b] , [Shu et al., 2010] , [Long et al., 2010] , [Long et al., 2011a] and [Long et al., 2011b]). Shu et al. (2010) reported two concordant $^{207}Pb/^{206}Pb$ ages of crystallization of magmatic zircons: 2469 ± 12 Ma (gneissic granite, n = 17) and 2470 ± 24 Ma (diorite, n = 17) in the Kuruqtagh area.

The rounded Archean zircons suggest a long-distance transport. Moreover, no Archean tectonic activity has been recorded in Central Tianshan, thus we consider that zircons of 2530–2380 Ma ages in Baluntai were likely derived from the Tarim Block.

Regarding the second population of ca. 1900–1790 Ma, Paleoproterozoic magmatic rocks have been reported from the Tarim Block, thus the period is considered as an important time of crustal growth in Central Tianshan (Hu et al., 2000). In addition, Shu et al. (2010) determined an age peak of 1870 Ma for magmatic zircons in the Kuruqtagh massif in NE Tarim. These suggest that the analyzed zircons with middle Paleoproterozoic ages were sourced from both Tarim and Central Tianshan.

Detrital zircons with ages of ca. 1600–1500 Ma are markedly subrounded or rounded. We infer that both Central Tianshan and Tarim were the provenances of these detrital zircons. The direct evidence for synchronous magmatic rocks or contemporaneous deformational events have not yet been found in the two areas, and a possible interpretation is that the source rocks have now been eroded and reworked, or were deeply buried.

A prominent period from 1000 to 900 Ma can be singled out in the age spectra. The population of 1000–900 Ma is considered to mark an important tectonic episode for Tarim and Central Tianshan ([Lu et al., 2008a] , [Zhang et al., 2009a] and [Shu et al., 2010]). As reported by Hu et al. (2010), two zircon U–Pb ages of 942 ± 7 Ma and 919 ± 6 Ma have been determined for gneissic granites from Central Tianshan. In fact, magmatic and metamorphic ages of ca. 1.1–0.9 Ga are abundantly recorded in the Tarim Block. The 0.9–1.0 Ga metamorphic event recognized in the northern Kunlun Orogen (SW Tarim) has been interpreted as a result of the response of the Tarim Block to the assembly of Rodinia (Zhang et al., 2007c). Guo et al. (2005) obtained zircon ages of 890–932 Ma for a granodiorite drilled core (7200 m depth) from the desert of the central Tarim Block. Therefore, we conclude that Central Tianshan and the Tarim Block were the sources for the zircons with ages around 0.95 Ga.

The Tarim Block has been regarded as a component of Rodinia, and its break-up from Rodinia is considered to have occurred during the Meso-Neoproterozoic time ([Li et al., 2003a] and [Huang et al., 2005]). The zircons with U–Pb ages of 821 ± 11 Ma, 798 ± 8 Ma and 707 ± 7 Ma have been obtained for the gneisses of Central Tianshan (Chen et al., 1999b). This age range is similar to that of the widely exposed Kuruqtagh diabase dyke swarms, which were dated at 824 ± 9 Ma, 777 ± 9 Ma and 760 ± 6 Ma (SHRIMP U–Pb zircon ages) ([Zhang et al., 2009a] , [Zhang et al., 2009b] and [Zhang et al., 2011]). Similar ages 806 ± 8 Ma and 798 ± 7 Ma for granites (LA-ICPMS zircon ages) were reported by Shu et al. (2010).

The age spectra shown in Fig. 8 revealed a prominent age peak at 447 Ma. These zircons have euhedral shape (Fig. 5), so they were likely derived from a nearby source. We argue that the provenance of these zircons was Central Tianshan based on the two facts: (1) no early Paleozoic magmatism occurred in the Tarim Block, and (2) Central Tianshan was an Ordovician island arc, as evidenced by the 432 ± 1 Ma and 435 ± 2 Ma Weiya granulite ([Shu et al., 2004] and [Charvet et al., 2007]) and ~430 Ma Jingbulake mafic-ultramafic intrusion in Western Tianshan (Yang and Zhou, 2009), and zircon with age of 456.2 ± 0.6 Ma from the Baluntai granite (Han et al., 2004). Hopson et al. (1989) also reported a 435 Ma Silurian granite from Central Tianshan.

In summary, except the age peaks of 447 Ma (Central Tianshan) and 2470 Ma (Tarim), other populations of detrital zircons from the Baluntai sandstones were sourced from both Central Tianshan and Tarim Block.

5.2. Evolution of the provenance of the Southern Tianshan belt

As mentioned above, Central Tianshan was a member of the proto-Tarim block in the Precambrian, and was rifted away from Tarim during middle Cambrian time. In the Silurian, collision between the Central Tianshan arc and the Tarim Block occurred due to the closure of the South Tianshan ocean, forming the Central-Southern Tianshan orogen. U–Pb dating of detrital zircons from Baluntai provides a broad view of the Precambrian geodynamic history and crustal evolution of the study area.

Archean to Paleoproterozoic igneous rocks sporadically occurred in the Tarim Block ([Hu and Rogers, 1992] and [XBGMR, 1999]). The available age data indicate that the Tarim Block underwent an intense Neoarchean to Paleoproterozoic magmatic event, represented by 2.5–2.7 Ga TTG suites and TIMS U–Pb ages of zircons of ~2.5 Ga for lasurquarz-bearing gneiss (Lu, 1992), and 2492 ± 19 Ma for amphibolite in the Kuruqtagh area (Guo et al., 2003). The magmatic zircons derived from the TTG rocks in Western Kunlun (SW Tarim) yielded concordant $^{207}Pb/^{206}Pb$ ages of 2534 ± 19 Ma (potassic granite) and 2602 ± 27 Ma (tonalite), indicating that these rocks were mainly emplaced at 2.6–2.5 Ga (Zhang et al., 2007b). More recently, Long et al. (2010) obtained a U–Pb age of 2516 ± 6 Ma from TTG suite in Kuruqtagh, which display typical geochemical features of an island arc tectonic setting. Furthermore, Shu et al. (2010) reported the U–Pb ages of 2469 ± 12 Ma for gneissic granite and 2470 ± 24 Ma for meta-diorite from Kuruqtagh, reflecting that a marked tectonomagmatic event took place in the early Paleoproterozoic.

Considering the negative $\varepsilon_{Hf}(t)$ values for most zircons with ages of 2530–2380 Ma, the early Paleoproterozoic rocks in Tarim were likely derived from reworking of the Archean crust. A minor amount of zircons with positive $\varepsilon_{Hf}(t)$ values suggest the presence of some juvenile crust.

The 1.9–1.8 Ga tectonomagmatic event in the proto-Tarim block is inferred from the age population of 1900–1790 Ma (peak at 1858 Ma) (Fig. 8). In both northeastern (Kuruqtagh) and southeastern (Altyn) parts of Tarim, Mesoproterozoic greenschist facies strata unconformably overlie the Paleoproterozoic amphibolite facies khondalites ([XBGMR, 1993] and [Feng et al., 1995]). In the Altyn Tagh and Tieklik areas of the Tarim Block, metamorphic zircons yielded SHRIMP U–Pb ages of 2.0–1.8 Ga (Zhang et al., 2007b). Most recently, Shu et al. (2010) obtained an age peak of 1870 Ma for magmatic zircons from the rocks in Kuruqtagh. All these suggest that like Laurentia, North China, Baltica, Antarctica, Amazonia, India, West Africa, South Africa and Australia ([Daly et al., 2001] , [Hanski et al., 2001] , [Wilde et al., 2002] , [Kroner et al., 2005] , [Santosh et al., 2004] , [Santosh et al., 2006] , [Zhao et al., 2002b] , [Zhao et al., 2003] , [Zhao et al., 2004] , [Zhao et al., 2009] , [Rogers and Santosh, 2002] , [Rogers and Santosh, 2009] , [Hou et al., 2008] , [Kusky and Santosh, 2009] and [Santosh, 2010]), the Tarim Block also underwent a tectonothermal event at 1900–1790 Ma, broadly coincident with the global collisional events that led to the assembly of the Columbia supercontinent ([Zhao et al., 2002b] , [Zhao et al., 2002c] and [Zhao et al., 2004]). Therefore, the argument for the Tarim Block as a component of the Columbia supercontinent is further supported.

The most characteristic feature of the global Mesoproterozoic geology is the widespread continental rifting and occurrence of anorogenic magmatism ([Green, 1992] , [Tarney, 1992] , [Windley, 1993] and [Zhao et al., 2006]). This could be related to mantle plume or asthenospheric upwelling. The Mesoproterozoic rifting event is considered to be equal to the breakup of Columbia ([Rogers and Santosh, 2002] , [Zhao et al., 2002b] and [Zhao et al., 2004]). As a response to the breakup of Columbia, a Mesoproterozoic tectonomagmatic event took place, and it is likely represented by the zircon population of 1600–1500 Ma as revealed in the studied area (Fig. 8). However, direct evidence has not been found in Tarim or Central Tianshan.

The age population of 1000–900 Ma (peak at 952 Ma; Fig. 8) might indicate an event related to the Grenville orogeny in Central Tianshan and Tarim. The Grenville Orogeny (ca. 1300–900 Ma) was widely known in Laurentia and East Antarctica (Hoffman, 1991), forming a

global-scale orogenic belt that welded together the older continental blocks to form the Rodinia supercontinent (Li et al., 2008).

Neoproterozoic gneisses occur in Tianshan of Kyrgyzstan (Brookfield, 2000). It could be a fragment of Tarim. Two zircon U–Pb ages of 942 ± 7 Ma and 919 ± 6 Ma from gneissic granites have been reported in Central Tianshan (Hu et al., 2010). Zhang et al. (2007c) reported a metamorphic zircon age of 0.9–1.0 Ga for paragneisses from the northern Kunlun Orogen, SW Tarim. The authors interpreted the age as a result of the response of the Tarim Block to the convergence of Rodinia. Ages of 890–932 Ma were reported for granodiorites from the central Tarim Block beneath the desert about 7200 m by Guo et al. (2005). Relevant dating data also include (1) the late Mesoproterozoic to early Neoproterozoic amphibolite facies metamorphic rocks with ^{40}Ar–^{39}Ar ages at 1050–1020 Ma, (2) the tightly folded metamorphic rocks with metamorphic zircon U–Pb ages of 1000–900 Ma along the southwestern margin of the Tarim (Zhang et al., 2009a), and (3) the magmatic zircons with an age of 933 ± 11 Ma in the Kuruqtagh foliated granite (Shu et al., 2010). Most recently, Cao et al. (2011) recognized Neoproterozoic granites in the Kuruqtagh area. Therefore, the age peak of 952 Ma may represent the record of the assembly of Rodinia in the Tarim Block.

The break-up of Rodinia seems to have been taken place in the middle Neoproterozoic (Rogers and Santosh, 2003), initiated by a mantle plume upwelling ([Park et al., 1995] , [Wingate et al., 1998] , [Li et al., 2003a] and [Li et al., 2003b]). The most typical characteristics of the breakup of supercontinent are the emplacement of continental flood basalt, mafic dyke swarms and rift sequences, as well as large igneous provinces (LIPs) ([Cox, 1978] , [Richards et al., 1989] , [Campbell and Griffiths, 1990] and [Ernst et al., 2008]). Our detrital zircon dating shows a cluster of middle Neoproterozoic ages (820–750 Ma). This result might be a fingerprint of the breakup event in the Tarim Block.

Diabase dyke swarms, alkaline igneous complexes and bimodal volcanic rocks crop out widely around the Tarim Block (Liou et al., 1996). Mafic-ultramafic and felsic intrusions (bimodal igneous complex) at 825–800 Ma have also been reported, including a 825 Ma bimodal igneous complex in Kuruqtagh (NE Tarim) (Zhang et al., 2007a), a late Neoproterozoic rift-basin in the northwest Tarim (Turner, 2010), a 807 ± 12 Ma dyke swarm in Aksu (NW Tarim) ([Chen et al., 2004] and [Liou et al., 1996]) and a 783 ± 10 Ma bimodal intrusion in Kudi (SW Tarim) (Zhang et al., 2006).

The present geochronological data and available geological information allow us to conclude that the breakup of the Tarim Block from Rodinia was a protracted tectonic process.

5.3. Position of the Tarim Block in the Precambrian supercontinents

For a better understanding of the affinity of the Tarim Block with other major continents, the Precambrian age distributions of ancient blocks around the world are compared and shown in Fig. 13. The tectonic event of ca. 450 Ma is not discussed here as it is not relevant to the Precambrian reconstruction of Tarim.

University (No. 2008-I-01) and the State Key Laboratory of Continental Dynamics of Northwest University.

References

Allen et al., 1993a M.B. Allen, B.F. Windley and C. Zhang, Paleozoic collisional tectonics and magmatism of the Chinese Tien Shan, central Asia. *Tectonophysics*, **220** (1993), pp. 89–115.

Allen et al., 1993b M.B. Allen, B.F. Windley, C. Zhang and J.H. Guo, Evolution of the Turfan basin, Chinese Central Asia. *Tectonics*, **12** (1993), pp. 889–896

Andersen, 2002 T. Andersen, Correction of common Pb in U–Pb analyses that do not report ^{204}Pb. *Chem. Geol.*, **192** (2002), pp. 59–79

Belousova et al., 1998 E.A. Belousova, W.L. Griffin and N.J. Pearson, Trace element composition and cathodoluminescence properties of southern African kimberlitic zircons. *Miner. Mag.*, **62** (1998), pp. 355–366.

Belousova et al., 2002 E.A. Belousova, W.L. Griffin, S.Y. O'Reilly and N.I. Fisher, Igneous zircon: trace element composition as an indicator of source rock type. *Contrib. Miner. Petrol.*, **143** (2002), pp. 602–622

Belyatsky et al., 2008 B. Belyatsky, E. Lepekhina, A. Antonov, O. Shuliatin and S. Sergeev, Age and genesis of accessory zircon from MAR gabbroids, . *Geophysical Res. (Abstr.)*, (2008), p. 10 (EGU2008-A-01314).

Berry et al., 2001 R. Berry, G.A. Jenner, S. Meffre and M.N. Tubrett, A North American provenance for Neoproterozoic to Cambrian sandstones in Tasmania?. *Earth Planet. Sci. Lett.*, **192** (2001), pp. 207–222.

Bingen et al., 2004 B. Bingen, H. Austrheim, M.J. Whitehouse and W.J. Davis, Trace element signature and U–Pb geochronology of eclogite-facies zircon, Bergen Arcs, Caledonides of W Norway. *Contrib. Miner. Petrol.*, **147** (2004), pp. 671–683

Biske and Seltmann, 2010 Yu.S. Biske and R. Seltmann, Paleozoic Tian-Shan as a transitional region between the Rheic and Urals-Turkestan oceans. *Gondwana Res.*, **17** (2010), pp. 602–613.

Black and Gulson, 1978 L.P. Black and B.L. Gulson, The age of the Mud Tank carbonatite, Strangways Range, Northern Territory. *BMR J. Aust. Geol. Geophys.*, **3** (1978), pp. 227–232.

Blichert-Toft and Albarede, 1997 J. Blichert-Toft and F. Albarede, The Lu–Hf isotope geochemistry of chondrites and the evolution of the mantle–crust system. *Earth Planet. Sci. Lett.*, **148** (1997), pp. 243–258.

Boger et al., 2000 S.D. Boger, C.J. Carson, C.J.L. Wilson and C.M. Fanning, Neoproterozoic deformation in the Radok Lake region of the Northern Prince Charles Mountains, east

Antarctica: evidence for a single protracted orogenic event. *Precambrian Res.*, **104** (2000), pp. 1–24

Boynton, 1984 W.V. Boynton, Cosmochemistry of the rare earth elements: meteorite studies, P. Henderson, Editor, *Rare Earth Element Geochemistry*, Elsevier, Amsterdam (1984), pp. 63–114.

Brookfield, 2000 M.E. Brookfield, Geological development and Phanerozoic crustal accretion in the western segment of the southern Tien Shan (Kyrgyzstan, Uzbekistan and Tajikistan). *Tectonophysics*, **328** (2000), pp. 1–14.

Bruguier et al., 1997 O. Bruguier, J.R. Lancelot and J. Malavieille, U–Pb dating on single detrital zircon grains from the Triassic Songpan-Ganze flysch (Central China): provenance and tectonic correlations. *Earth Planet. Sci. Lett.*, **152** (1997), pp. 217–231.

Campbell and Griffiths, 1990 I.H. Campbell and R.W. Griffiths, Implications of mantle plume structure for the evolution of flood basalts. *Earth Planet. Sci. Lett*, **99** 1–2 (1990), pp. 79–93.

Cao et al., 2011 X.F. Cao, X.B. Lü, S.T. Liu, P. Zhang, X. Gao, C. Chen and Y.L. Mo, LA-ICP-MS zircon dating, geochemistry, petrogenesis and tectonic implications of the Dapingliang Neoproterozoic granites at Kuluketage block, NW China. *Precambrian Res.*, **186** (2011), pp. 205–219.

Carroll et al., 1995 A.R. Carroll, S.A. Graham, M.S. Hendrix, D. Ying and D. Zhou, Late Paleozoic tectonic amalgamation of NW China: sedimentary records of the northern Tarim, northwestern Turpan, and southern Junggar basins. *Geol. Am. Soc. Bull.*, **107** (1995), pp. 571–594.

Carson et al., 2002 C.J. Carson, J.J. Ague and C.D. Coath, U–Pb geochronology from Tonagh Island, East Antarctica: implications for the timing of ultra-high temperature metamorphism of the Napier complex. *Precambrian Res.*, **116** (2002), pp. 237–263.

Charvet et al., 2007 J. Charvet, L.S. Shu and S. Laurent-Charvet, Paleozoic structural and geodynamic evolution of eastern Tianshan (NW China): welding of the Tarim and Junggar plates. *Episodes*, **30** (2007), pp. 162–186.

Charvet et al., 2011 J. Charvet, L.S. Shu, S. Laurent-Charvet, B. Wang, M. Faure, D. Cluzel, Y. Chen and K. De Jong, Paleozoic tectonic evolution of the Tianshan belt, NW China. *Sci. China Ser. D Earth Sci.*, **54** 2 (2011), pp. 166–184.

Chen et al., 2009 X.Y. Chen, Y.J. Wang, L.H. Sun and W.M. Fan, Zircon SHRIMP U–Pb dating of the granitic gneisses from Bingdaban and Laerdundaban (Tianshan Orogen) and their geological significances, . *Geochimica*, **38** (2009), pp. 424–431 (in Chinese with English abstract).

Chen et al., 2004 Y. Chen, B. Xu, S. Zhan and Y. Li, First mid-Neoproterozoic paleomagnetic results from the Tarim Basin (NW China) and their geodynamic implications. *Precambrian Res.*, **133** (2004), pp. 271–281.

Chen et al., 1999a C.M. Chen, H.F. Lu, D. Jia, D.S. Cai and S.M. Wu, Closing history of the southern Tianshan oceanic basin, western China: An oblique collisional orogeny. *Tectonophysics*, **302** (1999), pp. 23–40.

Chen et al., 1999b Y.B. Chen, A.Q. Hu, G.X. Zhang and Q.F. Zhang, Zircon U–Pb age and Nd–Sr isotopic composition of granitic gneiss and its geological implications from Precambrian window of western Tianshan, NW China, . *Geochimica*, **28** (1999), pp. 515–520 (in Chinese with English abstract).

Coleman, 1989 R.G. Coleman, Continental growth of northwest China. *Tectonics*, **8** 3 (1989), pp. 621–635.

Condie et al., 2009 K.C. Condie, E. Belousova, W.L. Griffin and K.N. Sircombe, Granitoid events in space and time: constraints from igneous and detrital zircon age spectra. *Gondwana Res.*, **15** 3–4 (2009), pp. 228–242.

Corfu et al., 2003 F. Corfu, J.M. Hanchar, P.W.O. Hoskin and P. Kinny, Atlas of zircon textures. *Rev. Miner. Geochem.*, **53** (2003), pp. 469–500.

Cox, 1978 K.G. Cox, Flood basalts, subduction and the break-up of Gondwanaland. *Nature*, **274** (1978), pp. 47–49.

Daly et al., 2001 J.S. Daly, V.V. Balagansky, M.J. Timmerman, M.J. Whitehouse, K. de Jong, P.G. Guise, S. Bogdanova, R. Gorbatchev and D. Bridgwater, Ion microprobe U–Pb zircon geochronology and isotopic evidence for a trans-crustal suture in the Lapland-Kola Orogen, northern Fennoscandian Shield. *Precambrian Res.*, **105** (2001), pp. 289–314.

Ernst et al., 2008 R.E. Ernst, M.T.D. Wingate, K.L. Buchan and Z.X. Li, Global record of 1600–700 Ma large igneous provinces (LIPs): implications for the reconstruction of the proposed Nuna (Columbia) and Rodinia supercontinents. *Precambrian Res.*, **160** (2008), pp. 159–178.

Faure et al., 2007 M. Faure, P. Trap, W. Lin, P. Monie and O. Bruguier, Polyorogenic evolution of the Paleoproterozoic Trans-North China Belt, new insights from the Lüliangshan-Hengshan-Wutaishan and Fuping massifs. *Episodes*, **30** (2007), pp. 95–106.

Feng et al., 1995 B.Z. Feng, Y.W. Zhou, S.F. Chi, T.Q. Yang, C.X. Zhong, S.Q. Ye, Q.M. Peng, Z.H. Liu, Q.G. Jiang and L.X. Xing, The Pre-Sinian Geology and Precious-nonferrous Ore Deposits in Kuluketage Area, Xinjiang, Geol. Publ. House, Beijing (1995), (in Chinese with English abstract).

Fitzsimons, 2000 I.C.W. Fitzsimons, Grenville-age basement provinces in East Antarctica: evidence for three separate collisional orogens. *Geology*, **28** (2000), pp. 879–882.

Gao et al., 1998 J. Gao, M.S. Li, X.C. Xiao, Y.Q. Tang and G.Q. He, Paleozoic tectonic evolution of the Tianshan Orogen, northwestern China. *Tectonophysics*, **287** (1998), pp. 213–231.

Gao et al., 2009 J. Gao, L.L. Long, R. Klemd, Q. Qian, D.Y. Liu, X.M. Xiong, W. Su, W. Liu, Y.T. Wang and F.Q. Yang, Tectonic evolution of the South Tianshan orogen and

adjacent regions, NW China: geochemical and age constraints of granitoid rocks. *Int. J. Earth Sci.*, **98** (2009), pp. 1221–1238.

Gao et al., 1993 Z.J. Gao, J.Z. Chen and S.N. Lu, Precambrian System of the Northern Xinjiang, Geol. Publ. House, Beijing (1993), pp. 1–153.

Gehrels et al., 2003 G.E. Gehrels, P.G. DeCelles, A. Martin, T.P. Ojha, G. Pinhassi and B.N. Upreti, Initiation of the Himalayan Orogen as an early Paleozoic thin-skinned thrust belt. *GSA Today*, **13** (2003), pp. 4–9.

Green, 1992 J.C. Green, Proterozoic rifts, K.C. Condie, Editor, *Proterozoic Crustal Evolution*, Elsevier, Amsterdam (1992), pp. 97–150.

Griffin et al., 2004 W.L. Griffin, E.A. Belousova, S.R. Shee, N.J. Pearson and S.Y. O'Reilly, Archean crustal evolution in the northern Yilgarn Craton: U–Pb and Hf-isotope evidence from detrital zircons. *Precambrian Res.*, **131** (2004), pp. 231–282.

Guo et al., 2003 Z.J. Guo, Z.C. Zhang, S.W. Liu and H.M. Li, U–Pb geochronological evidence for the early Precambrian complex of the Tarim Craton, NW China, . *Acta Petrol. Sin.*, **19** 3 (2003), pp. 537–542 (in Chinese with English abstract).

Guo et al., 2005 Z.J. Guo, A. Yin, A. Robinson and C.Z. Jia, Geochronology and geochemistry of deep-drill-core samples from the basement of the central Tarim basin. *J. Asian Earth Sci.*, **25** (2005), pp. 45–56.

Han et al., 2004 B.F. Han, G.Q. He, T.R. Wu and H.M. Li, Zircon U–Pb dating and geochemical features of Early Paleozoic granites from Tianshan, Xinjiang: implication for tectonic evolution, . *Xinjiang Geol.*, **22** (2004), pp. 4–11 (in Chinese with English abstract).

Hanski et al., 2001 E. Hanski, H. Huhma and M. Vaasjoki, Geochronology of northern Finland: a summary and discussion, M. Vaasjoki, Editor, *Radiometric Age Determinations from Finnish Lapland and their Bearing on the Timing of Precambrian Volcano-sedimentary Sequences. Geological Survey of Finland, Special Paper 33* (2001), pp. 255–279.

Harley and Black, 1997 S.L. Harley and L.P. Black, A revised Archaean chronology for the Napier Complex, Enderby Land from SHRIMP ion-microprobe studies. *Antarctic Sci.*, **9** (1997), pp. 74–91.

Heaman et al., 1990 L.M. Heaman, R. Bowins and J. Crocket, The chemical composition of igneous zircon suites: implications for geochemical tracer studies. *Geochim. Cosmochim. Acta*, **54** (1990), pp. 1597–1607.

Hinton and Upton, 1991 R.W. Hinton and B.G.J. Upton, The chemistry of zircon: variations within and between large crystals from syenite and alkali basalt xenoliths. *Geochim. Cosmochim. Acta*, **55** (1991), pp. 3287–3302.

Hoffman, 1991 P.F. Hoffman, Did the breakout of Laurentia turn Gondwanaland inside out?. *Science*, **252** (1991), pp. 1409–1412.

Hokada et al., 2003T. Hokada, K. Misawa, K. Shiraishi and S. Suzuki, Mid to late Archaean (3.3–2.5 Ga) tonalitic crustal formation and high-grade metamorphism at Mt. Riiser-Larsen, Napier Complex, East Antarctica. *Precambrian Res.*, **127** (2003), pp. 215–228.

Hokada et al., 2004 T. Hokada, K. Misawa, K. Yokoyama, K. Shiraishi and A. Yamaguchi, SHRIMP and electron microprobe chronology of UHT metamorphism in the Napier complex, East Antarctica: implications for zircon growth at >1000 °C. *Contrib. Mineral. Petrol.*, **147** (2004), pp. 1–20.

Hopson et al., 1989 C. Hopson, J. Wen, G. Tilton, Y. Tang, B. Zhu and M. Zhao, Palaeozoic plutonism in East Junggar, Bogdashan, and eastern Tianshan, NW China. *EOS Trans. Am. Geophys. Union*, **70** (1989), pp. 1403–1404.

Hoskin and Ireland, 2000 P.W.O. Hoskin and T.R. Ireland, Rare earth element chemistry of zircon and its use as a provenance indicator. *Geology*, **7** (2000), pp. 627–630.

Hoskin et al., 2000 P.W.O. Hoskin, P.D. Kinny, D. Wyborn and B.W. Chappell, Identifying accessory mineral saturation during differentiation in granitoid magmas: an integrated approach. *J. Petrol.*, **41** (2000), pp. 1365–1396.

Hoskin and Schaltegger, 2003 P.W.O. Hoskin and U. Schaltegger, The composition of zircon and igneous and metamorphic petrogenesis. *Rev. Miner. Geochem.*, **53** (2003), pp. 27–55.

Hou et al., 2008 G.T. Hou, M. Santosh, X.L. Qian, G.S. Lister and J.H. Li, Configuration of the Late Paleoproterozoic supercontinent Columbia: insights from radiating mafic dyke swarms. *Gondwana Res.*, **14** (2008), pp. 395–409.

Hu and Rogers, 1992 A.Q. Hu and G. Rogers, Discovery of 3.3 Ga Archaen rocks in north Tarim Block of Xinjiang, western China. *Chin. Sci. Bull.*, **37** (1992), pp. 1546–1549.

Hu et al., 2000 A.Q. Hu, B.M. Jahn, G.X. Zhang, Y.B. Chen and Q.F. Zhang, Crustal evolution and Phanerozoic crustal growth in northern Xinjiang: Nd isotopic evidence. Part I. Isotopic characterization of basement rocks. *Tectonophysics*, **328** (2000), pp. 15–51.

Hu et al., 2006 A.Q. Hu, G.J. Wei, W.F. Deng, J.B. Zhang and L.L. Chen, 1.4 Ga SHRIMP U–Pb age for zircons of granodiorite and its geological significance from the eastern segment of the Tianshan Mountains, Xinjiang, China, . *Geochimica*, **35** (2006), pp. 333–345 (in Chinese with English abstract).

Hu et al., 2010 A.Q. Hu, G.J. Wei, B.M. Jahn, J.B. Zhang, W.F. Deng and L.L. Chen, Formation of the 0.9 Ga Neoproterozoic granitoids in the Tianshan Orogen, NW China: constraints from the SHRIMP zircon age determination and its tectonic significance, . *Geochimica*, **39** (2010), pp. 197–212 (in Chinese with English abstract).

Huang et al., 2005 B.C. Huang, B. Xu, C.X. Zhang, Y.A. Li and R.X. Zhu, Paleomagnetism of the Baiyisi volcanic rocks (ca. 740 Ma) of Tarim, Northwest China: a continental fragment of Neoproterozoic Western Australia?. *Precambrian Res.*, **142** (2005), pp. 83–92.

Iizuka et al., 2005 T. Iizuka, T. Hirata, T. Komiya, S. Rino, I. Katayama, A. Motoki and S. Maruyama, U–Pb and Lu–Hf isotope systematics of zircons from the Mississippi River sand:

implications for reworking and growth of continental crust. *Geology*, **33** (2005), pp. 485–488.

Ireland and Wlotzka, 1992 T.R. Ireland and F. Wlotzka, The oldest zircons in the solar system. *Earth Planet. Sci. Lett.*, **109** (1992), pp. 1–10.

Ireland et al., 1998 T.R. Ireland, T. Flöttmann, C.M. Fanning, G.M. Gibson and W.V. Preiss, Development of the early Paleozoic Pacific margin of Gondwana from detrital-zircon ages across the Delamerian Orogen. *Geology*, **26** (1998), pp. 243–246.

Jackson et al., 2004 S.E. Jackson, N.J. Pearson and W.L. Griffin, The application of laser ablation microprobe-inductively coupled plasma-mass spectrometry (LAM-ICP-MS) to in situ U–Pb zircon geochronology. *Chem. Geol.*, **211** (2004), pp. 47–69.

Jahn, 2004 B.M. Jahn, The Central Asian Orogenic Belt and growth of the continental crust in the Phanerozoic, J. Malpas, C.J.N. Fleitcher, J.R. Ali, J.C. Aitchison, Editors , *Aspects of the Tectonic Evolution of China. Geol. Soc. Spec. Publ. 226* (2004), pp. 73–100.

Jahn et al., 2004 B.M. Jahn, B. Natal'in, B.F. Windley and N. Dobretsov, Phanerozoic continental growth in Central Asia. *J. Asian Earth Sci.*, **23** (2004), pp. 599–603.

Jahn, 2011 B.M. Jahn, Accretionary orogen and evolution of the Japanese islands—implications from a Sr–Nd isotopic study of the Phanerozoic granitoids from SW Japan. *Am. J. Sci.*, **310** (2011).

Jayananda et al., 2000 M. Jayananda, J.F. Moyen, H. Martin, J.J. Peucat, B. Auvray and B. Mahabaleswar, Late Archaean (2550–2520 Ma) juvenile magmatism in the Eastern Dharwar craton, southern India: constraints from geochronology, Nd–Sr isotopes and whole rock geochemistry. *Precambrian Res.*, **99** (2000), pp. 225–254.

Kelly et al., 2002 N.M. Kelly, G.L. Clarke and C.M. Fanning, A two-stage evolution of the Neoproterozoic Rayner structural episode: new U–Pb sensitive high resolution ion microprobe constraints from the Oygarden Group, Kemp Land, East Antarctica. *Precambrian Res.*, **116** (2002), pp. 307–330.

Kinny et al., 1990 P.D. Kinny, J.R. Wijbrans, D.O. Froude, I.S. Williams and W. Compston, Age constraints on the geological evolution of the Narryer Gneiss Complex, Western Australia. *Aust. J. Earth Sci.*, **37** (1990), pp. 51–69.

Konopelko et al., 2007 D. Konopelko, G. Biske, R. Seltmann, O. Eklund and B. Belyatsky, Hercynian post-collisional A-type granites of the Kokshaal Range, Southern Tien Shan, Kyrgyzstan. *Lithos*, **97** (2007), pp. 140–160.

Konopelko et al., 2009 D. Konopelko, R. Seltmann, G. Biske, E. Lepekhina and S. Sergeev, Possible source dichotomy of contemporaneous post-collisional barren I-type versus tin-bearing A-type granites, lying on opposite sides of the South Tien Shan suture. *Ore Geol. Rev.*, **35** (2009), pp. 206–216.

Kostitsyn et al., 2009 Y.A. Kostitsyn, E.A. Belousova, N.S. Bortnikov and E.V. Sharkov, Zircons in Gabbroid Formations from the Axial Zone of the Mid-Atlantic Ridge: U–Pb Age

and $^{176}Hf/^{177}Hf$ ratio (results of investigations by the laser ablation method). *Doklady Earth Sci.*, **429** (2009), pp. 1305–1309.

Kroner et al., 2005 A. Kroner, S.A. Wilde, J.H. Li and K.Y. Wang, Age and evolution of a late Archean to early Palaeozoic upper to lower crustal section in the Wutaishan/Hengshan/Fuping terrain of northern China. *J. Asian Earth Sci.*, **24** (2005), pp. 577–595.

Kusky and Santosh, 2009 T.M. Kusky and M. Santosh, The Columbia connection in North China. *Geol. Soc. Spec. Publ.*, **323** (2009), pp. 49–71.

Lei et al., 2011 R.X. Lei, C.Z. Wu, L.X. Gu, Z.Z. Zhang, G.X. Chi and Y.H. Jiang, Zircon U–Pb chronology and Hf isotope of the Xingxingxia granodiorite from the Central Tianshan zone (NW China): Implications for the tectonic evolution of the southern Altaids. *Gondwana Res.*, (2011), p. 010.

Li, 1981 C.Y. Li, Endogenic metallogeny and plate tectonics of China, . *Acta Geol. Sin.*, **55** (1981), pp. 195–204 (in Chinese with English abstract).

Li et al., 2001 Q. Li, H.F. Yu and Q.Y. Xiu, On the Precambrian basement of the eastern Tianshan mountains, Xinjiang, . *Xinjiang Geol.*, **20** 4 (2001), pp. 346–351 (in Chinese with English abstract).

Li et al., 2003a Z.X. Li, X.H. Li, P.D. Kinny, J. Wang, S. Zhang and H. Zhou, Geochronology of Neoproterozoic syn-rift magmatism in the Yangtze Craton, South China and correlations with other continents: evidence for a mantle superplume that broke up Rodinia. *Precambian Res.*, **122** (2003), pp. 85–109.

Li et al., 2003b X.H. Li, Z.X. Li, W.C. Ge, H.W. Zhou, W.X. Li, Y. Liu and M.T.D. Wingate, Neoproterozoic granitoids in South China: crustal melting above a mantle plume at ca. 825 Ma?. *Precambrian Res.*, **122** (2003), pp. 45–83.

Li et al., 2008 Z.X. Li, S.V. Bogdanova, A.S. Collins, A. Davidson, B. De Waele, R.E. Ernst, I.C.W. Fitzsimons, R.A. Fuck, D.P. Gladkochub, J. Jacobs, K.E. Karlstrom, L.M. Natapovm, S. Lu, L.M. Natapov, V. Pease, S.A. Pisarevsky, K. Thrane and V. Vernikovsky, Assembly, configuration, and break-up history of Rodinia: a synthesis. *Precambrian Res.*, **160** (2008), pp. 179–210.

Liou et al., 1996 J.G. Liou, S.A. Graham, S. Maruyama and R.Y. Zhang, Characteristics and tectonic significance of the late Proterozoic Aksu blueschists and diabasic dikes northwest Xinjiang, China. *Int. Geol. Rev.*, **38** (1996), pp. 228–244.

Liu et al., 2004 S.W. Liu, Z.J. Guo, Z.C. Zhang, Q.G. Li and H.F. Zheng, Nature of Precambrian metamorphic blocks in eastern segment of the Central Tianshan: constraints from geochronology and Nd geochemistry. *Sci. China Ser. D Earth Sci.*, **47** (2004), pp. 1085–1094.

Long et al., 2010 X.P. Long, C. Yuan, M. Sun, G.C. Zhao, W.J. Xiao, Y.J. Wang, Y.H. Yang and A.Q. Hu, Archean crustal evolution of the northern Tarim craton, NW China: Zircon U–Pb and Hf isotopic constraints. *Precambrian Res.*, **180** (2010), pp. 272–284.

Long et al., 2011a X.P. Long, C. Yuan, M. Sun, A. Kröner, G.C. Zhao, S.A. Wilde and A.Q. Hu, Reworking of the Tarim Craton by underplating of mantle plume-derived magmas: evidence from Neoproterozoic adakitic rocks and I-type granites in the Kuluketage area, NW China. *Precambrian Res.*, **187** (2011), pp. 1–14.

Long et al., 2011b X.P. Long, C. Yuan, M. Sun, W.J. Xiao, G.C. Zhao, K.F. Zhou, Y.J. Wang and A.Q. Hu, The discovery of the oldest rocks in the Kuluketage area and its geological implications. *Sci. China Ser. D Earth Sci.*, **54** (2011), pp. 342–348.

Lu, 1992 Lu, S.N., 1992. Geological evolution of Proterozoic in Kuruktage, Xinjiang. Bulletin of the Tianjin Institute of Geology and Mineral Resources, CAGS, No. 26–27, pp. 279–292 (in Chinese)..

Lu and Yuan, 2003 S.N. Lu and G.B. Yuan, Geochronology of early Precambrian magmatic activities in Aketasdhtage, east Altyn tagh, . *Acta Geol. Sin.*, **77** (2003), pp. 61–68 (in Chinese with English abstract).

Lu et al., 2008a S.N. Lu, H.K. Li, C.L. Zhang and G.H. Liu, Geological and geochronological evidence for the Precambrian evolution of the Tarim Craton and surrounding continental fragments. *Precambrian Res.*, **160** (2008), pp. 94–107.

Lu et al., 2008b S.N. Lu, G.C. Zhao, H.C. Wang and G.J. Hao, Precambrian metamorphic basement and sedimentary cover of the North China Craton: Review. *Precambrian Res.*, **160** (2008), pp. 77–93.

Ludwig, 2001 K.R. Ludwig, Berkeley Geochronology Center (2001), p. 55, (special publication).

Luo, 1989 F.Z. Luo, On Precambrian of Mid-Tianshan uplift (metamorphic) zone, . *Xinjiang Geol.*, **7** (1989), pp. 24–33 (in Chinese).

Maas et al., 1992 R. Maas, P.D. Kinny, I.S. Williams, D.O. Froude and W. Compston, The Earth's oldest known crust: a geochronological and geochemical study of 3900–4200 Ma old detrital zircons from Mt. Narryer and Jack Hills, Western Australia. *Geochim. Cosmochim. Acta*, **56** (1992), pp. 1281–1300.

Mishra et al., 1999 S. Mishra, M.P. Deomurari, M. Wiedenbeck, J.N. Goswami, S. Ray and A.K. Saha, $^{207}Pb/^{206}Pb$ zircons ages and the evolution of the Singhbhum Craton, eastern India: an ion microprobe study. *Precambrian Res.*, **93** (1999), pp. 139–151.

Mondal et al., 2002 M.E.A. Mondal, J.N. Goswami, M.P. Deomurari and K.K. Sharma, Ion microprobe $^{207}Pb/^{206}Pb$ ages of zircons from the Bundelkhand massif, Northern India: implications for crustal evolution of the Bundelkhand-Aravalli protocontinent. *Precambrian Res.*, **117** (2002), pp. 85–100.

Park et al., 1995 J.K. Park, K.L. Buchan and S.S. Harlan, A proposed giant radiating dyke swarm fragmented by the separation of Laurentia and Australia based on paleomagnetism of ca. 780 Mamafic intrusions in western North America. *Earth Planet. Sci. Lett.*, **132** (1995), pp. 129–139.

Pirajno et al., 2008 F. Pirajno, J.W. Mao, Z.C. Zhang, Z.H. Zhang and F.M. Chai, The association of mafic-ultramafic intrusions and A-type magmatism in the Tian Shan and Altay orogens, NW China: implications for geodynamic evolution and potential for the discovery of new ore deposits. *J. Asian Earth Sci.*, **32** (2008), pp. 165–183.

Qian et al., 2009 Q. Qian, J. Gao, R. Klemd, G.Q. He, B. Song, D.Y. Liu and R.H. Xu, Early Paleozoic tectonic evolution of the Chinese South Tianshan Orogen: constraints from SHRIMP zircon U–Pb geochronology and geochemistry of basaltic and dioritic rocks from Xiate, NW China. *Int. J. Earth Sci.*, **98** (2009), pp. 551–569.

Qiu et al., 2000 Y.M. Qiu, S. Gao, N.J. McNaughton, D.I. Groves and W.L. Ling, First evidence of >3.2 Ga continental crust in the Yangtze craton of South China and its implications for Archean crustal evolution and Phanerozoic tectonics. *Geology*, **28** (2000), pp. 11–14.

Ren et al., 2011 R. Ren, B.F. Han, J.Q. Ji, L. Zhang, Z. Xu and L. Su, U–Pb age of detrital zircons from the Tekes River, Xinjiang, China, and implications for tectonomagmatic evolution of the South Tian Shan Orogen. *Gondwana Res.*, **19** (2011), pp. 460–470.

Richards et al., 1989 M.A. Richards, R.A. Duncan and V.E. Courtillot, Flood basalts and hotspot tracks: Plume heads and tails. *Science*, **246** (1989), pp. 103–107.

Rino et al., 2004 S. Rino, T. Komiya, B.F. Windley, I. Katayama, A. Motoki and T. Hirata, Major episodic increases of continental crustal growth determined from zircon ages of river sands: implications for mantle overturns in the early Precambrian. *Phys. Earth Planet. Interiors*, **146** (2004), pp. 369–394.

Rino et al., 2008 S. Rino, Y. Kon, W. Sato, S. Maruyama, M. Santosh and D. Zhao, The Grenvillian and Pan-African orogens: world's largest orogenies through geologic time, and their implications on the origin of superplume. *Gondwana Res.*, **14** 1-2 (2008), pp. 51–72.

Rogers and Santosh, 2002 J.J.W. Rogers and M. Santosh, Configuration of Columbia, a Mesoproterozoic Supercontinent. *Gondwana Res.*, **5** (2002), pp. 5–22.

Rogers and Santosh, 2003 J.J.W. Rogers and M. Santosh, Supercontinents in Earth History. *Gondwana Res.*, **6** 3 (2003), pp. 357–368.

Rogers and Santosh, 2004 J.J.W. Rogers and M. Santosh, Continents and Supercontinents, Oxford University Press (2004), p. 289.

Rogers and Santosh, 2009 J.J.W. Rogers and M. Santosh, Tectonics and surface effects of the supercontinent Columbia. *Gondwana Res.*, **15** (2009), pp. 373–380.

Rubatto, 2002 D. Rubatto, Zircon trace element geochemistry: partitioning with garnet and the link between U–Pb ages and metamorphism. *Chem. Geol.*, **184** (2002), pp. 123–138.

Santosh et al., 2004 M. Santosh, K. Yokoyama and S.K. Acharyya, Geochronology and tectonic evolution of Karimnagar and Bhopalpatnam granulite belts, central India. *Gondwana Res.*, **7** (2004), pp. 501–518.

Santosh et al., 2006 M. Santosh, K. Sajeev and J.H. Li, Extreme crustal metamorphism during Columbia supercontinent assembly: evidence from North China Craton. *Gondwana Res.*, **10** (2006), pp. 256–266.

Santosh, 2010 M. Santosh, Assembling North China Craton within the Columbia supercontinent: the role of double-sided subduction. *Precambrian Res.*, **178** (2010), pp. 149–167.

Schaltegger et al., 1999 U. Schaltegger, C.M. Fanning, D. Günther, J.C. Maurin, K. Schulmann and D. Gebauer, Growth, annealing and recrystallization of zircon and preservation of monazite in high-grade metamorphism: conventional and in-situ U–Pb isotope, cathodoluminescence and microchemical evidence. *Contrib. Miner. Petrol.*, **134** (1999), pp. 186–201.

Scherer et al., 2001 E. Scherer, C. Munker and K. Mezger, Calibration of the Lutetium–Hafnium clock. *Science*, **293** (2001), pp. 683–687.

Sengör et al., 1993 A.M.C. Sengör, B.A. Natalin and V.S. Burtman, Evolution of the Altaid tectonic collage and Paleozoic crustal growth in Eurasia. *Nature*, **364** (1993), pp. 299–307. |

Shu et al., 2002 L.S. Shu, J. Charvet, H.F. Lu and S. Laurent-Charvet, Paleozoic accretion–collision events and kinematics of ductile deformation in the eastern part of the Southern-Central Tianshan Belt, China. *Acta Geol. Sin.*, **76** (2002), pp. 308–323.

Shu et al., 2004 L.S. Shu, J.H. Yu, J. Charvet, S. Laurent-Charvet, H.Q. Sang and R.G. Zhang, Geological, geochronological and geochemical features of granulites in the Eastern Tianshan, NW China. *J. Asian Earth Sci.*, **24** (2004), pp. 25–41.

Shu et al., 2010 L.S. Shu, X.L. Deng, W.B. Zhu, D.S. Ma and W.J. Xiao, Precambrian tectonic evolution of the Tarim Block, NW China: New geochronological insights from the Quruqtagh domain. *J. Asian Earth Sci.*, (2010).

Shu et al., 2011 L.S. Shu, M. Faure, J.H. Yu and B.M. Jahn, Geochronological and geochemical features of the Cathaysia block (South China): new evidence for the Neoproterozoic breakup of Rodinia. *Precambrian Res.*, **187** (2011), pp. 263–276.

Sun et al., 2009 W.H. Sun, M.F. Zhou, J.F. Gao, Y.H. Yang, X.F. Zhao and J.H. Zhao, Detrital zircon U–Pb geochronological and Lu–Hf isotopic constraints on the Precambrian magmatic and crustal evolution of the western Yangtze Block, SW China. *Precambrian Res.*, **172** (2009), pp. 99–126.

Tarney, 1992 J. Tarney, Geochemistry and significance of mafic dyke swarms in the Proterozoic, K.C. Condie, Editor, *Proterozoic Crustal Evolution*, Elsevier, Amsterdam (1992), pp. 151–179.

Turner, 2010 S.A. Turner, Sedimentary record of Late Neoproterozoic rifting in the NW Tarim Basin, China. *Precambrian Res.*, **181** (2010), pp. 85–96.

Veevers et al., 2005 J.J. Veevers, A. Saeed, E.A. Belousova and W.L. Griffin, U–Pb ages and source composition by Hf-isotope and trace-element analysis of detrital zircons in Permian

sandstone and modern sand from Southwestern Australia and a review of the paleogeographical and denudational history of the Yilgarn Craton. *Earth Sci. Rev.*, **68** (2005), pp. 245–279.

Vervoort et al., 1999 J.D. Vervoort, P.J. Patchett, J. Blichert-Toft and F. Albarède, Relationships between Lu–Hf and Sm–Nd isotopic systems in the global sedimentary system. *Earth Planet. Sci. Lett.*, **168** (1999), pp. 79–99.

Wang et al., 2007 B. Wang, Y. Chen, S. Zhan, L.S. Shu, M. Faure, D. Cluzel, J. Charvet and S. Laurent-Charvet, Primary Carboniferous and Permian palaeomagnetic results from the Yili Block (NW China) and their implications on the geodynamic evolution of Chinese Tianshan Belt. *Earth Planet. Sci. Lett.*, **263** (2007), pp. 288–308.

Wang et al., 2008 B. Wang, M. Faure, L.S. Shu, D. Cluzel, J. Charvet, K. de Jong and Y. Chen, Paleozoic tectonic evolution of the Yili Block, Western Chinese Tianshan. *Bull. Soc. Géol. France*, **179** (2008), pp. 483–490.

Wang et al., 2011 B. Wang, L.S. Shu, M. Faure, B.M. Jahn, D. Cluzel, J. Charvet, S.L. Chung and S. Meffre, Paleozoic tectonics of the southern Chinese Tianshan: insights from structural, chronological and geochemical studies of the Heiyingshan ophiolitic melange (NW China). *Tectonophysics*, **497** (2011), pp. 85–104.

Wang et al., 2010a L.J. Wang, W.L. Griffin, J.H. Yu and S.Y. O'Reilly, Precambrian crustal evolution of the Yangtze Block tracked by detrital zircons from Neoproterozoic sedimentary rocks. *Precambrian Res.*, **177** (2010), pp. 131–144.

Wang et al., 2010b X.L. Wang, S.Y. Jiang and B.Z. Dai, Melting of enriched Archean subcontinental lithospheric mantle: Evidence from the ca. 1760 Ma volcanic rocks of the Xiong'er Group, southern margin of the North China Craton. *Precambrian Res.*, **182** (2010), pp. 204–216.

Whitehouse and Platt, 2003 M.J. Whitehouse and J.P. Platt, Dating high-grade metamorphism constraints from rare-earth elements in zircons and garnet. *Contrib. Mineral. Petrol.*, **145** (2003), pp. 61–74.

Wilde et al., 2002 S.A. Wilde, G.C. Zhao and M. Sun, Development of the North China Craton during the Late Archaean and its final amalgamation at 1.8 Ga; some speculations on its position within a global Palaeoproterozoic supercontinent. *Gondwana Res.*, **5** (2002), pp. 85–94.

Wilde and Zhao, 2005 S.A. Wilde and G.C. Zhao, Archean to Paleoproterozoic evolution of the North China Craton. *J. Asian Earth Sci.*, **24** (2005), pp. 519–522.

Windley et al., 1990 B.F. Windley, M.B. Allen, C. Zhang, Z.Y. Zhao and G.R. Wang, Paleozoic accretion and Cenozoic red formation of the Chinese Tianshan range, central Asia. *Geology*, **18** (1990), pp. 128–131.

Windley, 1993 B.F. Windley, Proterozoic anorogenic magmatism and its orogenic connections. *J. Geol. Soc. Lond.*, **150** (1993), pp. 39–50

Windley et al., 2007 B.F. Windley, D. Alexeiev, W.J. Xiao, A. Kroner and G. Badarch, Tectonic models for accretion of the central Asian orogenic belt. *J. Geol. Soc. Lond.*, **164** (2007), pp. 31–47.

Wingate et al., 1998 M.T.D. Wingate, I.H. Campbell, W. Compston and G.M. Gibson, Ion microprobe U–Pb ages for Neoproterozoic basaltic magmatism in south-central Australia and implications for the breakup of Rodinia. *Precambrian Res.*, **87** (1998), pp. 135–159.

Xiang and Shu, 2010 L. Xiang and L.S. Shu, Pre-Devonian tectonic evolution of the eastern South China Block: Geochronological evidence from detrital zircons. *Sci. China Ser. D Earth Sci.*, **53** (2010), pp. 1427–1444.

Xiao et al., 2002 W.J. Xiao, B.F. Windley, H.L. Chen, G.C. Zhang and J.L. Li, Carboniferous–Triassic subduction and accretion in the Western Kunlun, China: implications for the collisional and accretionary tectonics of the Northern Tibetan Plateau. *Geology*, **30** 4 (2002), pp. 295–298.

Xiao et al., 2003 W.J. Xiao, F.L. Han, B.F. Windley, C. Yuan, H. Zhou and J.L. Li, Multiple accretionary orogenesis and episodic growth of continents: insights from the Western Kunlun Range, Central Asia. *Int. Geol. Rev.*, **45** (2003), pp. 303–328.

Xiao et al., 200 W.J. Xiao, C.M. Han, C. Yuan, M. Sun, S.F. Lin, H.L. Chen, Z.L. Li, J.L. Li and S. Sun, Middle Cambrian to Permian subduction-related accretionary orogenesis of Northern Xinjiang, NW China: implications for the tectonic evolution of central Asia. *J. Asian Earth Sci.*, **32** (2008), pp. 102–117.

Xiao and Kusky, 2009 W.J. Xiao and T. Kusky, Geodynamic processes and metallogenesis of the Central Asian and related orogenic belts: introduction. *Gondwana Res.*, **16** (2009), pp. 167–169.

XBGMR, 1993 XBGMR (Xinjiang Bureau of Geology and Mineral Resources), Regional Geology of Xinjiang Uygur Autonomous Region, Geol. Publ. House, Beijing (1993), pp. 11–125, (in Chinese).

XBGMR, 1999 XBGMR (Xinjiang Bureau of Geology and Mineral Resources), Stratigraphy of Xinjiang Uygur Autonomous Region, China University of Geosciences Press, Wuhan (1999), pp. 2–19 (in Chinese).

Xu et al., 2003 B. Xu, H.F. Zheng, H.T. Yao and Y.A. Li, C-isotope composition and significance of the Sinian on the Tarim plate. *Chin. Sci. Bull.*, **48** 4 (2003), pp. 385–389.

Xu et al., 2005 B. Xu, P. Jian, H.F. Zheng, H.B. Zou, L.F. Zhang and D.Y. Liu, U–Pb zircon geochronology and geochemistry of Neoproterozoic volcanic rocks in the Tarim Block of northwest China: implications for the break-up of Rodinia supercontinent and Neoproterozoic glaciations. *Precambrian Res.*, **136** 2 (2005), pp. 107–123.

Xu et al., 2009 B. Xu, S.H. Xiao, H.B. Zou, Y. Chen, Z.X. Li, B. Song, D.Y. Liu, C.M. Zhou and X.L. Yuan, SHRIMP zircon U–Pb age constraints on Neoproterozoic Quruqtagh diamictites in NW China. *Precambrian Res.*, **168** (2009), pp. 247–258.

Yang and Zhou, 2009 S.H. Yang and M.F. Zhou, Geochemistry of the ~430-Ma Jingbulake mafic-ultramafic intrusion in Western Xinjiang, NW China: implications for subduction related magmatism in the South Tianshan orogenic belt. *Lithos*, **113** (2009), pp. 259–273.

Yang et al., 2007 T.N. Yang, Y. Wang, J.Y. Li and G.H. Sun, Vertical and horizontal strain partitioning of the Central Tianshan (NW China): evidence from structures and $^{40}Ar/^{39}Ar$ geochronology. *J. Struct. Geol.*, **29** (2007), pp. 1605–1621.

Yao et al., 2011 J.L. Yao, L.S. Shu and M. Santosh, Detrital zircon U–Pb geochronology, Hf-isotopes and geochemistry-New clues for the Precambrian crustal evolution of Cathaysia Block, South China. *Gondwana Res.*, (2011).

Yu et al., 2008 J.H. Yu, S.Y. O'Reilly, L.J. Wang, W.L. Griffin, M. Zhang, R.C. Wang, S.Y. Jiang and L.S. Shu, Where was South China in the Rodinia supercontinent? Evidence from U–Pb geochronology and Hf isotopes of detrital zircons. *Precambrian Res.*, **164** (2008), pp. 1–15.

Yu et al., 2010 J.H. Yu, S.Y. O'Reilly, L.J. Wang, W.L. Griffin, M.F. Zhou, M. Zhang and L.S. Shu, Components and episodic growth of Precambrian crust in the Cathaysia Block, South China: Evidence from U–Pb ages and Hf isotopes of zircons in Neoproterozoic sediments. *Precambrian Res.*, **181** (2010), pp. 97–114.

Yuan et al., 2008 H.L. Yuan, S. Gao, M.N. Dai, C.L. Zong, D. Günther, G.H. Fontaine, X.M. Liu and C.R. Di Wu, Simultaneous determinations of U–Pb age, Hf isotopes and trace element compositions of zircon by excimer laser ablation quadrupole and multiple collector ICP-MS. *Chem. Geol.*, **247** 1-2 (2008), pp. 100–118.

Zhang et al., 2006 C.L. Zhang, Z.X. Li, X.H. Li, A.G. Wang and K.Y. Guo, Neoproterozoic bimodal intrusive complex in southwestern Tarim block, Northwest China: age, geochemistry, and implications for the rifting of Rodinia. *Int. Geol. Rev.*, **48** (2006), pp. 112–128.

Zhang et al., 2007a C.L. Zhang, X.H. Li, Z.X. Li, S.N. Lu, H.M. Ye and H.M. Li, Neoproterozoic ultramafic-mafic-carbonatite complex and granitoids in Quruqtagh of northeastern Tarim Block, western China: geochronology, geochemistry and tectonic implications. *Precambrian Res.*, **152** (2007), pp. 149–169.

Zhang et al., 2007b C.L. Zhang, Z.X. Li, X.H. Li, H.F. Yu and H.M. Ye, An early Palaeoproterozoic high-K intrusive complex in southwestern Tarim Block, NW China: age, geochemistry, and tectonic implications. *Gondwana Res.*, **12** (2007), pp. 101–112.

Zhang et al., 2007c C.L. Zhang, S.N. Lu, H.F. Yu and H.M. Ye, Tectonic evolution of the Western Kunlun orogenic belt in northern Qinghai-Tibet Plateau: evidence from zircon SHRIMP and LA-ICP-MS U–Pb geochronology. *Sci. China Ser. D Earth Sci.*, **50** 6 (2007), pp. 825–835.

Zhang et al., 2009a C.L. Zhang, Z.X. Li, X.H. Li and H.M. Ye, Neoproterozoic mafic dyke swarms at the northern margin of the Tarim Block, NW China: age, geochemistry, petrogenesis and tectonic implications. *J. Asian Earth Sci.*, **35** (2009), pp. 167–179.

Zhang et al., 2010a C.L. Zhang, Z.X. Li, X.H. Li, Y.G. Xu, G. Zhou and H.M. Ye, A Permian large igneous province in Tarim and Central Asian orogenic belt, NW China: results of a ca. 275 Ma mantle plume?. *Geol. Soc. Am. Bull.*, **122** (2010), pp. 2020–2040.

Zhang et al., 2010b C.L. Zhang, Y.G. Xu, Z.X. Li, H.Y. Wang and H.M. Ye, Diverse Permian magmatism in the Tarim Block, NW China: genetically linked to the Permian Tarim mantle plume?. *Lithos*, **119** (2010), pp. 537–552.

Zhang et al., 2011 C.L. Zhang, D.S. Yang, H.Y. Wang, Y. Takahashi and H.M. Ye, Neoproterozoic mafic-ultramafic layered intrusion in Quruqtagh of northeastern Tarim Block, NW China: two phases of mafic igneous activity with different mantle sources. *Gondwana Res.*, **19** (2011), pp. 177–190.

Zhang et al., 2009b Z.Y. Zhang, W.B. Zhu, L.S. Shu, J.B. Su and B.H. Zheng, Neoproterozoic ages of the Kuluketage diabase dyke swarm in Tarim, NW China, and its relationship to the breakup of Rodinia. *Geol. Mag.*, **146** 1 (2009), pp. 150–154.

Zhao and Cawood, 1999 G.C. Zhao and P.A. Cawood, Tectonothermal evolution of the Mayuan assemblage in the Cathaysia Block: new evidence for Neoproterozoic collisional-related assembly of the South China craton. *Am. J. Sci.*, **299** (1999), pp. 309–339.

Zhao, 2001 G.C. Zhao, Paleoproterozoic assembly of the North China Craton. *Geol. Mag.*, **138** (2001), pp. 87–91.

Zhao et al., 2001 G.C. Zhao, S.A. Wilde, P.A. Cawood and M. Sun, Archean blocks and their boundaries in the North China Craton: lithological, geochemical, structural and P–T path constraints and tectonic evolution. *Precambrian Res.*, **107** (2001), pp. 45–73.

Zhao et al., 2002a G.C. Zhao, S.A. Wilde, P.A. Cawood and M. Sun, SHRIMP U–Pb zircon ages of the Fuping complex: implications for accretion and assembly of the North China Craton. *Am. J. Sci.*, **302** (2002), pp. 191–226.

Zhao et al., 2002b G.C. Zhao, P.A. Cawood, S.A. Wilde and M. Sun, Review of global 2.1–1.8 Ga orogens: implications for a pre-Rodinia supercontinent. *Earth Sci. Rev.*, **59** (2002), pp. 125–162.

Zhao et al., 2002c G.C. Zhao, M. Sun and S.A. Wilde, Reconstruction of a pre-Rodinia Supercontinent: new advances and perspectives. *Chin. Sci. Bull.*, **47** (2002), pp. 1585–1588.

Zhao et al., 2003 G.C. Zhao, M. Sun, S.A. Wilde and S.Z. Li, Assembly, accreation and breakup of the Paleo-Mesoproterozoic Columbia supercontinent: records in the North China Craton. *Gondwana Res.*, **6** (2003), pp. 417–434.

Zhao et al., 2004 G.C. Zhao, M. Sun, S.A. Wilde and S.Z. Li, A Paleo-Mesoproterozoic supercontinent: assembly, growth, and breakup. *Earth Sci. Rev.*, **67** (2004), pp. 91–123.

Zhao et al., 2005 G.C. Zhao, M. Sun, S.A. Wilde and S.Z. Li, Late Archean to Paleoproterozoic evolution of the North China Craton: key issues revisited. *Precambrian Res.*, **136** (2005), pp. 177–202.

Zhao et al., 2006 G.C. Zhao, M. Sun, S.A. Wilde, S.Z. Li and J. Zhang, Some key issues in reconstructions of Proterozoic supercontinents. *J. Asian Earth Sci.*, **28** (2006), pp. 3–19.

Zhao et al., 2008 G.C. Zhao, S.A. Wilde, M. Sun, J.H. Guo, A. Kroner, S.Z. Li, X.P. Li and C.M. Wu, SHRIMP U–Pb zircon geochronology of the Huai'an complex: constraints on Late Archean to Paleoproterozoic custal accretion and collision of the Trans-North China Orogen. *Am. J. Sci.*, **308** (2008), pp. 270–303

Zhao et al., 2009 G.C. Zhao, Y. He and M. Sun, The Xiong'er volcanic belt at the southern margin of the North China Craton: petrographic and geochemical evidence for its outboard position in the Paleo-Mesoproterozoic Columbia Supercontinent. *Gondwana Res.*, **16** (2009), pp. 170–181.

Zhao et al., 2010 G.C. Zhao, S.A. Wilde, J.H. Guo, P.A. Cawood, M. Sun and X.P. Li, Single zircon grains record two continental collisional events in the North China craton. *Precambrian Res.*, **177** (2010), pp. 266–276.

Zhu et al., 2004 W.B. Zhu, L.S. Shu, R.S. Ma and Y. Sun, Comment on character-characteristics and dynamic origin of the large-scale Jiaoluotage ductile compressional zone in the eastern Tianshan Mountains, China by X.W. Xu, T.L. Ma, L.Q. Sun and X.P. Cai. *J. Struct. Geol.*, **26** (2004), pp. 2331–2335.

Zhu et al., 2008 W.B. Zhu, Z.Y. Zhang, L.S. Shu, H.F. Lu, J.B. Su and W. Yang, SHRIMP U–Pb zircon geochronology of Neoproterozoic Korla mafic dykes in the northern Tarim Block, NW China: implications for the long lasting break-up process of Rodinia. *J. Geol. Soc. Lond.*, **165** (2008), pp. 887–890.

Zhu et al., 2010 W.B. Zhu, Z.Y. Zhang, L.S. Shu, J.L. Wan, H.F. Lu, S.L. Wang, W. Yang and J.B. Su, Thermotectonic evolution of Precambrian basement rocks of the Kuruktag uplift, NE Tarim craton, China: evidence from apatite fission-track data. *Int. Geol. Rev*, **52** (2010), pp. 941–954.

Zhu et al., 2011a W.B. Zhu, B.H. Zheng, L.S. Shu, D.S. Ma, H.L. Wu, Y.X. Li, W.T. Huang and J.J. Yu, Neoproterozoic tectonic evolution of the Precambrian Aksu blueschist terrane, northwestern Tarim, China: Insights from LA-ICP-MS zircon U–Pb ages and geochemical data. *Precambrian Res.*, **185** (2011), pp. 215–230.

Zhu et al., 2011b W.B. Zhu, B.H. Zheng, L.S. Shu, D.S. Ma, J.L. Wan, D.W. Zheng, Z.Y. Zhang and X.Q. Zhu, Geochemistry and SHRIMP U–Pb zircon geochronology of the Korla mafic dykes: constrains on the Neoproterozoic continental breakup in the Tarim Block, northwest China. *J. Asian Earth Sci*, (2011).

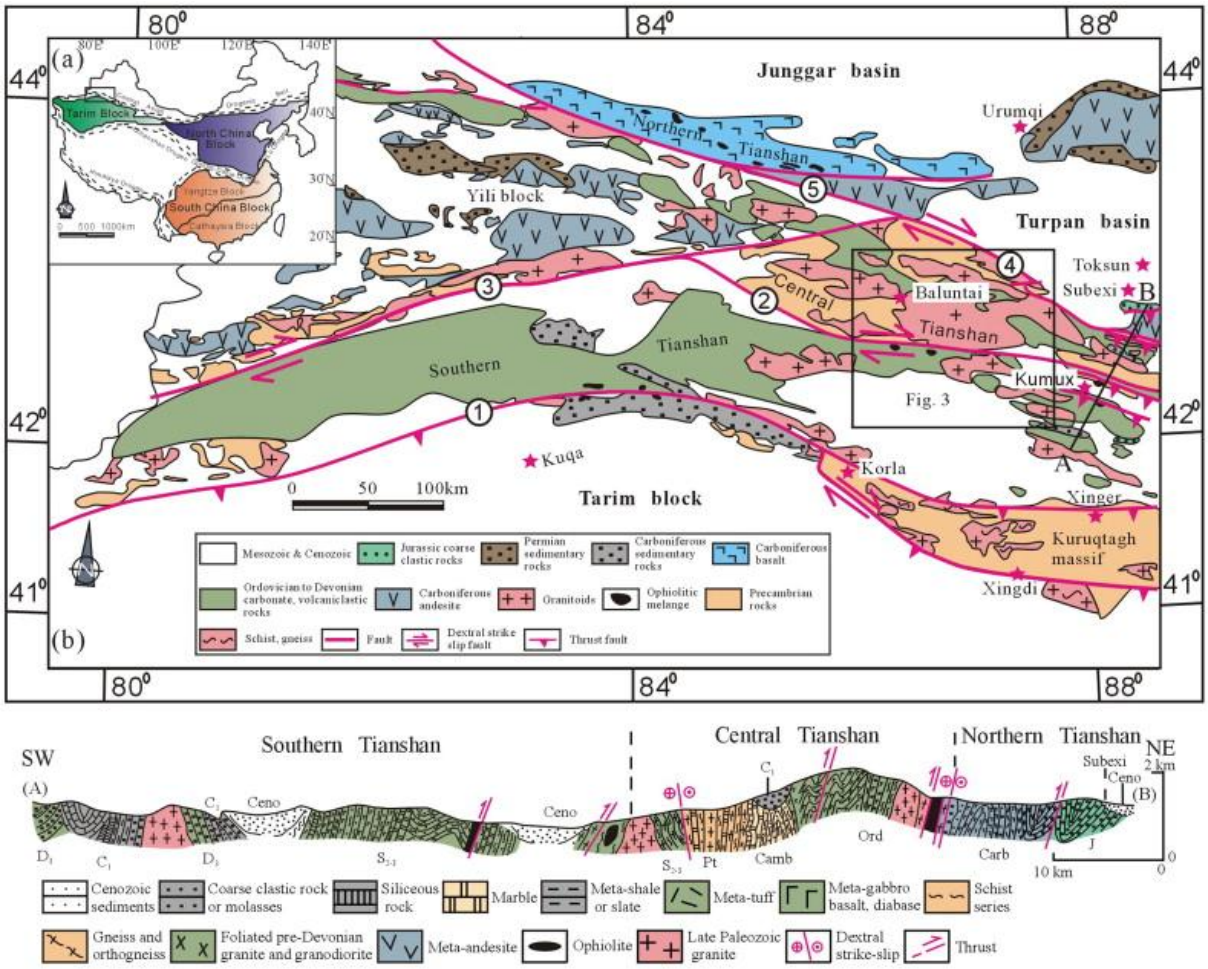

Fig. 1. : Simplified geological map of the Chinese Tianshan belt and cross-section (modified from [Shu et al., 2002] , [Zhao et al., 2005] , [Charvet et al., 2007] and [Wang et al., 2008]). Numbers in circles refer to the main faults: 1, South Tianshan fault (STF); 2, Baluntai fault; 3, Qingbulak-Nalati fault (QNF); 4, Main Tianshan shear zone (MTSZ); 5, North Tianshan fault (NTF).

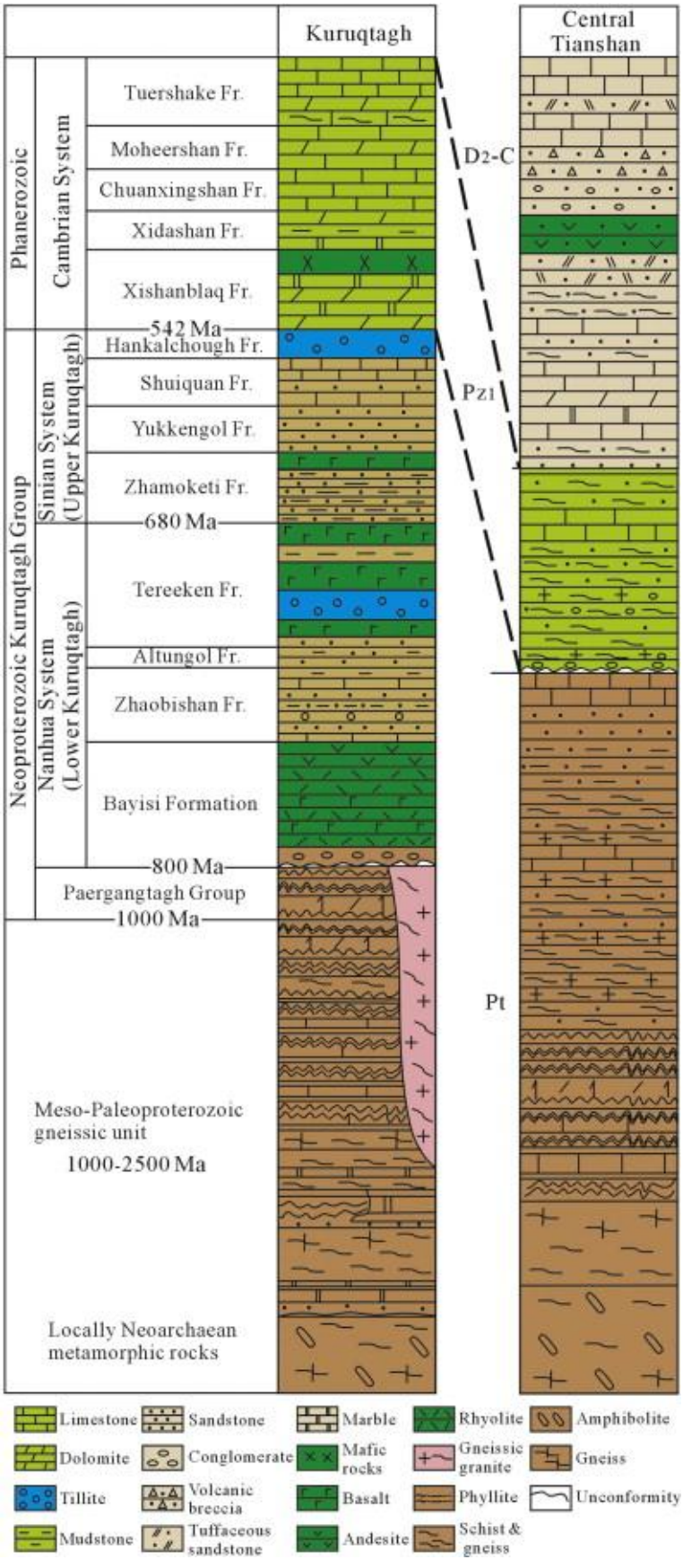

Fig. 2. :Columns of petrological features in both the Tarim Block and the Central Tianshan belt.

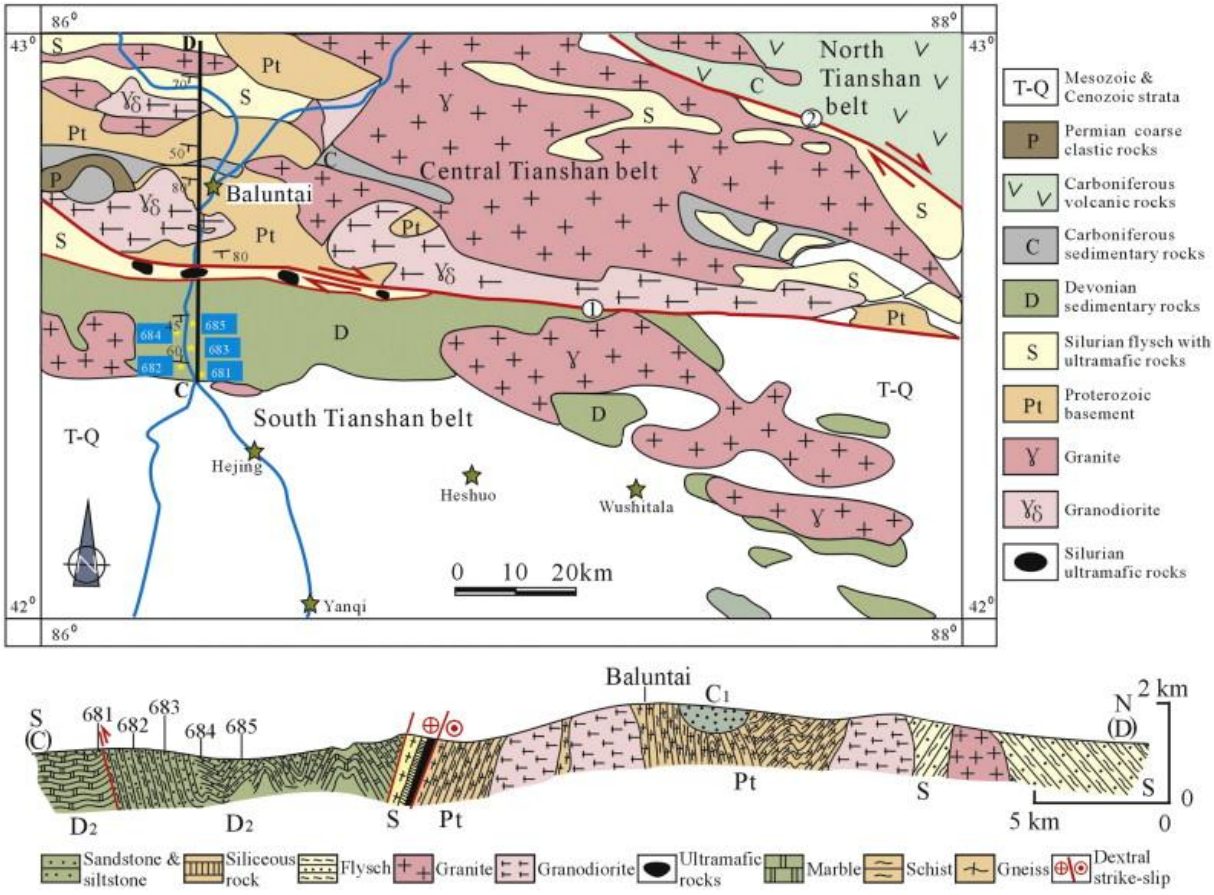

Fig. 3. : Geological map and cross-section of the Baluntai area showing the sampling sites. 1, Baluntai fault; 2, Main Tianshan shear zone.

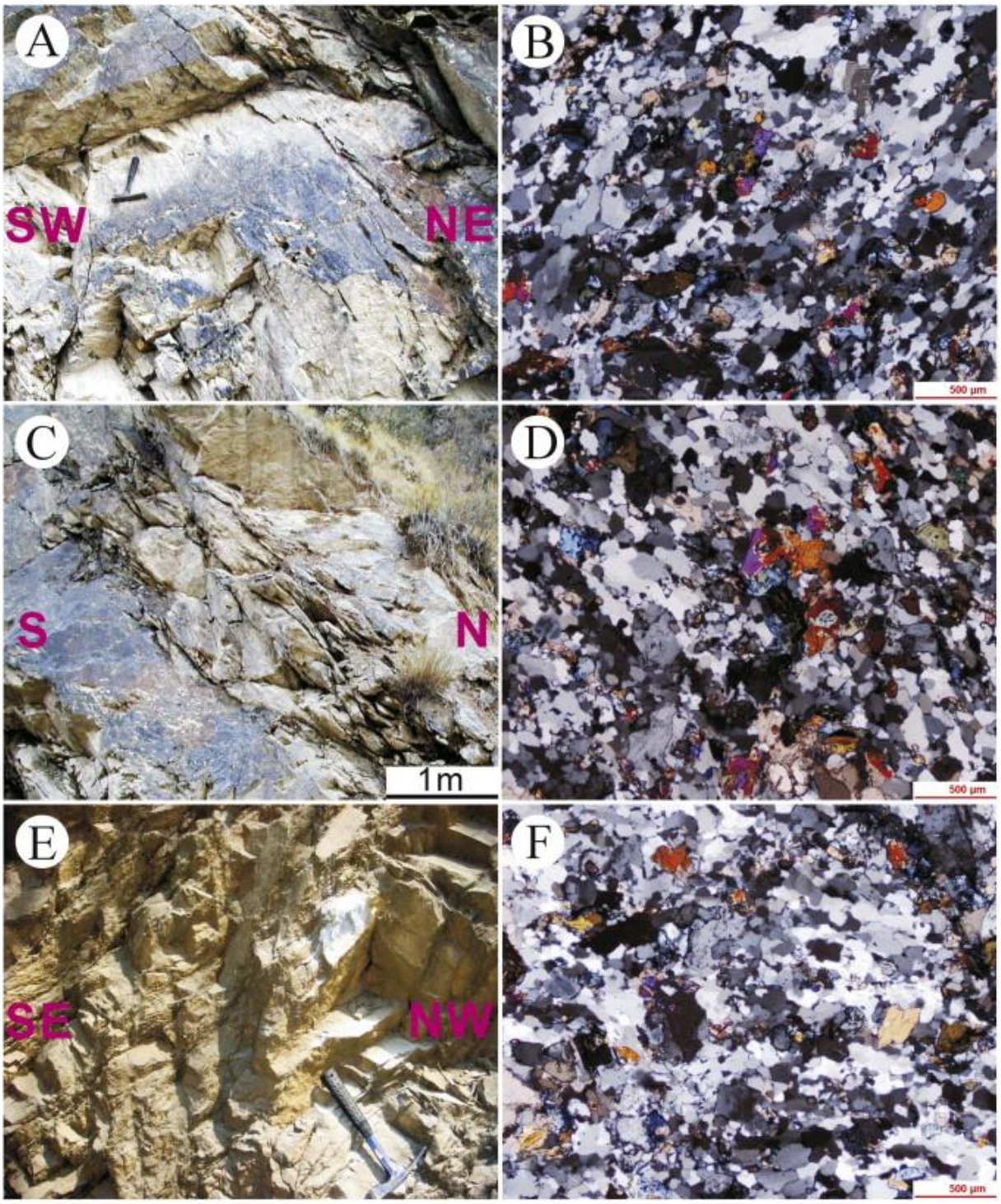

Fig. 4. : Representative field photos along the Baluntai section and the related photomicrographs used for zircon geochronology. (A) Sample 681, Devonian greywacke; (B) photomicrograph (crossed nicols) of sample 681; (C) Sample 682, Devonian greywacke; (D) photomicrograph (crossed nicols) of sample 682; (E) Sample 685, Devonian arkose; (F) photomicrograph (crossed nicols) of sample 685.

Table 1. Petrological features of five dating samples.

Sample	**681**	**682**	**683**	**684**	**685**
Location	Southern Tianshan				
Coordinate	42°27′18.62″N	42°28′10.84″N	42°28′51.31″N	42°29′41.41″N	42°30′12.47″N
	86°14′26.85″E	86°14′02.67″E	86°14′51.45″E	86°14′54.11″E	86°15′48.54″E
Horizon	D2	D2	D2	D2	D2
Texture	Coarse-grained sandy texture	Coarse-grained sandy texture	Coarse-grained sandy texture	Inequigranular sandy texture	Inequigranular sandy texture
Structure	Massive	Massive	Massive	Massive	Massive
Mineralogy	Quartz (70%), rock fragments (15%), feldspar (10%), biotite + epidote (2%); interstitial material: siliceous and little argillaceous (3%)	Quartz (70%), rock fragments (15%), feldspar (10%), biotite + epidote (2%); interstitial material: siliceous and little argillaceous (3%)	Quartz (65%), rock fragments (10%), feldspar (15%), biotite + epidote (5%); interstitial material: siliceous and little calcareous (5%)	Quartz (65%), rock fragments (10%), feldspar (15%), biotite + epidote (5%); interstitial material: siliceous and little calcareous (5%)	Quartz (80%), feldspar (10%), rock fragments (5%); interstitial material: siliceous (5%)
Name	Greywacke sandstone	Greywacke sandstone	Greywacke sandstone	Greywacke sandstone	Arkose

Table 2. U–Pb dating data for zircons from Devonian sandstones.

Spots	Isotopic ratios			Age/Ma			Th (ppm)	U (ppm)	Th/U	Concordance
	$^{207}Pb/^{206}Pb$	$^{207}Pb/^{235}U$	$^{206}Pb/^{238}U$	$^{207}Pb/^{206}Pb$	$^{207}Pb/^{235}U$	$^{206}Pb/^{238}U$				
681 Devonian greywacke from the South of Baluntai										
681-01	0.19306 ± 0.0033	14.07224 ± 0.2675	0.52847 ± 0.00793	2768 ± 14	2755 ± 18	2735 ± 33	110	90	1.22	101
681-02	0.05791 ± 0.00138	0.69402 ± 0.01731	0.08689 ± 0.00134	526 ± 29	535 ± 10	537 ± 8	659	413	1.60	100
681-03	0.07121 ± 0.00194	1.63055 ± 0.04598	0.16594 ± 0.00269	963 ± 32	982 ± 18	990 ± 15	140	252	0.56	99
681-04	0.07452 ± 0.00216	1.90359 ± 0.05642	0.18518 ± 0.00331	1056 ± 32	1082 ± 20	1095 ± 18	217	243	0.89	96
681-05	0.06254 ± 0.00151	1.11473 ± 0.02835	0.12936 ± 0.00211	693 ± 28	760 ± 14	784 ± 12	396	465	0.85	97
681-06	0.07727 ± 0.00258	2.06367 ± 0.06901	0.19387 ± 0.00337	1128 ± 39	1137 ± 23	1142 ± 18	202	112	1.81	99
681-07	0.16664 ± 0.00557	10.85825 ± 0.36479	0.47335 ± 0.00836	2524 ± 33	2511 ± 31	2498 ± 37	258	209	1.24	101
681-08	0.07364 ± 0.00197	1.73921 ± 0.04744	0.17181 ± 0.0028	1032 ± 30	1023 ± 18	1022 ± 15	2465	841	2.93	101
681-09	0.09771 ± 0.006	3.77365 ± 0.22366	0.27997 ± 0.00708	1581 ± 73	1587 ± 48	1591 ± 36	663	461	1.44	99
681-10	0.13003 ± 0.00265	6.92705 ± 0.14948	0.38758 ± 0.00578	2098 ± 19	2102 ± 19	2112 ± 27	390	476	0.82	99
681-11	0.07395 ± 0.00181	1.7927 ± 0.04608	0.17689 ± 0.00311	1040 ± 26	1043 ± 17	1050 ± 17	170	491	0.35	99
681-12	0.0715 ± 0.00394	1.2124 ± 0.06543	0.12321 ± 0.00268	972 ± 75	806 ± 30	749 ± 15	230	119	1.94	108
681-	0.08086	2.30545	0.20767	1218 ±	1214 ±	1216 ±	194	1388	0.14	100

Spots	Isotopic ratios			Age/Ma			Th (ppm)	U (ppm)	Th/U	Concordance
	$^{207}Pb/^{206}Pb$	$^{207}Pb/^{235}U$	$^{206}Pb/^{238}U$	$^{207}Pb/^{206}Pb$	$^{207}Pb/^{235}U$	$^{206}Pb/^{238}U$				
13	± 0.00484	± 0.13496	± 0.00486	78	41	26				
681-14	0.1023 ± 0.00541	4.17697 ± 0.21812	0.29683 ± 0.0066	1666 ± 64	1670 ± 43	1676 ± 33	135	205	0.66	99
681-15	0.07428 ± 0.00629	1.78862 ± 0.14686	0.17466 ± 0.0053	1049 ± 117	1041 ± 53	1038 ± 29	58	74	0.79	101
681-16	0.12753 ± 0.00446	6.52253 ± 0.23292	0.37184 ± 0.00667	2064 ± 38	2049 ± 31	2038 ± 31	1158	2098	0.55	101
681-17	0.08243 ± 0.00212	2.4535 ± 0.06743	0.21608 ± 0.00373	1256 ± 28	1258 ± 20	1261 ± 20	704	3613	0.19	100
681-18	0.10273 ± 0.00493	4.16297 ± 0.19682	0.29412 ± 0.00601	1674 ± 57	1667 ± 39	1662 ± 30	284	339	0.84	101
681-19	0.06142 ± 0.00454	0.80417 ± 0.05785	0.09508 ± 0.00245	654 ± 110	599 ± 33	586 ± 14	434	420	1.04	102
681-20	0.07418 ± 0.00227	1.8099 ± 0.05722	0.17718 ± 0.00308	1046 ± 36	1049 ± 21	1052 ± 17	468	586	0.80	99
681-21	0.06624 ± 0.00854	1.01981 ± 0.12527	0.11204 ± 0.0044	814 ± 193	714 ± 63	685 ± 26	295	506	0.58	104
681-22	0.11174 ± 0.00324	4.78021 ± 0.14011	0.31138 ± 0.00552	1828 ± 29	1781 ± 25	1747 ± 27	305	176	1.74	105
681-23	0.05859 ± 0.00154	0.70111 ± 0.01892	0.08703 ± 0.00141	552 ± 32	539 ± 11	538 ± 8	403	581	0.69	100
681-24	0.06765 ± 0.00094	1.31863 ± 0.02179	0.14138 ± 0.002	858 ± 15	854 ± 10	852 ± 11	176	270	0.65	100
681-25	0.05612 ± 0.00115	0.54832 ± 0.01141	0.07089 ± 0.00096	457 ± 24	444 ± 7	442 ± 6	168	523	0.32	100
681-26	0.10185 ±	4.11458 ±	0.29313 ±	1658 ± 20	1657 ± 18	1657 ± 21	154	133	1.16	100

Spots	Isotopic ratios			Age/Ma			Th (ppm)	U (ppm)	Th/U	Concordance
	$^{207}Pb/^{206}Pb$	$^{207}Pb/^{235}U$	$^{206}Pb/^{238}U$	$^{207}Pb/^{206}Pb$	$^{207}Pb/^{235}U$	$^{206}Pb/^{238}U$				
	0.00218	0.08855	0.00414							
681-27	0.07063 ± 0.00089	1.54223 ± 0.02293	0.15839 ± 0.0021	947 ± 14	947 ± 9	948 ± 12	176	990	0.18	100
681-28	0.06943 ± 0.00097	1.44993 ± 0.02244	0.1515 ± 0.00195	912 ± 14	910 ± 9	909 ± 11	169	304	0.56	100
681-29	0.05544 ± 0.00135	0.53196 ± 0.01299	0.0696 ± 0.00099	430 ± 30	433 ± 9	434 ± 6	250	374	0.67	100
681-30	0.05606 ± 0.00098	0.5669 ± 0.0105	0.07336 ± 0.00098	455 ± 20	456 ± 7	456 ± 6	253	426	0.59	100
681-31	0.07633 ± 0.00158	1.97188 ± 0.04419	0.18738 ± 0.00295	1104 ± 22	1106 ± 15	1107 ± 16	341	539	0.63	100
681-32	0.24044 ± 0.00597	20.71934 ± 0.54391	0.62382 ± 0.0114	3123 ± 21	3126 ± 25	3125 ± 45	152	118	1.29	100
681-33	0.06045 ± 0.01018	0.85716 ± 0.13799	0.10298 ± 0.00578	620 ± 255	629 ± 75	632 ± 34	40	25	1.62	100
681-34	0.22178 ± 0.01404	18.18135 ± 1.12513	0.59304 ± 0.02095	2994 ± 56	2999 ± 60	3002 ± 85	42	33	1.28	100
681-35	0.07468 ± 0.00113	1.64307 ± 0.02814	0.15958 ± 0.00222	1060 ± 16	987 ± 11	954 ± 12	577	718	0.80	103
681-36	0.05592 ± 0.00097	0.55296 ± 0.01017	0.07171 ± 0.00096	449 ± 20	447 ± 7	446 ± 6	403	505	0.80	100
681-37	0.05631 ± 0.001	0.5682 ± 0.0107	0.07319 ± 0.00098	465 ± 20	457 ± 7	455 ± 6	875	583	1.50	100
681-38	0.11455 ± 0.00387	4.48167 ± 0.15123	0.283 ± 0.00578	1873 ± 33	1728 ± 28	1606 ± 29	241	1286	0.19	117
681-39	0.09284 ± 0.00576	3.22662 ± 0.19223	0.25204 ± 0.00714	1485 ± 70	1464 ± 46	1449 ± 37	167	151	1.10	102

Spots	Isotopic ratios			Age/Ma			Th (ppm)	U (ppm)	Th/U	Concordance
	$^{207}Pb/^{206}Pb$	$^{207}Pb/^{235}U$	$^{206}Pb/^{238}U$	$^{207}Pb/^{206}Pb$	$^{207}Pb/^{235}U$	$^{206}Pb/^{238}U$				
681-40	0.11053 ± 0.00058	4.98372 ± 0.06817	0.32553 ± 0.0041	1808 ± 11	1817 ± 12	1817 ± 20	185	420	0.44	100
681-41	0.06409 ± 0.00086	1.09323 ± 0.01741	0.12375 ± 0.00172	745 ± 15	750 ± 8	752 ± 10	755	1031	0.73	100
681-42	0.07082 ± 0.00149	1.55062 ± 0.03331	0.15883 ± 0.00222	952 ± 23	951 ± 13	950 ± 12	194	271	0.72	100
681-43	0.05586 ± 0.00088	0.54665 ± 0.00942	0.07098 ± 0.00095	447 ± 18	443 ± 6	442 ± 6	388	561	0.69	100
681-44	0.0971 ± 0.00129	3.69113 ± 0.05837	0.27575 ± 0.00381	1569 ± 13	1569 ± 13	1570 ± 19	399	337	1.18	100
681-45	0.09423 ± 0.00145	3.43263 ± 0.05898	0.26424 ± 0.00367	1513 ± 15	1512 ± 14	1511 ± 19	124	97	1.28	100
681-46	0.05685 ± 0.00273	0.60329 ± 0.02812	0.07699 ± 0.00147	486 ± 69	479 ± 18	478 ± 9	43	47	0.91	100
681-47	0.08131 ± 0.00271	2.34349 ± 0.08095	0.20904 ± 0.0042	1229 ± 37	1226 ± 25	1224 ± 22	74	1358	0.05	100
681-48	0.07263 ± 0.00159	1.68202 ± 0.03894	0.16794 ± 0.00255	1004 ± 24	1002 ± 15	1001 ± 14	257	205	1.26	100
681-49	0.09575 ± 0.00162	3.56613 ± 0.06948	0.27012 ± 0.00406	1543 ± 17	1542 ± 15	1541 ± 21	172	606	0.28	100
681-50	0.05747 ± 0.00149	0.64503 ± 0.0177	0.08142 ± 0.0015	510 ± 30	505 ± 11	505 ± 9	568	1030	0.55	100
681-51	0.15226 ± 0.00413	6.66709 ± 0.18699	0.31767 ± 0.00565	2371 ± 25	2068 ± 25	1778 ± 28	587	616	0.95	133
681-52	0.11349 ± 0.00169	5.21611 ± 0.08649	0.33336 ± 0.0046	1856 ± 14	1855 ± 14	1855 ± 22	82	52	1.58	100
681-	0.0707 ±	1.51985	0.15593	949 ± 15	938 ±	934 ±	110	222	0.49	100

Spots	Isotopic ratios			Age/Ma			Th (ppm)	U (ppm)	Th/U	Concordance
	$^{207}Pb/^{206}Pb$	$^{207}Pb/^{235}U$	$^{206}Pb/^{238}U$	$^{207}Pb/^{206}Pb$	$^{207}Pb/^{235}U$	$^{206}Pb/^{238}U$				
53	0.00104	± 0.02493	± 0.0021		10	12				
681-54	0.05725 ± 0.00097	0.62719 ± 0.01151	0.07946 ± 0.00109	501 ± 19	494 ± 7	493 ± 7	372	238	1.57	100
681-55	0.09448 ± 0.00248	3.284 ± 0.08686	0.25184 ± 0.00401	1518 ± 27	1477 ± 21	1448 ± 21	21	166	0.13	105
681-56	0.07122 ± 0.00109	1.7069 ± 0.02892	0.17384 ± 0.00235	964 ± 16	1011 ± 11	1033 ± 13	26	1074	0.02	93
681-57	0.06656 ± 0.00231	1.16837 ± 0.07901	0.12836 ± 0.01218	824 ± 96	786 ± 37	779 ± 70	516	1468	0.35	101
681-58	0.1685 ± 0.00475	11.78902 ± 0.33232	0.50646 ± 0.00882	2543 ± 25	2588 ± 26	2641 ± 38	69	69	1.01	96
681-59	0.16225 ± 0.00129	10.53735 ± 0.14676	0.46947 ± 0.00508	2479 ± 11	2483 ± 13	2481 ± 22	153	202	0.76	100
681-60	0.06476 ± 0.00194	1.1218 ± 0.03315	0.12566 ± 0.00197	767 ± 36	764 ± 16	763 ± 11	199	75	2.64	100
681-61	0.20275 ± 0.00677	15.48749 ± 0.52233	0.55398 ± 0.01095	2848 ± 30	2846 ± 32	2842 ± 45	11	464	0.02	100
681-62	0.05699 ± 0.00119	0.60453 ± 0.01291	0.07694 ± 0.00106	491 ± 24	480 ± 8	478 ± 6	171	208	0.82	100
681-63	0.11431 ± 0.00178	5.17649 ± 0.08647	0.32847 ± 0.00437	1869 ± 14	1849 ± 14	1831 ± 21	90	120	0.75	102
681-64	0.16536 ± 0.00281	10.7609 ± 0.19386	0.472 ± 0.00647	2511 ± 14	2503 ± 17	2492 ± 28	188	207	0.91	101
681-65	0.06578 ± 0.00132	1.19381 ± 0.02539	0.13163 ± 0.00194	799 ± 22	798 ± 12	797 ± 11	270	170	1.59	100
681-66	0.07839 ±	2.11334 ±	0.19567 ±	1157 ± 23	1153 ± 16	1152 ± 17	210	175	1.20	100

Spots	Isotopic ratios			Age/Ma			Th (ppm)	U (ppm)	Th/U	Concordance
	$^{207}Pb/^{206}Pb$	$^{207}Pb/^{235}U$	$^{206}Pb/^{238}U$	$^{207}Pb/^{206}Pb$	$^{207}Pb/^{235}U$	$^{206}Pb/^{238}U$				
	0.00176	0.05038	0.00322							
681-67	0.07143 ± 0.00091	1.56946 ± 0.02331	0.15938 ± 0.0021	970 ± 14	958 ± 9	953 ± 12	188	360	0.52	101
681-68	0.08294 ± 0.00242	2.46741 ± 0.07298	0.21649 ± 0.00395	1268 ± 31	1263 ± 21	1263 ± 21	46	107	0.43	100
681-69	0.09533 ± 0.00116	3.50252 ± 0.05046	0.26651 ± 0.00351	1535 ± 12	1528 ± 11	1523 ± 18	142	635	0.22	101
681-70	0.05606 ± 0.00078	0.55753 ± 0.00881	0.07214 ± 0.00096	455 ± 16	450 ± 6	449 ± 6	612	590	1.04	100
681-71	0.07173 ± 0.00098	1.61656 ± 0.02536	0.16348 ± 0.00219	978 ± 14	977 ± 10	976 ± 12	190	271	0.70	100
681-72	0.1786 ± 0.00555	10.07741 ± 0.31085	0.41288 ± 0.00823	2640 ± 26	2442 ± 28	2228 ± 38	167	261	0.64	118
681-73	0.05576 ± 0.00169	0.55036 ± 0.01653	0.07161 ± 0.00109	443 ± 40	445 ± 11	446 ± 7	165	80	2.06	100
681-74	0.07106 ± 0.00124	1.56953 ± 0.02905	0.16023 ± 0.00216	959 ± 18	958 ± 11	958 ± 12	238	200	1.19	100
681-75	0.08492 ± 0.00241	2.5825 ± 0.07317	0.22268 ± 0.00394	1314 ± 29	1296 ± 21	1296 ± 21	359	1086	0.33	101
681-76	0.1642 ± 0.00227	10.69419 ± 0.16991	0.47243 ± 0.00641	2499 ± 12	2497 ± 15	2494 ± 28	76	186	0.41	100
681-77	0.07255 ± 0.00104	1.68595 ± 0.02758	0.16858 ± 0.00228	1001 ± 15	1003 ± 10	1004 ± 13	230	400	0.57	100
682 Devonian greywacke from the South of Baluntai										
682-01	0.09819 ± 0.00192	3.63414 ± 0.07675	0.26842 ± 0.00408	1590 ± 19	1557 ± 17	1533 ± 21	187	154	1.21	104
682-02	0.19687 ±	14.62763 ±	0.5386 ±	2800 ± 16	2791 ± 20	2778 ± 36	380	124	3.07	101

Spots	Isotopic ratios			Age/Ma			Th (ppm)	U (ppm)	Th/U	Concordance
	$^{207}Pb/^{206}Pb$	$^{207}Pb/^{235}U$	$^{206}Pb/^{238}U$	$^{207}Pb/^{206}Pb$	$^{207}Pb/^{235}U$	$^{206}Pb/^{238}U$				
	0.00363	0.30265	0.00854							
682-03	0.07516 ± 0.0017	1.92075 ± 0.04655	0.18541 ± 0.0029	1073 ± 25	1088 ± 16	1096 ± 16	94	330	0.29	98
682-04	0.17064 ± 0.00392	11.18471 ± 0.2718	0.47533 ± 0.00799	2564 ± 20	2539 ± 23	2507 ± 35	268	236	1.14	102
682-05	0.15735 ± 0.00547	9.67304 ± 0.33625	0.44668 ± 0.00818	2427 ± 35	2404 ± 32	2380 ± 36	183	197	0.93	102
682-06	0.17593 ± 0.00359	12.10116 ± 0.26697	0.49928 ± 0.00782	2615 ± 18	2612 ± 21	2611 ± 34	496	487	1.02	100
682-07	0.09605 ± 0.00423	3.54907 ± 0.1524	0.26834 ± 0.00531	1549 ± 51	1538 ± 34	1532 ± 27	534	866	0.62	101
682-08	0.07634 ± 0.00204	1.98013 ± 0.05395	0.18859 ± 0.00297	1104 ± 30	1109 ± 18	1114 ± 16	650	503	1.29	99
682-09	0.06931 ± 0.00131	1.54751 ± 0.03212	0.16241 ± 0.00252	908 ± 20	950 ± 13	970 ± 14	509	1119	0.45	98
682-10	0.15655 ± 0.00512	9.33157 ± 0.30329	0.43311 ± 0.00758	2419 ± 32	2371 ± 30	2320 ± 34	228	269	0.85	104
682-11	0.06421 ± 0.00289	1.14708 ± 0.05094	0.12989 ± 0.00247	749 ± 62	776 ± 24	787 ± 14	189	111	1.71	99
682-12	0.07686 ± 0.00192	2.14001 ± 0.05522	0.20278 ± 0.00332	1118 ± 27	1162 ± 18	1190 ± 18	288	371	0.78	94
682-13	0.06501 ± 0.00162	1.20654 ± 0.03158	0.13559 ± 0.00234	775 ± 28	804 ± 15	820 ± 13	632	932	0.68	98
682-14	0.07051 ± 0.00204	1.56484 ± 0.04591	0.16139 ± 0.00266	943 ± 34	956 ± 18	964 ± 15	372	378	0.98	99
682-15	0.07114 ± 0.00213	1.58871 ± 0.04824	0.16232 ± 0.00271	961 ± 35	966 ± 19	970 ± 15	346	485	0.71	100

Spots	Isotopic ratios			Age/Ma			Th (ppm)	U (ppm)	Th/U	Concordance
	$^{207}Pb/^{206}Pb$	$^{207}Pb/^{235}U$	$^{206}Pb/^{238}U$	$^{207}Pb/^{206}Pb$	$^{207}Pb/^{235}U$	$^{206}Pb/^{238}U$				
682-16	0.16089 ± 0.00702	10.31177 ± 0.45537	0.46527 ± 0.01018	2465 ± 45	2463 ± 41	2463 ± 45	179	367	0.49	100
682-17	0.16807 ± 0.00904	11.25875 ± 0.59306	0.48578 ± 0.01069	2539 ± 59	2545 ± 49	2552 ± 46	118	171	0.69	99
682-18	0.3401 ± 0.01327	35.84084 ± 1.4114	0.76455 ± 0.01368	3663 ± 38	3662 ± 39	3661 ± 50	724	1129	0.64	100
682-19	0.07639 ± 0.00227	1.97977 ± 0.06099	0.18817 ± 0.0032	1105 ± 35	1109 ± 21	1111 ± 17	257	1046	0.25	99
682-20	0.06835 ± 0.00257	1.34816 ± 0.05044	0.14343 ± 0.00274	879 ± 46	867 ± 22	864 ± 15	410	598	0.69	100
682-21	0.06694 ± 0.00761	1.2423 ± 0.13765	0.13484 ± 0.00461	836 ± 175	820 ± 62	815 ± 26	135	103	1.32	101
682-22	0.07581 ± 0.00506	1.90539 ± 0.12167	0.18199 ± 0.00465	1090 ± 87	1083 ± 43	1078 ± 25	165	175	0.95	101
682-23	0.09541 ± 0.00564	3.52083 ± 0.19812	0.26762 ± 0.00714	1536 ± 66	1532 ± 44	1529 ± 36	282	261	1.08	100
682-24	0.06792 ± 0.00201	1.44419 ± 0.0428	0.15475 ± 0.0027	866 ± 34	907 ± 18	928 ± 15	707	777	0.91	98
682-25	0.06245 ± 0.00362	1.16205 ± 0.0647	0.13576 ± 0.00324	690 ± 78	783 ± 30	821 ± 18	593	154	3.86	95
682-26	0.05608 ± 0.00437	0.59272 ± 0.04439	0.07666 ± 0.00216	456 ± 116	473 ± 28	476 ± 13	490	325	1.51	99
682-27	0.13653 ± 0.0018	7.57749 ± 0.11718	0.40265 ± 0.00558	2184 ± 12	2182 ± 14	2181 ± 26	51	71	0.72	100
682-28	0.11467 ± 0.00182	5.37449 ± 0.09384	0.34024 ± 0.00462	1875 ± 15	1881 ± 15	1888 ± 22	485	724	0.67	99
682-	0.11897	5.09603	0.31097	1941 ±	1835 ±	1745 ±	45	172	0.26	111

Spots	Isotopic ratios			Age/Ma			Th (ppm)	U (ppm)	Th/U	Concordance
	$^{207}Pb/^{206}Pb$	$^{207}Pb/^{235}U$	$^{206}Pb/^{238}U$	$^{207}Pb/^{206}Pb$	$^{207}Pb/^{235}U$	$^{206}Pb/^{238}U$				
29	± 0.00245	± 0.10897	± 0.00452	19	18	22				
682-30	0.06899 ± 0.00153	1.41497 ± 0.03277	0.14878 ± 0.00232	898 ± 24	895 ± 14	894 ± 13	191	230	0.83	100
682-31	0.11136 ± 0.00653	4.74189 ± 0.26576	0.30957 ± 0.00789	1822 ± 65	1775 ± 47	1739 ± 39	75	112	0.67	105
682-32	0.05406 ± 0.00488	0.43898 ± 0.03812	0.05896 ± 0.00194	374 ± 137	370 ± 27	369 ± 12	1576	1081	1.46	100
682-33	0.05467 ± 0.00197	0.4731 ± 0.01694	0.0628 ± 0.00108	399 ± 50	393 ± 12	393 ± 7	790	1060	0.74	100
682-34	0.06783 ± 0.00148	1.41512 ± 0.03219	0.15137 ± 0.00226	863 ± 24	895 ± 14	909 ± 13	89	69	1.30	98
682-35	0.10974 ± 0.00326	4.85809 ± 0.14408	0.32142 ± 0.00525	1795 ± 31	1795 ± 25	1797 ± 26	141	128	1.10	100
682-36	0.07314 ± 0.00133	1.72309 ± 0.03392	0.17091 ± 0.00246	1018 ± 19	1017 ± 13	1017 ± 14	201	225	0.89	100
682-37	0.09909 ± 0.00151	3.85261 ± 0.06714	0.28204 ± 0.004	1607 ± 15	1604 ± 14	1602 ± 20	346	241	1.44	100
682-38	0.07948 ± 0.0013	2.25554 ± 0.04074	0.20592 ± 0.00291	1184 ± 16	1199 ± 13	1207 ± 16	298	399	0.75	98
682-39	0.05643 ± 0.00103	0.5653 ± 0.01102	0.07268 ± 0.00102	469 ± 21	455 ± 7	452 ± 6	457	432	1.06	101
682-40	0.05623 ± 0.0018	0.58079 ± 0.0184	0.0749 ± 0.00121	461 ± 42	465 ± 12	466 ± 7	146	172	0.85	100
682-41	0.06859 ± 0.00116	1.38767 ± 0.02544	0.14674 ± 0.00204	886 ± 18	884 ± 11	883 ± 11	143	165	0.87	100
682-42	0.05514 ±	0.48615 ±	0.06409 ±	418 ± 101	402 ± 23	400 ± 12	271	640	0.42	101

Spots	Isotopic ratios			Age/Ma			Th (ppm)	U (ppm)	Th/U	Concordance
	$^{207}Pb/^{206}Pb$	$^{207}Pb/^{235}U$	$^{206}Pb/^{238}U$	$^{207}Pb/^{206}Pb$	$^{207}Pb/^{235}U$	$^{206}Pb/^{238}U$				
	0.00401	0.03391	0.00199							
682-43	0.05895 ± 0.00212	0.74268 ± 0.02616	0.09141 ± 0.00158	565 ± 47	564 ± 15	564 ± 9	284	237	1.20	100
682-44	0.07286 ± 0.00105	1.69459 ± 0.0283	0.16868 ±v0.00235	1010 ± 15	1006 ± 11	1005 ± 13	384	483	0.80	100
682-45	0.11339 ± 0.00208	5.19155 ± 0.10035	0.33201 ± 0.00478	1854 ± 17	1851 ± 16	1848 ± 23	50	42	1.18	100
682-46	0.07042 ± 0.00313	1.51712 ± 0.06481	0.1562 ± 0.00306	941 ± 56	937 ± 26	936 ± 17	693	697	1.00	100
682-47	0.14529 ± 0.00976	8.25359 ± 0.52919	0.41534 ± 0.01332	2291 ± 67	2259 ± 58	2239 ± 61	113	94	1.20	102
682-48	0.17344 ± 0.0033	11.42485 ± 0.22329	0.47742 ± 0.00657	2591 ± 16	2558 ± 18	2516 ± 29	414	288	1.44	103
682-49	0.07103 ± 0.00172	1.56487 ± 0.03849	0.15974 ± 0.00243	958 ± 27	956 ± 15	955 ± 14	161	85	1.90	100
682-50	0.10096 ± 0.00191	3.9357 ± 0.0781	0.2825 ± 0.00402	1642 ± 18	1621 ± 16	1604 ± 20	391	111	3.51	102
682-51	0.05618 ± 0.00167	0.56753 ± 0.01686	0.07326 ± 0.00117	459 ± 38	456 ± 11	456 ± 7	296	438	0.67	100
682-52	0.07083 ± 0.00105	1.50604 ± 0.02516	0.15419 ± 0.0021	953 ± 16	933 ± 10	924 ± 12	161	377	0.43	101
682-53	0.07183 ± 0.00113	1.57679 ± 0.02729	0.15914 ± 0.00215	981 ± 16	961 ± 11	952 ± 12	193	675	0.29	101
682-54	0.11793 ± 0.00405	5.52997 ± 0.18797	0.34025 ± 0.00676	1925 ± 34	1905 ± 29	1888 ± 33	45	33	1.35	102
682-55	0.16065 ± 0.00247	10.29342 ± 0.17745	0.46466 ± 0.00638	2463 ± 13	2462 ± 16	2460 ± 28	410	924	0.44	100

Spots	Isotopic ratios			Age/Ma			Th (ppm)	U (ppm)	Th/U	Concordance
	$^{207}Pb/^{206}Pb$	$^{207}Pb/^{235}U$	$^{206}Pb/^{238}U$	$^{207}Pb/^{206}Pb$	$^{207}Pb/^{235}U$	$^{206}Pb/^{238}U$				
682-56	0.12453 ± 0.00615	6.16934 ± 0.29186	0.35993 ± 0.00932	2022 ± 48	2000 ± 41	1982 ± 44	36	20	1.76	102
682-57	0.08355 ± 0.00171	2.53936 ± 0.05427	0.22032 ± 0.00316	1282 ± 21	1283 ± 16	1284 ± 17	257	310	0.83	100
682-58	0.07445 ± 0.00142	1.8764 ± 0.03839	0.18277 ± 0.00264	1054 ± 20	1073 ± 14	1082 ± 14	133	181	0.74	97
682-59	0.05624 ± 0.00135	0.56959 ± 0.01398	0.07344 ± 0.00108	462 ± 29	458 ± 9	457 ± 6	738	594	1.24	100
682-60	0.05758 ± 0.00213	0.65407 ± 0.02388	0.08237 ± 0.00142	514 ± 50	511 ± 15	510 ± 8	76	73	1.04	100
682-61	0.16109 ± 0.00243	10.14264 ± 0.18006	0.45674 ± 0.00675	2467 ± 14	2448 ± 16	2425 ± 30	85	75	1.13	102
682-62	0.07276 ± 0.00113	1.75792 ± 0.0314	0.17525 ± 0.00256	1007 ± 16	1030 ± 12	1041 ± 14	222	125	1.77	97
682-63	0.05617 ± 0.00081	0.5679 ± 0.00962	0.07333 ± 0.00105	459 ± 17	457 ± 6	456 ± 6	422	612	0.69	100
682-64	0.07129 ± 0.0011	1.52536 ± 0.02742	0.15528 ± 0.00232	966 ± 17	941 ± 11	930 ± 13	438	188	2.33	101
682-65	0.2692 ± 0.0039	24.80222 ± 0.41768	0.66836 ± 0.00974	3301 ± 12	3300 ± 16	3300 ± 38	85	68	1.26	100
682-66	0.09706 ± 0.00135	3.75075 ± 0.06204	0.28032 ± 0.00402	1568 ± 14	1582 ± 13	1593 ± 20	861	307	2.80	98
682-67	0.09376 ± 0.0045	3.35552 ± 0.15799	0.26313 ± 0.0063	1503 ± 53	1494 ± 37	1506 ± 32	163	354	0.46	100
682-68	0.05909 ± 0.00145	0.73614 ± 0.01858	0.09036 ± 0.00137	570 ± 30	560 ± 11	558 ± 8	105	68	1.55	100
682-	0.05942	0.74604	0.09107	583 ± 29	566 ±	562 ± 8	278	91	3.04	101

Spots	Isotopic ratios			Age/Ma			Th (ppm)	U (ppm)	Th/U	Concordance
	$^{207}Pb/^{206}Pb$	$^{207}Pb/^{235}U$	$^{206}Pb/^{238}U$	$^{207}Pb/^{206}Pb$	$^{207}Pb/^{235}U$	$^{206}Pb/^{238}U$				
69	± 0.00145	± 0.01858	± 0.00136		11					
682-70	0.15697 ± 0.00217	9.19359 ± 0.15015	0.42479 ± 0.00606	2423 ± 12	2357 ± 15	2282 ± 27	156	118	1.32	106
682-71	0.07435 ± 0.00126	1.76553 ± 0.0331	0.17223 ± 0.00251	1051 ± 18	1033 ± 12	1024 ± 14	110	100	1.09	103
682-72	0.06643 ± 0.00488	1.19317 ± 0.08131	0.13023 ± 0.0036	820 ± 96	797 ± 38	789 ± 21	122	520	0.23	101
682-73	0.05559 ± 0.00134	0.54867 ± 0.01379	0.07159 ± 0.00111	436 ± 30	444 ± 9	446 ± 7	137	112	1.22	100
682-74	0.05656 ± 0.00109	0.6093 ± 0.01216	0.07815 ± 0.00105	474 ± 22	483 ± 8	485 ± 6	341	208	1.64	100
682-75	0.09538 ± 0.00166	3.33985 ± 0.08038	0.25391 ± 0.00529	1536 ± 20	1490 ± 19	1459 ± 27	47.8	74.5	0.64	105
683 Devonian greywacke from the South of Baluntai										
683-01	0.11994 ± 0.00258	5.96272 ± 0.13624	0.36054 ± 0.00578	1955 ± 20	1970 ± 20	1985 ± 27	40	67	0.60	98
683-02	0.12069 ± 0.02157	5.84682 ± 0.99328	0.35396 ± 0.02576	1966 ± 203	1953 ± 147	1953 ± 123	95	81	1.17	101
683-03	0.28589 ± 0.01286	27.34072 ± 1.18892	0.69395 ± 0.01497	3395 ± 41	3396 ± 43	3398 ± 57	157	183	0.86	100
683-04	0.17176 ± 0.00777	11.59381 ± 0.51653	0.49117 ± 0.00992	2575 ± 48	2572 ± 42	2576 ± 43	471	1402	0.34	100
683-05	0.125 ± 0.00378	6.36655 ± 0.19586	0.3706 ± 0.00654	2029 ± 30	2028 ± 27	2032 ± 31	306	639	0.48	100
683-06	0.06795 ± 0.00645	1.44566 ± 0.13196	0.15463 ± 0.00513	867 ± 135	908 ± 55	927 ± 29	409	444	0.92	98
683-	0.06743	1.34744	0.14515	851 ± 34	866 ±	874 ±	2042	725	2.82	99

Spots	Isotopic ratios			Age/Ma			Th (ppm)	U (ppm)	Th/U	Concordance
	$^{207}Pb/^{206}Pb$	$^{207}Pb/^{235}U$	$^{206}Pb/^{238}U$	$^{207}Pb/^{206}Pb$	$^{207}Pb/^{235}U$	$^{206}Pb/^{238}U$				
07	± 0.00191	± 0.03981	± 0.00253		17	14				
683-08	0.05661 ± 0.00236	0.56525 ± 0.0233	0.07263 ± 0.0013	476 ± 60	455 ± 15	452 ± 8	198	197	1.01	101
683-09	0.07153 ± 0.00095	1.55404 ± 0.02352	0.1576 ± 0.00206	973 ± 14	952 ± 9	943 ± 11	145	152	0.95	101
683-10	0.07843 ± 0.00124	2.09796 ± 0.03577	0.19403 ± 0.00259	1158 ± 16	1148 ± 12	1143 ± 14	58	70	0.82	101
683-11	0.16521 ± 0.00509	10.57836 ± 0.3162	0.46566 ± 0.00844	2510 ± 27	2487 ± 28	2465 ± 37	72	35	2.04	102
683-12	0.06735 ± 0.00091	1.28156 ± 0.01966	0.13803 ± 0.00182	849 ± 14	838 ± 9	834 ± 10	159	193	0.82	100
683-13	0.05666 ± 0.00139	0.60263 ± 0.01486	0.07716 ± 0.00112	478 ± 30	479 ± 9	479 ± 7	9	561	0.02	100
683-14	0.05708 ± 0.00137	0.60707 ± 0.01482	0.07714 ± 0.00112	495 ± 29	482 ± 9	479 ± 7	87	67	1.30	101
683-15	0.1635 ± 0.00271	10.38159 ± 0.18761	0.46051 ± 0.0065	2492 ± 14	2469 ± 17	2442 ± 29	115	200	0.57	102
683-16	0.15113 ± 0.0025	9.18735 ± 0.17429	0.44078 ± 0.00696	2359 ± 15	2357 ± 17	2354 ± 31	328	336	0.97	100
683-17	0.08404 ± 0.00164	2.52896 ± 0.05434	0.21821 ± 0.00343	1293 ± 20	1280 ± 16	1272 ± 18	78	267	0.29	102
683-18	0.16839 ± 0.00217	11.14257 ± 0.1652	0.48 ± 0.00629	2542 ± 11	2535 ± 14	2527 ± 27	211	222	0.95	101
683-19	0.07608 ± 0.00118	1.29609 ± 0.02168	0.12358 ± 0.00162	1097 ± 15	844 ± 10	751 ± 9	76	690	0.11	112
683-20	0.12921 ±	6.79708 ±	0.38161 ±	2087 ± 12	2085 ± 14	2084 ± 24	150	266	0.56	100

Spots	Isotopic ratios			Age/Ma			Th (ppm)	U (ppm)	Th/U	Concordance
	$^{207}Pb/^{206}Pb$	$^{207}Pb/^{235}U$	$^{206}Pb/^{238}U$	$^{207}Pb/^{206}Pb$	$^{207}Pb/^{235}U$	$^{206}Pb/^{238}U$				
	0.00177	0.10573	0.00508							
683-21	0.07651 ± 0.00102	1.94515 ± 0.03147	0.1844 ± 0.00266	1108 ± 14	1097 ± 11	1091 ± 14	308	854	0.36	102
683-22	0.12086 ± 0.00364	5.91554 ± 0.17141	0.35461 ± 0.00572	1969 ± 29	1964 ± 25	1957 ± 27	355	287	1.24	101
683-23	0.06927 ± 0.00087	1.38177 ± 0.02017	0.14472 ± 0.00188	907 ± 13	881 ± 9	871 ± 11	102	664	0.15	101
683-24	0.06636 ± 0.00134	1.14495 ± 0.02397	0.12518 ± 0.0018	818 ± 22	775 ± 11	760 ± 10	271	149	1.81	102
683-25	0.07756 ± 0.00107	2.03925 ± 0.03168	0.19073 ± 0.00251	1136 ± 14	1129 ± 11	1125 ± 14	364	238	1.53	101
683-26	0.08337 ± 0.00145	2.40297 ± 0.04668	0.20906 ± 0.00317	1278 ± 18	1243 ± 14	1224 ± 17	85	125	0.68	104
683-27	0.07477 ± 0.00099	1.76195 ± 0.02725	0.17094 ± 0.00232	1062 ± 14	1032 ± 10	1017 ± 13	359	297	1.21	104
683-28	0.06943 ± 0.0012	1.35298 ± 0.02549	0.14136 ± 0.00202	912 ± 18	869 ± 11	852 ± 11	124	116	1.06	102
683-29	0.15965 ± 0.00223	10.18759 ± 0.16964	0.46286 ± 0.00666	2452 ± 13	2452 ± 15	2452 ± 29	413	539	0.77	100
683-30	0.07162 ± 0.00179	1.58461 ± 0.04152	0.16045 ± 0.00272	975 ± 28	964 ± 16	959 ± 15	132	92	1.43	101
683-31	0.07341 ± 0.00101	1.64679 ± 0.02587	0.16271 ± 0.00218	1025 ± 14	988 ± 10	972 ± 12	150	248	0.60	102
683-32	0.07194 ± 0.00109	1.63599 ± 0.02724	0.16495 ± 0.00222	984 ± 15	984 ± 10	984 ± 12	667	281	2.37	100
683-33	0.07068 ± 0.00114	1.49541 ± 0.02561	0.15343 ± 0.002	948 ± 16	929 ± 10	920 ± 11	7	85	0.08	101

Spots	Isotopic ratios			Age/Ma			Th (ppm)	U (ppm)	Th/U	Concordance
	$^{207}Pb/^{206}Pb$	$^{207}Pb/^{235}U$	$^{206}Pb/^{238}U$	$^{207}Pb/^{206}Pb$	$^{207}Pb/^{235}U$	$^{206}Pb/^{238}U$				
683-34	0.07614 ± 0.00101	1.94288 ± 0.02901	0.18506 ± 0.00237	1099 ± 13	1096 ± 10	1095 ± 13	121	181	0.67	100
683-35	0.06534 ± 0.00092	1.1602 ± 0.01781	0.12877 ± 0.00163	785 ± 15	782 ± 8	781 ± 9	919	395	2.33	100
683-36	0.05546 ± 0.00121	0.52877 ± 0.01225	0.06918 ± 0.00107	431 ± 26	431 ± 8	431 ± 6	288	223	1.29	100
683-37	0.06935 ± 0.00228	1.45774 ± 0.04848	0.15249 ± 0.0029	909 ± 38	913 ± 20	915 ± 16	18	222	0.08	100
683-38	0.06685 ± 0.0011	1.20425 ± 0.02124	0.13067 ± 0.00174	833 ± 17	803 ± 10	792 ± 10	164	191	0.86	101
683-39	0.12549 ± 0.00155	6.42665 ± 0.09497	0.37157 ± 0.005	2036 ± 12	2036 ± 13	2037 ± 24	300	300	1.00	100
683-40	0.06655 ± 0.00108	1.22263 ± 0.02103	0.1332 ± 0.00172	824 ± 17	811 ± 10	806 ± 10	143	266	0.54	101
683-41	0.06508 ± 0.00127	1.08515 ± 0.02181	0.12092 ± 0.00163	777 ± 21	746 ± 11	736 ± 9	210	135	1.55	101
683-42	0.12919 ± 0.00339	6.81126 ± 0.17819	0.38251 ± 0.00606	2087 ± 25	2087 ± 23	2088 ± 28	145	177	0.82	100
683-43	0.15006 ± 0.00547	8.9299 ± 0.33389	0.43106 ± 0.00847	2347 ± 38	2331 ± 34	2310 ± 38	81	44	1.83	102
683-44	0.12288 ± 0.00193	5.94851 ± 0.10487	0.35153 ± 0.00511	1998 ± 14	1968 ± 15	1942 ± 24	162	166	0.98	103
683-45	0.15862 ± 0.00253	10.10561 ± 0.18457	0.46254 ± 0.00691	2441 ± 14	2444 ± 17	2451 ± 30	202	193	1.04	100
683-46	0.10057 ± 0.00124	3.94703 ± 0.05773	0.2848 ± 0.0038	1635 ± 12	1623 ± 12	1615 ± 19	118	135	0.88	101
683-	0.08123	2.31459	0.20696	1227 ±	1217 ±	1213 ±	691	275	2.51	101

Spots	Isotopic ratios			Age/Ma			Th (ppm)	U (ppm)	Th/U	Concordance
	$^{207}Pb/^{206}Pb$	$^{207}Pb/^{235}U$	$^{206}Pb/^{238}U$	$^{207}Pb/^{206}Pb$	$^{207}Pb/^{235}U$	$^{206}Pb/^{238}U$				
47	± 0.00306	± 0.08679	± 0.00437	42	27	23				
683-48	0.07072 ± 0.00086	1.52556 ± 0.02209	0.15654 ± 0.00209	949 ± 13	941 ± 9	938 ± 12	195	326	0.60	100
683-49	0.16604 ± 0.00288	10.97553 ± 0.21291	0.47997 ± 0.00716	2518 ± 15	2521 ± 18	2527 ± 31	434	720	0.60	100
683-50	0.07099 ± 0.00128	1.54398 ± 0.02892	0.15777 ± 0.00212	957 ± 19	948 ± 12	944 ± 12	283	263	1.08	100
683-51	0.06844 ± 0.00093	1.15692 ± 0.01794	0.12263 ± 0.00164	882 ± 14	781 ± 8	746 ± 9	306	237	1.29	105
683-52	0.07788 ± 0.00108	2.07892 ± 0.03227	0.19366 ± 0.00254	1144 ± 14	1142 ± 11	1141 ± 14	163	179	0.91	100
683-53	0.05712 ± 0.00107	0.55418 ± 0.01081	0.07037 ± 0.00095	496 ± 21	448 ± 7	438 ± 6	650	397	1.64	102
683-54	0.08563 ± 0.00128	2.68708 ± 0.04381	0.22763 ± 0.00301	1330 ± 14	1325 ± 12	1322 ± 16	89	75	1.19	101
683-55	0.07056 ± 0.00325	1.48457 ± 0.06613	0.15259 ± 0.00365	945 ± 53	924 ± 27	915 ± 20	583	298	1.96	101
683-56	0.07214 ± 0.0012	1.61684 ± 0.02809	0.16258 ± 0.00212	990 ± 17	977 ± 11	971 ± 12	444	256	1.73	101
683-57	0.06548 ± 0.00097	1.14571 ± 0.01835	0.12692 ± 0.00162	790 ± 15	775 ± 9	770 ± 9	303	270	1.12	101
683-58	0.08396 ± 0.00158	2.48207 ± 0.04813	0.21448 ± 0.00294	1292 ± 18	1267 ± 14	1253 ± 16	45	74	0.60	103
683-59	0.05828 ± 0.00115	0.66176 ± 0.01363	0.08236 ± 0.00114	540 ± 23	516 ± 8	510 ± 7	77	127	0.61	101
683-60	0.10922 ±	4.82149 ±	0.32031 ±	1786 ± 27	1789 ± 24	1791 ± 27	54	50	1.09	100

Spots	Isotopic ratios			Age/Ma			Th (ppm)	U (ppm)	Th/U	Concordance
	$^{207}Pb/^{206}Pb$	$^{207}Pb/^{235}U$	$^{206}Pb/^{238}U$	$^{207}Pb/^{206}Pb$	$^{207}Pb/^{235}U$	$^{206}Pb/^{238}U$				
	0.00308	0.13627	0.00561							
683-61	0.07478 ± 0.0019	1.85657 ± 0.04704	0.18013 ± 0.00263	1063 ± 28	1066 ± 17	1068 ± 14	8	227	0.03	100
683-62	0.07877 ± 0.00148	2.12353 ± 0.04292	0.1955 ± 0.00284	1166 ± 19	1156 ± 14	1151 ± 15	138	161	0.85	101
683-63	0.06608 ± 0.00239	1.19243 ± 0.0421	0.13091 ± 0.00222	809 ± 46	797 ± 19	793 ± 13	45	28	1.63	101
683-64	0.07111 ± 0.00111	1.61027 ± 0.02754	0.16425 ± 0.00219	961 ± 16	974 ± 11	980 ± 12	187	209	0.90	99
683-65	0.12032 ± 0.00286	5.85869 ± 0.13984	0.3532 ± 0.00515	1961 ± 23	1955 ± 21	1950 ± 25	100	99	1.00	101
683-66	0.07126 ± 0.00099	1.5713 ± 0.02627	0.15992 ± 0.00232	965 ± 15	959 ± 10	956 ± 13	367	600	0.61	100
683-67	0.05605 ± 0.00195	0.54986 ± 0.01868	0.07118 ± 0.00116	454 ± 47	445 ± 12	443 ± 7	177	216	0.82	100
683-68	0.05978 ± 0.00179	0.8162 ± 0.02453	0.09903 ± 0.00163	596 ± 37	606 ± 14	609 ± 10	108	176	0.62	100
683-69	0.05543 ± 0.00067	0.60264 ± 0.00871	0.07887 ± 0.00105	430 ± 14	479 ± 6	489 ± 6	1312	967	1.36	98
683-70	0.1812 ± 0.00232	12.8231 ± 0.18783	0.51347 ± 0.00668	2664 ± 11	2667 ± 14	2671 ± 28	223	162	1.38	100
683-71	0.07378 ± 0.00103	1.74159 ± 0.02873	0.17121 ± 0.00246	1035 ± 15	1024 ± 11	1019 ± 14	101	571	0.18	102
683-72	0.07737 ± 0.00114	2.05471 ± 0.03305	0.19273 ± 0.00252	1131 ± 15	1134 ± 11	1136 ± 14	206	201	1.02	100
683-73	0.1909 ± 0.00241	13.98277 ± 0.20989	0.53134 ± 0.00728	2750 ± 11	2749 ± 14	2747 ± 31	119	122	0.97	100

Spots	Isotopic ratios			Age/Ma			Th (ppm)	U (ppm)	Th/U	Concordance
	$^{207}Pb/^{206}Pb$	$^{207}Pb/^{235}U$	$^{206}Pb/^{238}U$	$^{207}Pb/^{206}Pb$	$^{207}Pb/^{235}U$	$^{206}Pb/^{238}U$				
683-74	0.1674 ± 0.002	11.1281 ± 0.16057	0.48235 ± 0.00654	2532 ± 11	2534 ± 13	2537 ± 28	159	607	0.26	100
683-75	0.05589 ± 0.00096	0.51322 ± 0.00937	0.06664 ± 0.0009	448 ± 19	421 ± 6	416 ± 5	303	295	1.03	101
683-76	0.05692 ± 0.00106	0.64031 ± 0.01252	0.08161 ± 0.00113	488 ± 21	502 ± 8	506 ± 7	193	180	1.07	99
683-77	0.08775 ± 0.00127	2.87726 ± 0.04669	0.23789 ± 0.00325	1377 ± 14	1376 ± 12	1376 ± 17	94	106	0.88	100
683-78	0.07138 ± 0.001	1.63012 ± 0.02605	0.16562 ± 0.00227	968 ± 15	982 ± 10	988 ± 13	515	197	2.62	99
683-79	0.06491 ± 0.00116	1.15486 ± 0.02215	0.12904 ± 0.00182	771 ± 19	780 ± 10	782 ± 10	239	140	1.70	100
683-80	0.15713 ± 0.00224	9.89299 ± 0.15528	0.45697 ± 0.00608	2425 ± 12	2425 ± 14	2426 ± 27	136	142	0.96	100
683-81	0.07691 ± 0.00111	2.00872 ± 0.0333	0.18943 ± 0.00267	1119 ± 15	1118 ± 11	1118 ± 14	197	125	1.58	100
683-82	0.05588 ± 0.001	0.52798 ± 0.00995	0.06856 ± 0.00093	448 ± 20	430 ± 7	427 ± 6	520	448	1.16	101
683-83	0.05947 ± 0.00125	0.75254 ± 0.0165	0.09179 ± 0.00134	584 ± 24	570 ± 10	566 ± 8	393	217	1.82	101
683-84	0.17292 ± 0.00649	11.51427 ± 0.42106	0.48477 ± 0.00967	2586 ± 35	2566 ± 34	2548 ± 42	37	65	0.57	101
683-85	0.05625 ± 0.00118	0.56026 ± 0.01264	0.07221 ± 0.00113	462 ± 25	452 ± 8	449 ± 7	557	412	1.35	101
683-86	0.05659 ± 0.0008	0.57352 ± 0.00933	0.07352 ± 0.001	476 ± 16	460 ± 6	457 ± 6	1374	848	1.62	101
683-	0.07122	1.59922	0.16285	964 ± 16	970 ±	973 ±	277	158	1.76	100

Spots	Isotopic ratios			Age/Ma			Th (ppm)	U (ppm)	Th/U	Concordance
	$^{207}Pb/^{206}Pb$	$^{207}Pb/^{235}U$	$^{206}Pb/^{238}U$	$^{207}Pb/^{206}Pb$	$^{207}Pb/^{235}U$	$^{206}Pb/^{238}U$				
87	± 0.0011	± 0.02792	± 0.00231		11	13				
683-88	0.07572 ± 0.00273	1.92478 ± 0.06889	0.18449 ± 0.00321	1088 ± 44	1090 ± 24	1091 ± 17	232	315	0.74	100
683-89	0.08235 ± 0.00124	2.43978 ± 0.04204	0.21486 ± 0.00306	1254 ± 15	1254 ± 12	1255 ± 16	234	160	1.47	100
684 Devonian greywacke from the South of Baluntai										
684-01	0.18224 ± 0.00553	13.02018 ± 0.39849	0.51859 ± 0.00874	2673 ± 29	2681 ± 29	2693 ± 37	365	483	0.76	99
684-02	0.07301 ± 0.00196	1.72983 ± 0.04895	0.17196 ± 0.00311	1014 ± 30	1020 ± 18	1023 ± 17	425	495	0.86	99
684-03	0.07349 ± 0.00458	1.74804 ± 0.10705	0.17326 ± 0.00438	1027 ± 83	1026 ± 40	1030 ± 24	737	581	1.27	100
684-04	0.21321 ± 0.00841	16.80534 ± 0.66583	0.57205 ± 0.01055	2930 ± 40	2924 ± 38	2916 ± 43	259	299	0.87	100
684-05	0.21599 ± 0.01435	17.12741 ± 1.1067	0.5756 ± 0.01387	2951 ± 73	2942 ± 62	2931 ± 57	282	307	0.92	101
684-06	0.28251 ± 0.01101	26.67567 ± 1.04687	0.68622 ± 0.01262	3377 ± 38	3372 ± 38	3368 ± 48	213	149	1.43	100
684-07	0.10261 ± 0.00182	4.20066 ± 0.07734	0.29692 ± 0.00412	1672 ± 16	1674 ± 15	1676 ± 20	75	57	1.32	100
684-08	0.07396 ± 0.00181	1.60595 ± 0.03933	0.15751 ± 0.00238	1040 ± 26	973 ± 15	943 ± 13	63	58	1.09	103
684-09	0.06727 ± 0.00084	1.4405 ± 0.02141	0.15533 ± 0.00209	846 ± 14	906 ± 9	931 ± 12	515	1200	0.43	97
684-10	0.08222 ± 0.00134	2.42954 ± 0.04403	0.21439 ± 0.00307	1251 ± 16	1251 ± 13	1252 ± 16	415	433	0.96	100
684-	0.06826	1.43159	0.15214	876 ± 15	902 ±	913 ±	679	245	2.77	99

Spots	Isotopic ratios			Age/Ma			Th (ppm)	U (ppm)	Th/U	Concordance
	$^{207}Pb/^{206}Pb$	$^{207}Pb/^{235}U$	$^{206}Pb/^{238}U$	$^{207}Pb/^{206}Pb$	$^{207}Pb/^{235}U$	$^{206}Pb/^{238}U$				
11	± 0.00096	± 0.02305	± 0.00208		10	12				
684-12	0.05664 ± 0.00136	0.61802 ± 0.01522	0.07915 ± 0.00119	478 ± 29	489 ± 10	491 ± 7	80	74	1.09	100
684-13	0.12611 ± 0.00163	6.26631 ± 0.09324	0.36044 ± 0.00481	2044 ± 12	2014 ± 13	1984 ± 23	70	74	0.95	103
684-14	0.06413 ± 0.00123	1.07555 ± 0.02163	0.12166 ± 0.00171	746 ± 21	741 ± 11	740 ± 10	151	58	2.62	100
684-15	0.16764 ± 0.00332	11.03631 ± 0.22274	0.47803 ± 0.00667	2534 ± 17	2526 ± 19	2519 ± 29	152	192	0.79	101
684-16	0.0779 ± 0.00131	2.0178 ± 0.03578	0.18788 ± 0.00249	1144 ± 17	1122 ± 12	1110 ± 14	214	225	0.95	103
684-17	0.0729 ± 0.00777	1.70303 ± 0.17205	0.16959 ± 0.00698	1011 ± 139	1010 ± 65	1010 ± 38	18	15	1.18	100
684-18	0.05839 ± 0.00189	0.57228 ± 0.01825	0.07109 ± 0.00113	544 ± 42	459 ± 12	443 ± 7	46	54	0.86	104
684-19	0.07339 ± 0.00127	1.63864 ± 0.03048	0.16196 ± 0.00227	1025 ± 18	985 ± 12	968 ± 13	121	123	0.98	102
684-20	0.07279 ± 0.00102	1.69542 ± 0.02749	0.16892 ± 0.00235	1008 ± 15	1007 ± 10	1006 ± 13	123	147	0.83	100
684-21	0.09487 ± 0.00122	3.48689 ± 0.05285	0.26658 ± 0.00361	1525 ± 13	1524 ± 12	1523 ± 18	89	378	0.24	100
684-22	0.06847 ± 0.00114	1.39571 ± 0.02466	0.14785 ± 0.00196	883 ± 17	887 ± 10	889 ± 11	196	234	0.84	100
684-23	0.16651 ± 0.00978	11.20558 ± 0.61886	0.48698 ± 0.01319	2523 ± 57	2540 ± 51	2558 ± 57	56	39	1.46	99
684-24	0.0914 ± 0.00166	3.18092 ±	0.2524 ±	1455 ± 17	1453 ± 15	1451 ± 18	96	85	1.13	100

Spots	Isotopic ratios			Age/Ma			Th (ppm)	U (ppm)	Th/U	Concordance
	$^{207}Pb/^{206}Pb$	$^{207}Pb/^{235}U$	$^{206}Pb/^{238}U$	$^{207}Pb/^{206}Pb$	$^{207}Pb/^{235}U$	$^{206}Pb/^{238}U$				
		0.06015	0.00347							
684-25	0.10814 ± 0.00235	4.70258 ± 0.10378	0.31542 ± 0.00468	1768 ± 20	1768 ± 18	1767 ± 23	37	44	0.83	100
684-26	0.07234 ± 0.0028	1.5411 ± 0.05702	0.15421 ± 0.00269	996 ± 47	947 ± 23	925 ± 15	181	129	1.40	102
684-27	0.16213 ± 0.00286	10.38875 ± 0.19264	0.4648 ± 0.00649	2478 ± 15	2470 ± 17	2461 ± 29	238	36	6.64	101
684-28	0.07487 ± 0.00147	1.85553 ± 0.03778	0.17977 ± 0.00252	1065 ± 20	1065 ± 13	1066 ± 14	57	74	0.77	100
684-29	0.05596 ± 0.0009	0.52653 ± 0.00912	0.06825 ± 0.0009	451 ± 18	430 ± 6	426 ± 5	724	415	1.75	101
684-30	0.07609 ± 0.00114	1.88092 ± 0.0314	0.1793 ± 0.00246	1097 ± 15	1074 ± 11	1063 ± 13	955	267	3.58	103
684-31	0.05802 ± 0.00129	0.64219 ± 0.01463	0.08029 ± 0.00114	531 ± 26	504 ± 9	498 ± 7	196	101	1.93	101
684-32	0.06711 ± 0.00092	1.24763 ± 0.01973	0.13485 ± 0.00183	841 ± 15	822 ± 9	815 ± 10	267	315	0.85	101
684-33	0.08515 ± 0.00143	2.6395 ± 0.04749	0.22482 ± 0.00308	1319 ± 16	1312 ± 13	1307 ± 16	91	181	0.50	101
684-34	0.07813 ± 0.00376	2.10966 ± 0.09771	0.19593 ± 0.00439	1150 ± 57	1152 ± 32	1153 ± 24	96	22	4.43	100
684-35	0.07174 ± 0.00128	1.54777 ± 0.0295	0.15649 ± 0.00216	979 ± 19	950 ± 12	937 ± 12	258	478	0.54	101
684-36	0.09924 ± 0.00161	3.87962 ± 0.0694	0.28359 ± 0.004	1610 ± 15	1609 ± 14	1609 ± 20	98	67	1.46	100
684-37	0.20046 ± 0.00724	14.68115 ± 0.52015	0.5312 ± 0.01022	2830 ± 33	2795 ± 34	2747 ± 43	51	53	0.95	103

Spots	Isotopic ratios			Age/Ma			Th (ppm)	U (ppm)	Th/U	Concordance
	$^{207}Pb/^{206}Pb$	$^{207}Pb/^{235}U$	$^{206}Pb/^{238}U$	$^{207}Pb/^{206}Pb$	$^{207}Pb/^{235}U$	$^{206}Pb/^{238}U$				
684-38	0.14761 ± 0.00199	8.77655 ± 0.13777	0.43128 ± 0.00603	2318 ± 12	2315 ± 14	2311 ± 27	368	70	5.26	100
684-39	0.07034 ± 0.00123	1.54266 ± 0.02955	0.15909 ± 0.00232	938 ± 18	948 ± 12	952 ± 13	137	92	1.50	100
684-40	0.05602 ± 0.00118	0.55181 ± 0.01212	0.07142 ± 0.00104	453 ± 25	446 ± 8	445 ± 6	292	301	0.97	100
684-41	0.11427 ± 0.00197	5.26726 ± 0.09805	0.33438 ± 0.00491	1868 ± 15	1864 ± 16	1860 ± 24	37	28	1.33	100
684-42	0.08724 ± 0.00125	2.86967 ± 0.0476	0.2386 ± 0.00337	1366 ± 14	1374 ± 12	1379 ± 18	191	282	0.68	99
684-43	0.07653 ± 0.00111	2.08049 ± 0.03537	0.1972 ± 0.0029	1109 ± 15	1142 ± 12	1160 ± 16	519	268	1.94	96
684-44	0.18111 ± 0.0027	12.65474 ± 0.20874	0.50692 ± 0.00694	2663 ± 12	2654 ± 16	2643 ± 30	287	159	1.80	101
684-45	0.19797 ± 0.00312	14.72053 ± 0.25322	0.53922 ± 0.0077	2810 ± 13	2797 ± 16	2780 ± 32	48	38	1.26	101
684-46	0.07135 ± 0.00091	1.62616 ± 0.02464	0.16532 ± 0.00224	967 ± 14	980 ± 10	986 ± 12	361	528	0.68	99
684-47	0.0678 ± 0.00094	1.35894 ± 0.02167	0.14538 ± 0.00198	862 ± 15	871 ± 9	875 ± 11	91	848	0.11	100
684-48	0.11529 ± 0.00162	5.5103 ± 0.08899	0.34669 ± 0.00481	1884 ± 13	1902 ± 14	1919 ± 23	77	99	0.78	98
684-49	0.11274 ± 0.00188	5.03925 ± 0.09065	0.32418 ± 0.00448	1844 ± 15	1826 ± 15	1810 ± 22	251	234	1.07	102
684-50	0.06895 ± 0.0015	1.3607 ± 0.0307	0.14314 ± 0.00213	897 ± 24	872 ± 13	862 ± 12	117	70	1.67	101
684-	0.10906	4.71562	0.31375	1784 ±	1770 ±	1759 ±	160	468	0.34	101

Spots	Isotopic ratios			Age/Ma			Th (ppm)	U (ppm)	Th/U	Concordance
	$^{207}Pb/^{206}Pb$	$^{207}Pb/^{235}U$	$^{206}Pb/^{238}U$	$^{207}Pb/^{206}Pb$	$^{207}Pb/^{235}U$	$^{206}Pb/^{238}U$				
51	± 0.00168	± 0.08029	± 0.00432	14	14	21				
684-52	0.11308 ± 0.00227	5.1644 ± 0.10927	0.33104 ± 0.00505	1849 ± 18	1847 ± 18	1843 ± 24	177	158	1.12	100
684-53	0.06181 ± 0.00089	0.94875 ± 0.01589	0.11132 ± 0.00157	668 ± 16	677 ± 8	680 ± 9	80	294	0.27	100
684-54	0.16163 ± 0.00281	10.22278 ± 0.18991	0.45877 ± 0.00646	2473 ± 15	2455 ± 17	2434 ± 29	181	225	0.80	102
684-55	0.14625 ± 0.00477	8.60495 ± 0.27439	0.42688 ± 0.00774	2303 ± 31	2297 ± 29	2292 ± 35	205	114	1.79	100
684-56	0.05722 ± 0.00137	0.59955 ± 0.01473	0.07599 ± 0.00114	500 ± 29	477 ± 9	472 ± 7	255	130	1.96	101
684-57	0.09941 ± 0.00253	3.80018 ± 0.09855	0.27798 ± 0.00438	1613 ± 26	1593 ± 21	1581 ± 22	133	353	0.38	102
684-58	0.13698 ± 0.00247	7.53551 ± 0.14437	0.39932 ± 0.00576	2189 ± 16	2177 ± 17	2166 ± 27	93	64	1.45	101
684-59	0.10723 ± 0.00608	4.53041 ± 0.24856	0.307 ± 0.0073	1753 ± 66	1737 ± 46	1726 ± 36	71	303	0.23	102
684-60	0.07306 ± 0.00109	1.75567 ± 0.03031	0.17429 ± 0.0025	1016 ± 16	1029 ± 11	1036 ± 14	448	315	1.42	98
684-61	0.07334 ± 0.00207	1.74582 ± 0.04895	0.17264 ± 0.00271	1023 ± 32	1026 ± 18	1027 ± 15	237	311	0.76	100
684-62	0.05849 ± 0.00264	0.70038 ± 0.03061	0.08686 ± 0.00172	548 ± 61	539 ± 18	537 ± 10	102	228	0.45	100
684-63	0.06655 ± 0.00265	1.24289 ± 0.04816	0.13551 ± 0.00256	824 ± 50	820 ± 22	819 ± 15	49	52	0.93	100
684-64	0.10667 ± 0.0023	4.57114 ±	0.31098 ±	1743 ± 20	1744 ± 20	1746 ± 27	154	166	0.93	100

Spots	Isotopic ratios			Age/Ma			Th (ppm)	U (ppm)	Th/U	Concordance
	$^{207}Pb/^{206}Pb$	$^{207}Pb/^{235}U$	$^{206}Pb/^{238}U$	$^{207}Pb/^{206}Pb$	$^{207}Pb/^{235}U$	$^{206}Pb/^{238}U$				
		0.10806	0.00548							
684-65	0.07231 ± 0.00201	1.6017 ± 0.04457	0.16069 ± 0.00265	995 ± 31	971 ± 17	961 ± 15	43	51	0.85	101
684-66	0.10923 ± 0.00144	4.76467 ± 0.07583	0.31647 ± 0.00455	1787 ± 13	1779 ± 13	1772 ± 22	8	146	0.06	101
684-67	0.1111 ± 0.00507	4.9862 ± 0.21704	0.32565 ± 0.00799	1817 ± 45	1817 ± 37	1817 ± 39	44	23	1.92	100
684-68	0.07056 ± 0.00104	1.59829 ± 0.0272	0.16433 ± 0.00236	945 ± 16	970 ± 11	981 ± 13	133	174	0.77	99
684-69	0.05569 ± 0.0009	0.55731 ± 0.01012	0.07262 ± 0.00105	440 ± 19	450 ± 7	452 ± 6	629	424	1.48	100
684-70	0.06428 ± 0.001	1.08176 ± 0.01875	0.12206 ± 0.00171	751 ± 17	744 ± 9	742 ± 10	219	224	0.98	100
684-71	0.12225 ± 0.00377	5.97093 ± 0.17943	0.35412 ± 0.00603	1989 ± 30	1972 ± 26	1954 ± 29	348	315	1.11	102
684-72	0.16062 ± 0.00222	10.38363 ± 0.16861	0.46915 ± 0.00685	2462 ± 12	2470 ± 15	2480 ± 30	59	45	1.31	99
684-73	0.15267 ± 0.00512	9.2789 ± 0.30581	0.44111 ± 0.00789	2376 ± 32	2366 ± 30	2356 ± 35	112	285	0.39	101
684-74	0.09574 ± 0.00133	3.64402 ± 0.05882	0.27612 ± 0.00389	1543 ± 14	1559 ± 13	1572 ± 20	187	177	1.06	98
684-75	0.09794 ± 0.00132	3.81244 ± 0.0606	0.28238 ± 0.00397	1585 ± 13	1595 ± 13	1603 ± 20	388	132	2.94	99
684-76	0.05475 ± 0.00132	0.57399 ± 0.01434	0.07605 ± 0.0012	402 ± 29	461 ± 9	473 ± 7	264	208	1.27	97
684-77	0.0638 ± 0.00116	1.09054 ± 0.0214	0.12399 ± 0.00181	735 ± 20	749 ± 10	753 ± 10	291	145	2.01	99

Spots	Isotopic ratios			Age/Ma			Th (ppm)	U (ppm)	Th/U	Concordance
	$^{207}Pb/^{206}Pb$	$^{207}Pb/^{235}U$	$^{206}Pb/^{238}U$	$^{207}Pb/^{206}Pb$	$^{207}Pb/^{235}U$	$^{206}Pb/^{238}U$				
684-78	0.06405 ± 0.00096	1.14966 ± 0.01975	0.13019 ± 0.00186	743 ± 16	777 ± 9	789 ± 11	695	954	0.73	98
684-79	0.13553 ± 0.00623	7.46637 ± 0.33588	0.3996 ± 0.00942	2171 ± 46	2169 ± 40	2167 ± 43	221	721	0.31	100
684-80	0.19177 ± 0.00522	13.99558 ± 0.39287	0.53036 ± 0.00901	2757 ± 25	2749 ± 27	2743 ± 38	179	350	0.51	101
684-81	0.07851 ± 0.00166	2.25295 ± 0.05048	0.20821 ± 0.00323	1160 ± 22	1198 ± 16	1219 ± 17	9	181	0.05	95
684-82	0.05831 ± 0.00145	0.6444 ± 0.0164	0.08026 ± 0.00122	541 ± 30	505 ± 10	498 ± 7	282	506	0.56	101
685 Devonian arkose from the South of Baluntai										
685-01	0.11078 ± 0.00219	4.84382 ± 0.10389	0.31702 ± 0.00487	1812 ± 19	1793 ± 18	1775 ± 24	170	152	1.12	102
685-02	0.1109 ± 0.00226	4.93549 ± 0.10923	0.3227 ± 0.00498	1814 ± 20	1808 ± 19	1803 ± 24	266	196	1.36	101
685-03	0.1143 ± 0.00343	5.33346 ± 0.16538	0.33834 ± 0.00576	1869 ± 32	1874 ± 27	1879 ± 28	244	261	0.93	99
685-04	0.15972 ± 0.00392	9.97341 ± 0.25554	0.45291 ± 0.00723	2453 ± 23	2432 ± 24	2408 ± 32	165	445	0.37	102
685-05	0.15692 ± 0.00689	9.59985 ± 0.41817	0.44413 ± 0.00913	2423 ± 46	2397 ± 40	2369 ± 41	286	258	1.11	102
685-06	0.28589 ± 0.01286	27.34072 ± 1.18892	0.69395 ± 0.01497	3390 ± 28	3391 ± 33	3395 ± 47	141	163	0.87	100
685-07	0.1143 ± 0.00418	5.4035 ± 0.19421	0.34379 ± 0.00635	1869 ± 39	1885 ± 31	1905 ± 30	251	186	1.35	98
685-08	0.09822 ± 0.0039	3.89392 ± 0.1538	0.28766 ± 0.00545	1591 ± 46	1612 ± 32	1630 ± 27	412	255	1.62	98

Spots	Isotopic ratios			Age/Ma			Th (ppm)	U (ppm)	Th/U	Concordance
	$^{207}Pb/^{206}Pb$	$^{207}Pb/^{235}U$	$^{206}Pb/^{238}U$	$^{207}Pb/^{206}Pb$	$^{207}Pb/^{235}U$	$^{206}Pb/^{238}U$				
685-09	0.09703 ± 0.00468	3.8859 ± 0.18498	0.29145 ± 0.00677	1568 ± 55	1611 ± 38	1649 ± 34	206	226	0.91	95
685-10	0.17767 ± 0.00743	12.31917 ± 0.52583	0.5033 ± 0.00991	2631 ± 45	2629 ± 40	2628 ± 42	55	1581	0.03	100
685-11	0.1131 ± 0.00434	4.66222 ± 0.17928	0.29929 ± 0.0057	1850 ± 42	1760 ± 32	1688 ± 28	474	382	1.24	110
685-12	0.09651 ± 0.00394	3.80374 ± 0.15252	0.28599 ± 0.00561	1558 ± 46	1594 ± 32	1621 ± 28	96	82	1.17	96
685-13	0.16174 ± 0.00425	10.11165 ± 0.27586	0.4553 ± 0.00771	2474 ± 24	2445 ± 25	2419 ± 34	306	173	1.77	102
685-14	0.09655 ± 0.00322	3.43205 ± 0.11233	0.25894 ± 0.00443	1558 ± 36	1512 ± 26	1484 ± 23	81	670	0.12	105
685-15	0.05626 ± 0.00099	0.5973 ± 0.01144	0.07704 ± 0.00109	463 ± 20	476 ± 7	478 ± 7	366	331	1.11	100
685-16	0.05653 ± 0.00133	0.58823 ± 0.01405	0.07547 ± 0.0011	473 ± 28	470 ± 9	469 ± 7	146	145	1.01	100
685-17	0.11368 ± 0.00147	5.26737 ± 0.08046	0.33613 ± 0.0046	1859 ± 12	1864 ± 13	1868 ± 22	67	110	0.61	100
685-18	0.07443 ± 0.00175	1.82761 ± 0.04388	0.17827 ± 0.00275	1053 ± 25	1055 ± 16	1058 ± 15	82	142	0.58	100
685-19	0.16114 ± 0.00454	10.24259 ± 0.28307	0.46126 ± 0.00752	2468 ± 26	2457 ± 26	2445 ± 33	64	112	0.58	101
685-20	0.09521 ± 0.00135	3.5257 ± 0.057	0.26859 ± 0.00368	1532 ± 14	1533 ± 13	1534 ± 19	255	166	1.54	100
685-21	0.07159 ± 0.00132	1.65059 ± 0.0324	0.16724 ± 0.00242	974 ± 19	990 ± 12	997 ± 13	287	109	2.64	99
685-	0.06696	1.24656	0.13502	837 ± 20	822 ±	816 ±	75	104	0.72	101

Spots	Isotopic ratios			Age/Ma			Th (ppm)	U (ppm)	Th/U	Concordance
	$^{207}Pb/^{206}Pb$	$^{207}Pb/^{235}U$	$^{206}Pb/^{238}U$	$^{207}Pb/^{206}Pb$	$^{207}Pb/^{235}U$	$^{206}Pb/^{238}U$				
22	± 0.00123	± 0.02425	± 0.00189		11	11				
685-23	0.06698 ± 0.0009	1.29289 ± 0.02039	0.14001 ± 0.00191	837 ± 15	843 ± 9	845 ± 11	94	424	0.22	100
685-24	0.05608 ± 0.00084	0.58463 ± 0.00987	0.07565 ± 0.00104	456 ± 17	467 ± 6	470 ± 6	575	323	1.78	99
685-25	0.06925 ± 0.00086	1.29676 ± 0.01939	0.13588 ± 0.00184	906 ± 14	844 ± 9	821 ± 10	128	540	0.24	103
685-26	0.06305 ± 0.00232	0.9578 ± 0.0342	0.11022 ± 0.00189	710 ± 47	682 ± 18	674 ± 11	25	27	0.91	101
685-27	0.05536 ± 0.00092	0.5605 ± 0.01	0.07344 ± 0.00099	427 ± 19	452 ± 7	457 ± 6	185	251	0.74	99
685-28	0.07423 ± 0.00101	1.80636 ± 0.02785	0.17651 ± 0.00234	1048 ± 14	1048 ± 10	1048 ± 13	119	279	0.43	100
685-29	0.07009 ± 0.00117	1.61795 ± 0.02886	0.16739 ± 0.00226	931 ± 17	977 ± 11	998 ± 12	90	337	0.27	98
685-30	0.07177 ± 0.00101	1.58442 ± 0.0254	0.16015 ± 0.00215	979 ± 15	964 ± 10	958 ± 12	35	258	0.13	101
685-31	0.05968 ± 0.00115	0.78586 ± 0.01602	0.09553 ± 0.00136	592 ± 22	589 ± 9	588 ± 8	882	323	2.73	100
685-32	0.07125 ± 0.00121	1.5344 ± 0.02857	0.15623 ± 0.0022	965 ± 18	944 ± 11	936 ± 12	27	84	0.32	101
685-33	0.06068 ± 0.00113	0.92125 ± 0.0196	0.11023 ± 0.00177	628 ± 22	663 ± 10	674 ± 10	231	1443	0.16	98
685-34	0.05996 ± 0.00075	0.85046 ± 0.01312	0.10291 ± 0.00146	602 ± 15	625 ± 7	631 ± 9	728	745	0.98	99
685-35	0.05635 ± 0.001	0.56766 ±	0.07306 ±	466 ± 20	457 ± 7	455 ± 6	182	197	0.93	100

Spots	Isotopic ratios			Age/Ma			Th (ppm)	U (ppm)	Th/U	Concordance
	$^{207}Pb/^{206}Pb$	$^{207}Pb/^{235}U$	$^{206}Pb/^{238}U$	$^{207}Pb/^{206}Pb$	$^{207}Pb/^{235}U$	$^{206}Pb/^{238}U$				
		0.01091	0.00104							
685-36	0.19461 ± 0.00239	14.41866 ± 0.21861	0.53749 ± 0.00766	2782 ± 11	2778 ± 14	2773 ± 32	118	78	1.52	100
685-37	0.16275 ± 0.00231	10.19327 ± 0.16326	0.45424 ± 0.00619	2484 ± 12	2452 ± 15	2414 ± 27	204	99	2.07	103
685-38	0.0894 ± 0.00135	2.97676 ± 0.05023	0.24151 ± 0.00335	1413 ± 15	1402 ± 13	1395 ± 17	332	222	1.49	101
685-39	0.1599 ± 0.00257	10.11203 ± 0.17734	0.45861 ± 0.00635	2455 ± 14	2445 ± 16	2433 ± 28	237	157	1.51	101
685-40	0.0546 ± 0.00116	0.55904 ± 0.01248	0.07427 ± 0.00111	396 ± 25	451 ± 8	462 ± 7	156	193	0.81	98
685-41	0.05614 ± 0.00105	0.58596 ± 0.01178	0.07571 ± 0.00109	458 ± 22	468 ± 8	470 ± 7	222	219	1.01	100
685-42	0.0903 ± 0.00225	3.07792 ± 0.0776	0.24724 ± 0.00389	1432 ± 25	1427 ± 19	1424 ± 20	111	64	1.75	101
685-43	0.07159 ± 0.00119	1.63478 ± 0.03008	0.16566 ± 0.00236	974 ± 17	984 ± 12	988 ± 13	101	133	0.76	100
685-44	0.06453 ± 0.00243	0.95147 ± 0.03529	0.10696 ± 0.00193	759 ± 48	679 ± 18	655 ± 11	94	34	2.79	104
685-45	0.0726 ± 0.00113	1.68627 ± 0.02895	0.16848 ± 0.00232	1003 ± 16	1003 ± 11	1004 ± 13	748	268	2.79	100
685-46	0.05743 ± 0.0014	0.58829 ± 0.01451	0.07433 ± 0.00111	508 ± 29	470 ± 9	462 ± 7	161	193	0.84	102
685-47	0.09592 ± 0.00117	3.55674 ± 0.05355	0.26908 ± 0.00379	1546 ± 13	1540 ± 12	1536 ± 19	309	376	0.82	101
685-48	0.0559 ± 0.00123	0.51799 ± 0.0116	0.06722 ± 0.00093	448 ± 26	424 ± 8	419 ± 6	178	214	0.83	101

Spots	Isotopic ratios			Age/Ma			Th (ppm)	U (ppm)	Th/U	Concordance
	$^{207}Pb/^{206}Pb$	$^{207}Pb/^{235}U$	$^{206}Pb/^{238}U$	$^{207}Pb/^{206}Pb$	$^{207}Pb/^{235}U$	$^{206}Pb/^{238}U$				
685-49	0.05591 ± 0.00147	0.52271 ± 0.01365	0.06783 ± 0.00099	449 ± 33	427 ± 9	423 ± 6	232	150	1.55	101
685-50	0.12229 ± 0.00313	1.80843 ± 0.06099	0.1068 ± 0.00161	1990 ± 39	1049 ± 22	654 ± 9	0.00	1305		160
685-51	0.09939 ± 0.00189	3.82097 ± 0.07073	0.28115 ± .00355	1613 ± 17	1597 ± 15	1597 ± 18	162	204	0.79	101
685-52	0.07049 ± 0.00105	1.55065 ± 0.02282	0.15955 ± 0.0014	943 ± 16	951 ± 9	954 ± 8	104	184	0.56	100
685-53	0.06608 ± 0.00321	1.2294 ± 0.06541	0.13386 ± 0.00179	809 ± 89	814 ± 30	810 ± 10	109	68.8	1.59	100
685-54	0.10288 ± 0.00086	4.42777 ± 0.11251	0.30934 ± 0.00644	1677 ± 21	1718 ± 21	1737 ± 32	69.4	407	0.17	97
685-55	0.0713 ± 0.00071	1.53427 ± 0.03164	0.15546 ± 0.00264	966 ± 19	944 ± 13	932 ± 15	557	534	1.04	101
685-56	0.22506 ± 0.0053	20.19605 ± 0.86151	0.61805 ± 0.01571	3017 ± 37	3101 ± 41	3102 ± 63	19.6	101	0.19	97
685-57	0.07259 ± 0.00095	1.6692 ± 0.02262	0.16645 ± 0.00075	1003 ± 20	997 ± 9	993 ± 4	75.1	112	0.67	100
685-58	0.05727 ± 0.00138	0.69386 ± 0.01661	0.08825 ± 0.0007	502 ± 39	535 ± 10	545 ± 4	119	67.9	1.75	98
685-59	0.05545 ± 0.00172	0.5273 ± 0.01648	0.06883 ± 0.0005	430 ± 57	430 ± 11	429 ± 3	158	304	0.52	100
685-60	0.12767 ± 0.00085	7.17561 ± 0.0584	0.40679 ± 0.00248	2066 ± 7	2133 ± 7	2200 ± 11	102	114	0.89	94
685-61	0.10863 ± 0.0011	4.80582 ± 0.05644	0.32085 ± 0.00276	1777 ± 10	1786 ± 10	1794 ± 13	54.7	75.9	0.72	99
685-	0.07275	1.70431	0.16989	1007 ±	1010 ±	1011 ±	92.0	183	0.50	100

Spots	Isotopic ratios			Age/Ma			Th (ppm)	U (ppm)	Th/U	Concordance
	$^{207}Pb/^{206}Pb$	$^{207}Pb/^{235}U$	$^{206}Pb/^{238}U$	$^{207}Pb/^{206}Pb$	$^{207}Pb/^{235}U$	$^{206}Pb/^{238}U$				
62	± 0.00128	± 0.02685	± 0.00135	19	10	7				
685-63	0.12033 ± 0.00089	5.95113 ± 0.08373	0.35693 ± 0.00404	1961 ± 11	1969 ± 12	1968 ± 19	196	119	1.65	100
685-64	0.07453 ± 0.00101	1.8582 ± 0.03594	0.18021 ± 0.00343	1056 ± 18	1066 ± 13	1068 ± 19	96.8	618	0.16	99
685-65	0.06432 ± 0.00152	1.03498 ± 0.02466	0.1163 ± 0.00093	752 ± 37	721 ± 12	709 ± 5	112	113	1.00	102
685-66	0.05686 ± 0.00086	0.62198 ± 0.00863	0.07901 ± 0.0005	486 ± 20	491 ± 5	490 ± 3	243	402	0.60	100
685-67	0.07266 ± 0.00121	1.73067 ± 0.03287	0.17163 ± 0.00291	1004 ± 17	1020 ± 12	1021 ± 16	65.0	254	0.26	98
685-68	0.05625 ± 0.00142	0.63713 ± 0.01144	0.08093 ± 0.00053	462 ± 28	501 ± 7	502 ± 3	191	307	0.62	100
685-69	0.09219 ± 0.00132	3.25261 ± 0.0625	0.2544 ± 0.00383	1471 ± 17	1470 ± 15	1461 ± 20	225	237	0.95	101
685-70	0.07523 ± 0.0013	1.90828 ± 0.03538	0.18296 ± 0.00179	1075 ± 22	1084 ± 12	1083 ± 10	46.4	317	0.15	99
685-71	0.07509 ± 0.0013	1.98556 ± 0.038	0.19289 ± 0.00265	1071 ± 19	1111 ± 13	1137 ± 14	119	153	0.78	94
685-72	0.08787 ± 0.00138	2.87503 ± 0.05169	0.23762 ± 0.0039	1380 ± 15	1375 ± 14	1374 ± 20	61.2	181	0.34	100
685-73	0.15263 ± 0.00109	9.48068 ± 0.13527	0.4475 ± 0.00496	2376 ± 11	2386 ± 13	2384 ± 22	139	141	0.99	100
685-74	0.0661 ± 0.00127	1.22155 ± 0.02463	0.13352 ± 0.00132	810 ± 26	810 ± 11	808 ± 8	336	393	0.86	100
685-75	0.14474 ±	8.29147 ±	0.41309 ±	2285 ± 6	2263 ± 6	2229 ± 8	74.8	437	0.17	103

Spots	Isotopic ratios			Age/Ma			Th (ppm)	U (ppm)	Th/U	Concordance
	$^{207}Pb/^{206}Pb$	$^{207}Pb/^{235}U$	$^{206}Pb/^{238}U$	$^{207}Pb/^{206}Pb$	$^{207}Pb/^{235}U$	$^{206}Pb/^{238}U$				
	0.00061	0.05604	0.00176							
685-76	0.06757 ± 0.00077	1.38368 ± 0.01596	0.14799 ± 0.00086	855 ± 14	882 ± 7	890 ± 5	274	379	0.72	99
685-77	0.05716 ± 0.00121	0.64086 ± 0.01476	0.08086 ± 0.00074	498 ± 35	503 ± 9	501 ± 4	323	490	0.66	100

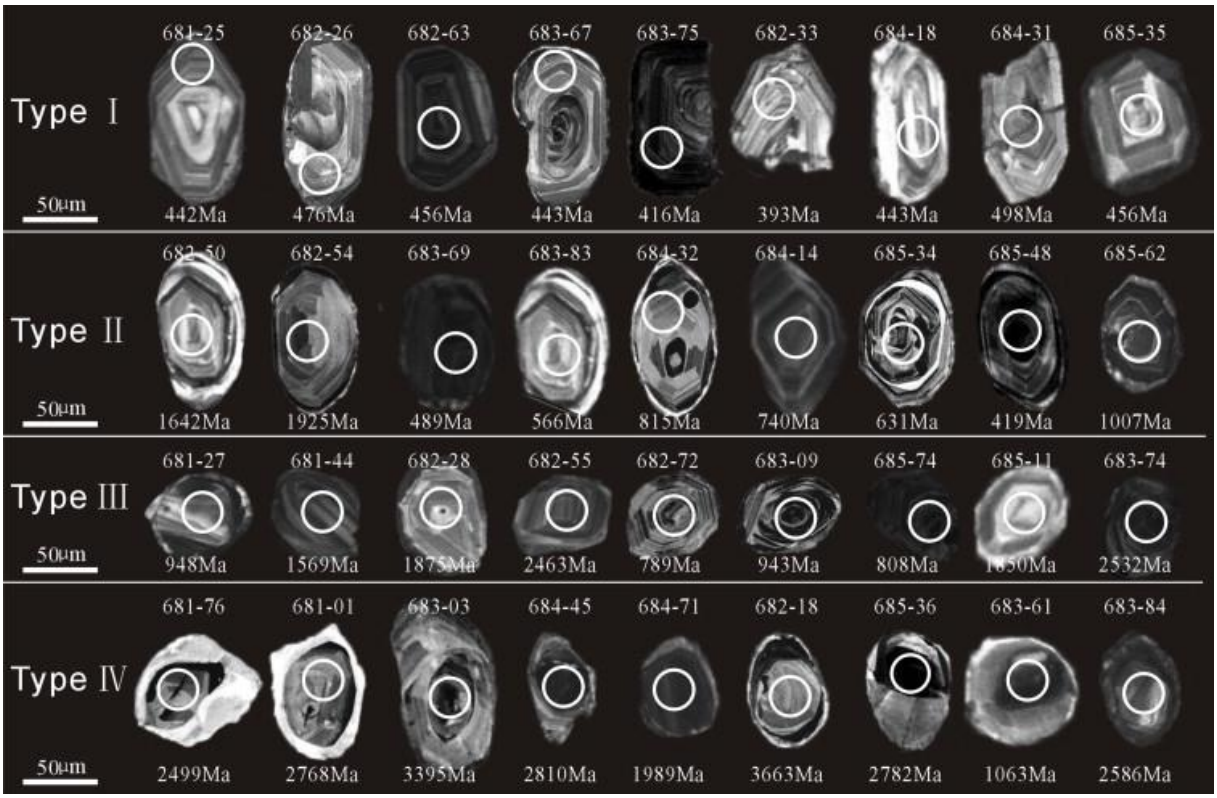

Fig. 5. : Cathodo-luminescence images of detrital zircons in sandstones from Baluntai. Type-I, zircons are characterized by euhedral shape; Type-II, zircons are subhedral, exhibiting clear oscillatory zoning; Type-III, zircons show rounded grain morphology; Type-IV, zircons show rounded-subrounded grain morphology, and featured by an anhedral inherited core with a narrow rim.

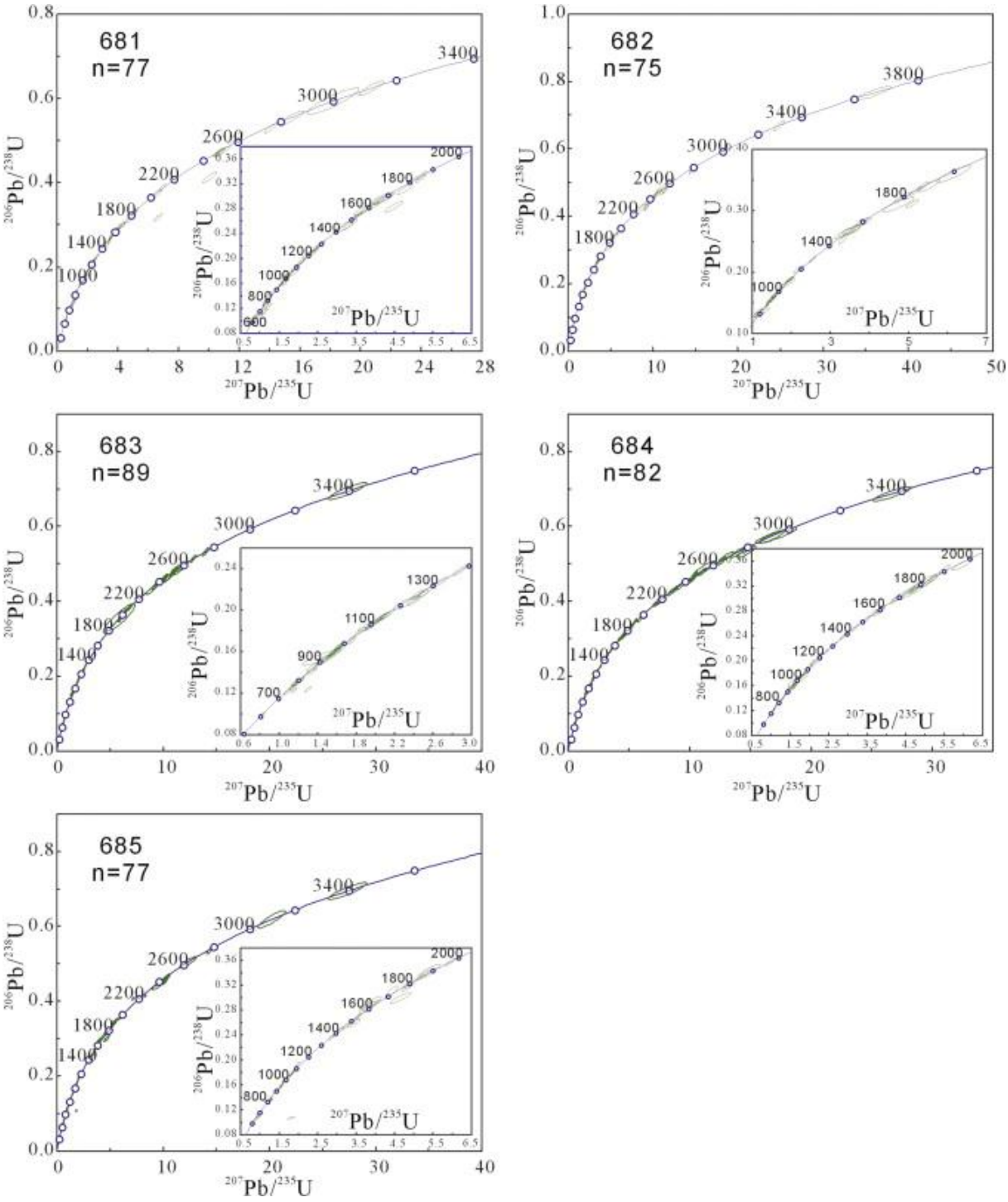

Fig. 6. :U–Pb concordia plots for detrital zircons from sandstones in Baluntai (age is in Ma and ellipse shows 1σ errors; *n* represents numbers of analyzed zircon grains).

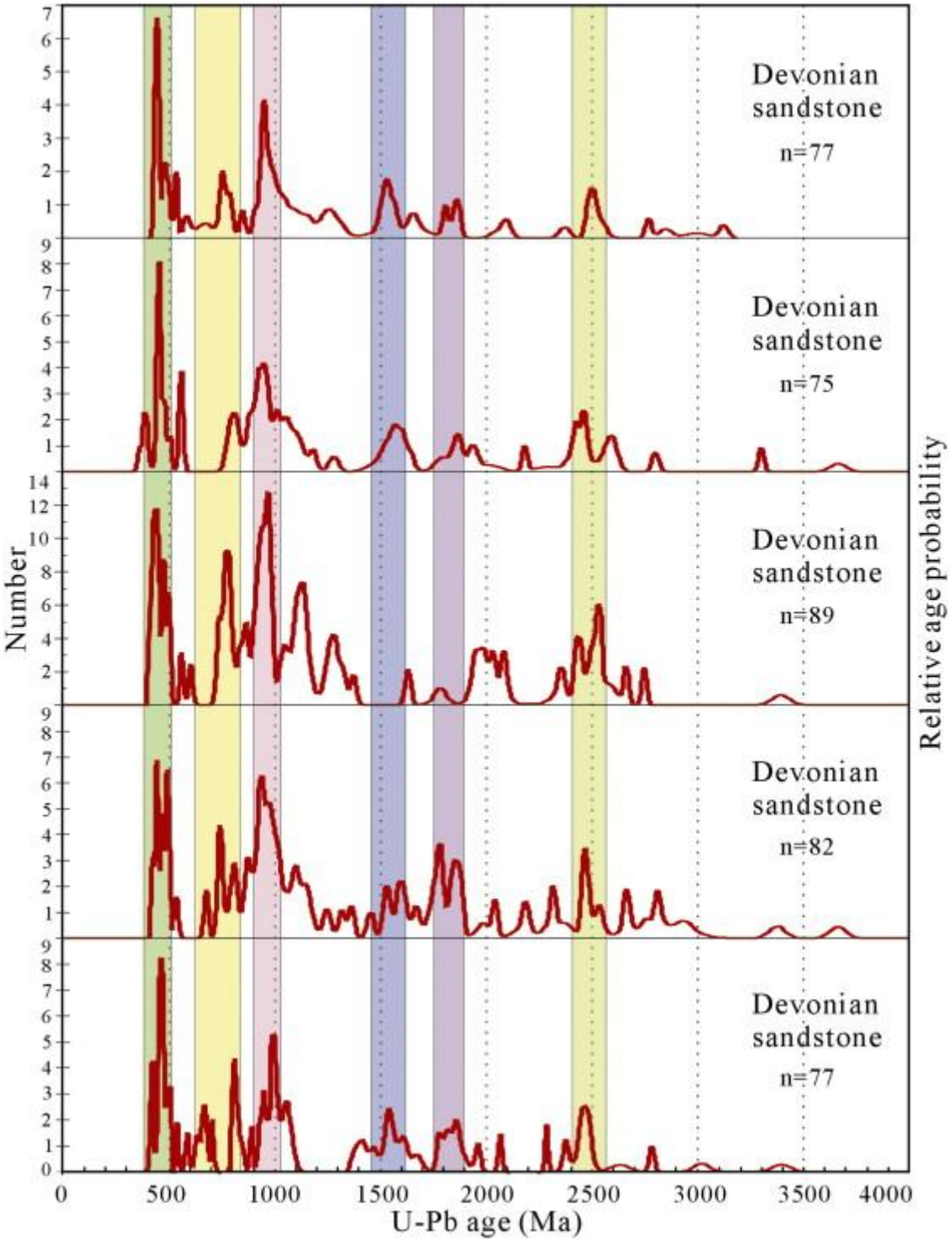

Fig. 7. : Relative U–Pb age probability for detrital zircons from sandstones in Baluntai.

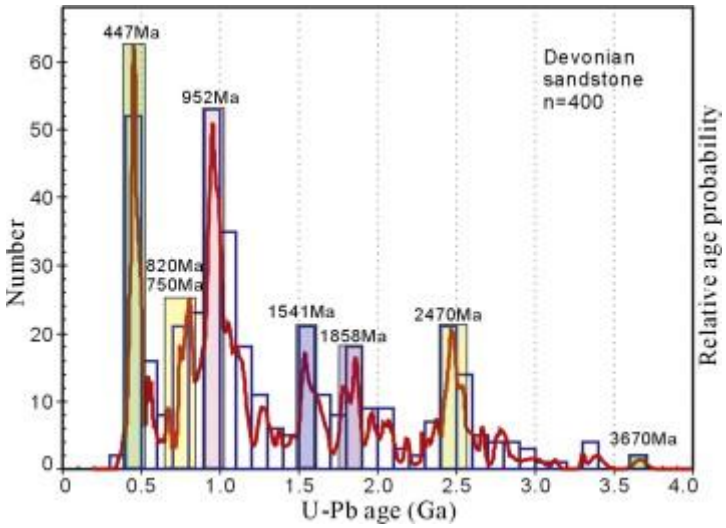

Fig. 8. :Distribution of zircon U–Pb ages from the five samples.

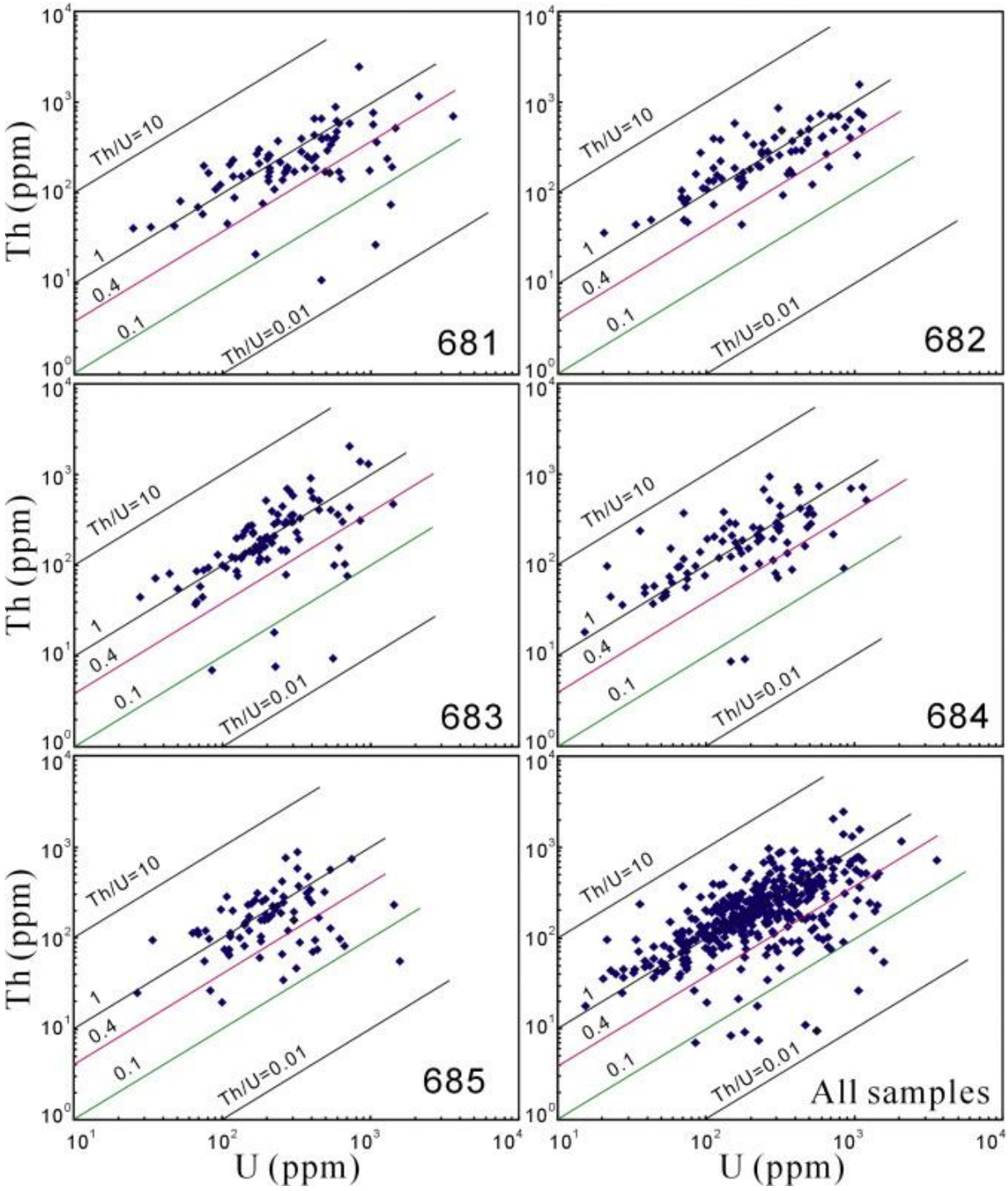

Fig. 9. :Th–U plots of zircons from all studied samples. As shown in the diagram, 343 zircons show Th/U ratios greater than 0.4, 10 zircon grains exhibit Th/U ratios less than 0.1.

Table 3. REE analysis of the zircons.

REE spots	La	Ce	Pr	Nd	Sm	Eu	Gd	Tb	Dy	Ho	Er	Tm	Yb	Lu	ΣREE	Ce/Ce*	Eu/Eu*	(Sm/La)N	(Yb/Sm)N
	ppm	ppm	ppm	ppm	ppm	ppm	ppm	ppm	ppm	ppm	ppm	ppm	ppm	ppm	ppm				
681-40	0.23	4.14	0.20	2.08	4.92	0.29	28.96	11.31	148.84	56.70	290.27	54.83	495.69	90.75	1189.2	4.32	0.06	34.26	94.05
681-57	0.46	18.03	0.26	2.40	3.02	1.00	14.09	4.02	41.87	13.68	66.46	11.64	105.82	21.21	303.9	12.32	0.39	10.35	32.69
681-59	17.4	98.42	11.8	65.28	27.86	4.42	28.90	4.77	47.57	15.89	109.33	21.16	234.12	55.89	742.8	1.59	0.47	2.54	7.84
682-75	1.32	12.14	0.48	2.70	2.61	0.94	12.30	4.03	48.63	18.68	97.75	20.19	204.33	42.23	468.3	3.68	0.42	3.15	73.07
685-51	1.37	32.64	0.61	3.83	3.84	0.81	18.43	6.99	93.00	36.05	198.52	37.76	357.32	73.02	864.2	8.61	0.24	4.46	86.88
685-52	0.01	10.67	0.12	2.03	3.74	0.38	19.02	6.35	78.49	27.74	141.42	25.36	226.28	44.60	586.2	25.68	0.11	999.24	56.38
685-53	6.78	108.7	2.53	8.16	5.35	0.88	20.76	6.58	81.48	31.28	170.72	31.65	298.52	62.68	836.1	6.31	0.22	1.25	52.10
685-54	0.18	5.53	0.16	1.58	3.03	0.55	22.49	10.03	146.13	60.16	339.07	65.39	622.34	124.03	1400.7	7.14	0.15	26.36	191.88
685-55	0.55	24.83	0.63	7.65	9.59	1.11	41.81	12.61	143.44	49.48	239.95	41.49	356.15	68.05	997.4	8.84	0.14	27.73	34.65
685-56	0.00	1.18	0.01	0.18	0.33	0.24	3.45	1.47	19.52	8.54	50.17	10.66	109.09	25.24	230.1	45.58	0.44	0.00	305.90
685-57	0.19	5.82	0.05	0.81	1.86	0.29	10.09	3.66	46.56	17.55	94.13	17.35	157.47	31.62	387.4	14.24	0.16	15.56	79.01
685-58	0.06	28.98	0.50	6.15	6.50	3.21	20.34	5.45	57.75	19.12	93.18	17.21	163.44	31.02	452.9	16.57	0.78	172.59	23.45
685-59	13.3	40.91	4.46	20.4	8.05	1.13	32.11	10.48	120.34	44.46	227.60	41.40	378.69	73.72	1017.0	1.28	0.19	0.96	43.89
685-60	70.6	211.2	24.7	106.7	20.91	1.70	25.44	5.62	57.86	20.92	109.77	21.71	212.34	44.33	933.8	1.22	0.22	0.47	9.48
685-61	0.63	15.61	0.29	2.75	3.88	0.52	17.66	5.32	62.84	22.53	112.25	20.70	187.54	36.93	489.5	8.71	0.16	9.79	45.04
685-62	0.11	15.88	0.11	1.16	2.42	0.34	13.27	5.47	73.70	28.54	147.98	28.77	264.31	50.94	633.0	30.41	0.14	35.40	101.70
685-63	7.43	48.26	3.38	20.15	12.39	2.16	39.63	11.15	117.54	37.98	172.11	30.50	262.00	47.03	811.7	2.31	0.27	2.65	19.73
685-64	1.31	71.37	3.82	35.91	30.30	6.44	68.65	19.83	194.66	57.25	253.50	44.44	369.95	69.87	1227.3	4.97	0.42	36.74	11.39
685-65	0.80	41.35	0.79	10.18	17.98	8.50	88.88	28.18	339.40	121.07	583.57	103.65	892.70	173.87	2410.9	11.32	0.53	35.69	46.31
685-66	6.24	26.77	1.89	9.60	4.92	0.71	18.95	6.40	82.23	31.86	170.32	33.94	327.50	67.58	788.9	1.86	0.20	1.25	62.10
685-67	0.50	3.29	0.19	1.84	5.90	0.94	36.69	11.18	111.58	31.74	125.20	20.19	166.36	26.05	541.7	2.55	0.15	18.65	26.29
685-68	0.00	10.04	0.08	1.41	2.18	1.09	11.22	4.11	54.67	23.32	135.64	30.53	336.95	82.30	693.5	39.10	0.54	0.00	144.17
685-69	0.05	11.81	0.23	3.65	5.10	1.59	25.58	8.05	93.07	34.17	179.69	35.95	362.91	75.56	837.4	14.14	0.35	168.99	66.43
685	0.1	1.0	0.0	0.7	3.5	0.1	26.	10.	134.	47.2	217.	40.3	366.	67.9	915.	4.01	0.02	44.92	95.58

REE spots	La	Ce	Pr	Nd	Sm	Eu	Gd	Tb	Dy	Ho	Er	Tm	Yb	Lu	ΣREE	Ce/Ce*	Eu/Eu*	(Sm/La)N	(Yb/Sm)N
	ppm	ppm	ppm	ppm	ppm	ppm	ppm	ppm	ppm	ppm	ppm	ppm	ppm	ppm	ppm				
-70	3	8	3	4	7	0	21	64	27	6	18	6	04	5	5				
685-71	0.13	5.13	0.11	1.64	3.67	0.19	23.21	8.38	109.11	40.55	201.38	38.81	346.75	63.92	843.0	9.81	0.05	44.30	88.20
685-72	205.2	489.7	64.5	286.6	56.65	1.90	59.02	10.51	88.95	25.82	113.01	21.57	195.79	34.60	1653.7	1.02	0.10	0.44	3.22
685-73	1.00	23.99	0.41	2.99	3.44	1.34	16.62	4.88	54.56	17.78	80.91	15.62	145.30	26.32	395.2	9.05	0.45	5.46	39.36
685-74	0.05	33.31	0.27	4.18	9.53	0.64	49.38	16.52	200.17	75.17	366.06	72.18	633.62	120.31	1581.4	34.20	0.07	284.39	62.03
685-75	0.56	1.59	0.18	1.19	3.03	0.19	18.07	7.24	83.68	24.96	94.17	14.48	106.37	16.11	371.8	1.20	0.06	8.59	32.71
685-76	2.41	28.37	0.81	5.06	5.39	0.96	22.02	7.43	90.34	33.90	172.64	35.35	343.73	69.71	818.1	4.86	0.23	3.56	59.45
685-77	2.17	33.81	0.97	4.52	4.31	1.59	21.78	7.28	94.12	36.21	195.08	42.87	452.96	96.07	993.7	5.59	0.41	3.16	97.98

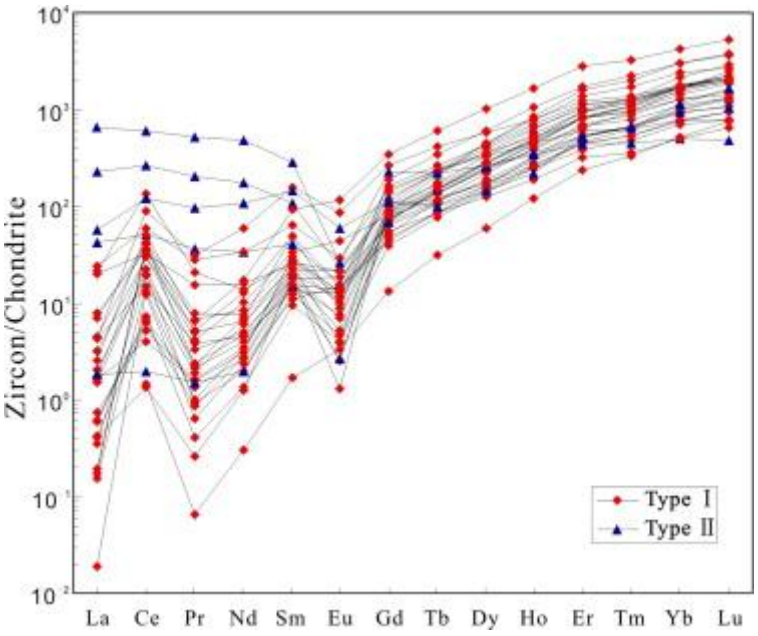

Fig. 10. : Chondrite-normalized REE patterns of zircons. Chondrite REE values are after Boynton (1984).

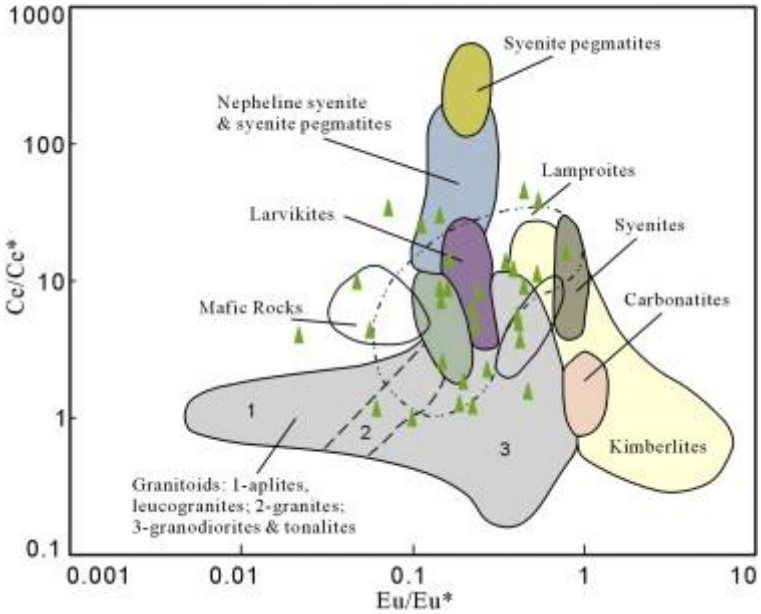

Fig. 11. : The fields of zircon compositions used as discriminants for different rock types (after Belousova et al., 2002). Ce/Ce* = 2*(Ce/0.808)/[(La/0.31) + (Pr/0.122)], Eu/Eu* = 2*(Eu/0.0735)/[(Sm/0.195) + (Gd/0.259)]. Chondrite REE values are after Boynton (1984).

Table 4. Hf isotope analysis for zircons from Devonian sandstones.

Sample	$^{176}Yb/^{177}Hf$	2σ	$^{176}Lu/^{177}Hf$	2σ	$^{176}Hf/^{177}Hf$	2σ	λ	$^{176}Hf/^{177}Hf_i$	$\varepsilon_{Hf}(t)$	εHf(0)	Age(Ma)	T_{DM}(Ma)	T_{DM2}(Ma)	$f_{Lu/Hf}$
681														
681-01	0.025	0.000	0.000971	0.000002	0.281073	0.000017	1.87E−11	0.281022	0.3	−60.1	2768	3031	3189	−0.97
681-03	0.023	0.000	0.000864	0.000011	0.282044	0.000015	1.87E−11	0.282028	−4.4	−25.7	990	1696	2122	−0.97
681-05	0.024	0.000	0.000937	0.000008	0.281917	0.000016	1.87E−11	0.281903	−13.5	−30.2	784	1875	2531	−0.97
681-07	0.001	0.000	0.000044	0.000001	0.280735	0.000014	1.87E−11	0.280733	−15.6	−72.0	2524	3405	3968	−1.00
681-09	0.027	0.000	0.001114	0.000026	0.282439	0.000019	1.87E−11	0.282406	22.3	−11.8	1581	1153	899	−0.97
681-12	0.013	0.000	0.000516	0.000003	0.282077	0.000016	1.87E−11	0.282070	−8.3	−24.6	749	1635	2184	−0.98
681-21	0.007	0.000	0.000276	0.000003	0.282390	0.000016	1.87E−11	0.282386	1.5	−13.5	685	1196	1518	−0.99
681-22	0.005	0.000	0.000184	0.000003	0.281444	0.000015	1.87E−11	0.281437	−6.5	−47.0	1828	2476	2887	−0.99
681-40	0.032	0.000	0.001054	0.000004	0.281553	0.000010	1.87E−11	0.281517	−4.1	−43.1	1808	2383	2725	−0.97
681-41	0.020	0.000	0.000747	0.000005	0.282083	0.000018	1.87E−11	0.282072	−8.2	−24.4	752	1637	2176	−0.98
681-42	0.012	0.000	0.000466	0.000002	0.281595	0.000096	1.87E−11	0.281586	−21.0	−41.6	950	2290	3123	−0.99
681-57	0.038	0.000	0.001666	0.000016	0.282752	0.000024	1.87E−11	0.282728	15.7	−0.7	779	721	689	−0.95
681-59	0.008	0.000	0.000311	0.000001	0.281294	0.000029	1.87E−11	0.281279	2.8	−52.3	2479	2685	2815	−0.99
682														
682-01	0.013	0.000	0.000508	0.000002	0.281499	0.000016	1.87E−11	0.281484	−10.3	−45.0	1590	2422	2938	−0.98
682-02	0.033	0.000	0.001270	0.000007	0.280972	0.000019	1.87E−11	0.280904	−3.1	−63.6	2800	3192	3423	−0.96
682-05	0.011	0.000	0.000426	0.000006	0.281277	0.000018	1.87E−11	0.281258	0.8	−52.9	2427	2715	2895	−0.99
682-07	0.005	0.000	0.000178	0.000002	0.281495	0.000027	1.87E−11	0.281490	−11.0	−45.2	1549	2407	2951	−0.99
682-09	0.027	0.001	0.000999	0.000024	0.282054	0.000015	1.87E−11	0.282036	−4.6	−25.4	970	1687	2117	−0.97
682-11	0.014	0.000	0.000596	0.000001	0.281730	0.000021	1.87E−11	0.281721	−19.8	−36.8	787	2114	2931	−0.98
682-13	0.035	0.000	0.001381	0.000018	0.282073	0.000022	1.87E−11	0.282052	−7.4	−24.7	820	1678	2177	−0.96
682-14	0.034	0.000	0.001330	0.000006	0.281261	0.000016	1.87E−11	0.281237	−33.1	−53.4	964	2802	3877	−0.96
682-16	0.014	0.000	0.000553	0.000005	0.282029	0.000023	1.87E−11	0.282003	28.2	−26.3	2465	1703	1232	−0.98
682-17	0.008	0.000	0.000349	0.000001	0.281294	0.000018	1.87E−11	0.281277	4.1	−52.3	2539	2688	2782	−0.99
682-18	0.020	0.000	0.000854	0.000004	0.281910	0.000014	1.87E−11	0.281849	50.8	−30.5	3663	1881	803	−0.97

Sample	$^{176}Yb/^{177}Hf$	2σ	$^{176}Lu/^{177}Hf$	2σ	$^{176}Hf/^{177}Hf$	2σ	λ	$^{176}Hf/^{177}Hf_i$	$\varepsilon_{Hf}(t)$	εHf(0)	Age(Ma)	T_{DM}(Ma)	T_{DM2}(Ma)	$f_{Lu/Hf}$
682-21	0.008	0.000	0.000354	0.000002	0.281896	0.000015	1.87E−11	0.281891	−13.2	−31.0	815	1875	2539	−0.99
682-23	0.014	0.000	0.000581	0.000002	0.281538	0.000035	1.87E−11	0.281521	−10.2	−43.6	1536	2374	2891	−0.98
682-28	0.015	0.000	0.000588	0.000002	0.281373	0.000018	1.87E−11	0.281352	−8.5	−49.5	1875	2597	3043	−0.98
682-31	0.020	0.000	0.000764	0.000002	0.281168	0.000018	1.87E−11	0.281142	−17.1	−56.7	1822	2887	3536	−0.98
682-45	0.012	0.000	0.000521	0.000002	0.282593	0.000017	1.87E−11	0.282575	34.5	−6.3	1854	922	345	−0.98
682-46	0.016	0.000	0.000613	0.000008	0.281984	0.000014	1.87E−11	0.281973	−7.6	−27.9	936	1767	2279	−0.98
682-49	0.012	0.000	0.000458	0.000004	0.281983	0.000017	1.87E−11	0.281975	−7.1	−27.9	955	1761	2262	−0.99
682-53	0.012	0.000	0.000431	0.000003	0.282029	0.000018	1.87E−11	0.282022	−5.5	−26.3	952	1697	2160	−0.99
682-55	0.030	0.000	0.001093	0.000003	0.280937	0.000014	1.87E−11	0.280886	−11.6	−64.9	2463	3225	3678	−0.97
682-61	0.005	0.000	0.000200	0.000001	0.281088	0.000023	1.87E−11	0.281079	−4.6	−59.5	2467	2951	3258	−0.99
682-65	0.012	0.000	0.000455	0.000004	0.280407	0.000019	1.87E−11	0.280378	−10.2	−83.6	3301	3874	4230	−0.99
682-66	0.015	0.000	0.000580	0.000007	0.281652	0.000019	1.87E−11	0.281635	−5.4	−39.6	1568	2219	2621	−0.98
682-67	0.021	0.000	0.000846	0.000003	0.281227	0.000018	1.87E−11	0.281203	−22.2	−54.7	1503	2814	3607	−0.97
682-70	0.011	0.000	0.000439	0.000001	0.281116	0.000014	1.87E−11	0.281096	−5.0	−58.6	2423	2933	3250	−0.99
682-72	0.031	0.000	0.000937	0.000006	0.282169	0.000026	1.87E−11	0.282155	−4.4	−21.3	789	1525	1968	−0.97
682-75	0.018	0.000	0.000661	0.000001	0.281947	0.000010	1.87E−11	0.281928	4.3	−29.2	1536	1820	1994	−0.98
683														
683-03	0.009	0.000	0.000392	0.000007	0.280966	0.000023	1.87E−11	0.280940	12.1	−63.9	3395	3129	2963	−0.99
683-09	0.012	0.000	0.000469	0.000005	0.281920	0.000018	1.87E−11	0.281912	−9.6	−30.1	943	1848	2410	−0.99
683-11	0.026	0.000	0.001159	0.000013	0.282408	0.000015	1.87E−11	0.282353	41.7	−12.9	2510	1198	422	−0.97
683-15	0.003	0.000	0.000103	0.000006	0.280956	0.000015	1.87E−11	0.280951	−8.6	−64.2	2492	3120	3519	−1.00
683-18	0.019	0.000	0.000769	0.000005	0.280884	0.000015	1.87E−11	0.280847	−11.1	−66.8	2542	3270	3712	−0.98
683-24	0.022	0.000	0.000985	0.000006	0.281953	0.000015	1.87E−11	0.281939	−12.7	−29.0	760	1827	2467	−0.97
683-29	0.028	0.000	0.000867	0.000006	0.281152	0.000018	1.87E−11	0.281111	−3.8	−57.3	2452	2917	3198	−0.97
683-30	0.015	0.000	0.000590	0.000007	0.282237	0.000017	1.87E−11	0.282227	1.9	−18.9	959	1417	1700	−0.98
683-31	0.014	0.000	0.000451	0.000006	0.282337	0.000019	1.87E−11	0.282329	5.8	−15.4	972	1275	1463	−0.99
683-35	0.059	0.000	0.002199	0.000012	0.281881	0.000018	1.87E−11	0.281849	−15.4	−31.5	781	1990	2652	−0.93

Sample	$^{176}Yb/^{177}Hf$	2σ	$^{176}Lu/^{177}Hf$	2σ	$^{176}Hf/^{177}Hf$	2σ	λ	$^{176}Hf/^{177}Hf_i$	$\varepsilon_{Hf}(t)$	εHf(0)	Age(Ma)	T_{DM}(Ma)	T_{DM2}(Ma)	$f_{Lu/Hf}$
683-38	0.027	0.000	0.001049	0.000007	0.282023	0.000019	1.87E−11	0.282007	−9.6	−26.5	792	1734	2295	−0.97
683-40	0.015	0.000	0.000804	0.000007	0.281778	0.000029	1.87E−11	0.281766	−17.8	−35.1	806	2059	2820	−0.98
683-45	0.010	0.000	0.000374	0.000003	0.281947	0.000018	1.87E−11	0.281929	25.0	−29.2	2441	1807	1410	−0.99
683-48	0.029	0.000	0.001053	0.000008	0.281974	0.000016	1.87E−11	0.281955	−8.2	−28.2	938	1801	2317	−0.97
683-49	0.028	0.000	0.001078	0.000005	0.281270	0.000015	1.87E−11	0.281218	1.5	−53.1	2518	2772	2923	−0.97
683-50	0.035	0.001	0.001316	0.000024	0.282354	0.000015	1.87E−11	0.282330	5.2	−14.8	944	1281	1478	−0.96
683-51	0.021	0.000	0.000813	0.000006	0.282152	0.000038	1.87E−11	0.282140	−5.9	−21.9	746	1544	2028	−0.98
683-56	0.019	0.000	0.000712	0.000008	0.281996	0.000018	1.87E−11	0.281983	−6.5	−27.5	971	1756	2235	−0.98
683-57	0.015	0.000	0.000520	0.000005	0.282025	0.000015	1.87E−11	0.282018	−9.7	−26.4	770	1706	2286	−0.98
683-63	0.028	0.000	0.001134	0.000010	0.282199	0.000022	1.87E−11	0.282182	−3.4	−20.3	793	1491	1906	−0.97
683-66	0.040	0.000	0.001520	0.000011	0.282095	0.000018	1.87E−11	0.282068	−3.8	−23.9	956	1654	2056	−0.95
683-73	0.024	0.000	0.000927	0.000018	0.280980	0.000016	1.87E−11	0.280931	−3.3	−63.4	2750	3153	3396	−0.97
683-74	0.016	0.000	0.000631	0.000003	0.281021	0.000014	1.87E−11	0.280991	−6.3	−61.9	2532	3074	3408	−0.98
683-79	0.019	0.000	0.000797	0.000005	0.281932	0.000018	1.87E−11	0.281920	−12.9	−29.7	782	1847	2494	−0.98
683-80	0.019	0.000	0.000735	0.000009	0.281197	0.000016	1.87E−11	0.281163	−2.6	−55.7	2425	2846	3102	−0.98
684														
684-06	0.021	0.000	0.000931	0.000010	0.281419	0.000019	1.87E−11	0.281358	26.5	−47.9	3377	2559	2066	−0.97
684-08	0.006	0.000	0.000255	0.000000	0.282443	0.000017	1.87E−11	0.282438	9.0	−11.6	943	1123	1237	−0.99
684-09	0.021	0.000	0.000941	0.000019	0.282145	0.000020	1.87E−11	0.282128	−2.2	−22.2	931	1559	1937	−0.97
684-14	0.030	0.000	0.000967	0.000004	0.282486	0.000019	1.87E−11	0.282473	5.7	−10.1	740	1083	1289	−0.97
684-15	0.017	0.000	0.000636	0.000002	0.280980	0.000015	1.87E−11	0.280949	−7.7	−63.4	2534	3130	3496	−0.98
684-19	0.020	0.000	0.000940	0.000008	0.282329	0.000015	1.87E−11	0.282312	5.1	−15.7	968	1303	1504	−0.97
684-21	0.037	0.001	0.001346	0.000039	0.281751	0.000016	1.87E−11	0.281712	−3.6	−36.1	1525	2126	2478	−0.96
684-23	0.042	0.000	0.001530	0.000011	0.281040	0.000019	1.87E−11	0.280966	−7.3	−61.3	2523	3121	3466	−0.95
684-27	0.011	0.000	0.000450	0.000003	0.281172	0.000032	1.87E−11	0.281151	−1.8	−56.6	2478	2858	3095	−0.99
684-32	0.022	0.001	0.000856	0.000031	0.282141	0.000013	1.87E−11	0.282127	−4.8	−22.3	815	1562	2013	−0.97
684-35	0.051	0.001	0.001923	0.000034	0.282141	0.000017	1.87E−11	0.282107	−2.8	−22.3	937	1606	1980	−0.94

Sample	$^{176}Yb/^{177}Hf$	2σ	$^{176}Lu/^{177}Hf$	2σ	$^{176}Hf/^{177}Hf$	2σ	λ	$^{176}Hf/^{177}Hf_i$	$\varepsilon_{Hf}(t)$	εHf(0)	Age(Ma)	T_{DM}(Ma)	T_{DM2}(Ma)	$f_{Lu/Hf}$
684-39	0.017	0.000	0.000623	0.000003	0.282176	0.000014	1.87E−11	0.282165	−0.4	−21.1	952	1503	1842	−0.98
684-41	0.016	0.000	0.000629	0.000003	0.281446	0.000020	1.87E−11	0.281423	−6.1	−46.9	1868	2502	2892	−0.98
684-45	0.024	0.000	0.000955	0.000010	0.281044	0.000016	1.87E−11	0.280993	0.2	−61.1	2810	3069	3225	−0.97
684-48	0.006	0.000	0.000242	0.000001	0.281546	0.000015	1.87E−11	0.281538	−1.7	−43.3	1884	2342	2631	−0.99
684-49	0.058	0.001	0.002255	0.000022	0.281659	0.000015	1.87E−11	0.281580	−1.1	−39.4	1844	2310	2564	−0.93
684-52	0.025	0.001	0.000988	0.000018	0.281549	0.000018	1.87E−11	0.281515	−3.3	−43.2	1849	2384	2704	−0.97
684-53	0.021	0.000	0.000837	0.000009	0.281715	0.000020	1.87E−11	0.281704	−22.8	−37.4	680	2148	3037	−0.97
684-54	0.018	0.000	0.000707	0.000010	0.280989	0.000017	1.87E−11	0.280956	−8.8	−63.0	2473	3123	3520	−0.98
684-63	0.022	0.000	0.000879	0.000010	0.282095	0.000016	1.87E−11	0.282081	−6.4	−24.0	819	1626	2114	−0.97
684-65	0.023	0.001	0.000977	0.000029	0.282502	0.000035	1.87E−11	0.282484	11.1	−9.6	961	1062	1122	−0.97
684-67	0.024	0.000	0.000884	0.000002	0.281635	0.000017	1.87E−11	0.281604	−0.8	−40.2	1817	2260	2528	−0.97
684-70	0.027	0.001	0.001068	0.000027	0.282065	0.000020	1.87E−11	0.282050	−9.2	−25.0	742	1676	2232	−0.97
684-72	0.015	0.000	0.000568	0.000006	0.280987	0.000016	1.87E−11	0.280961	−8.9	−63.1	2462	3115	3518	−0.98
684-74	0.021	0.000	0.000786	0.000001	0.281481	0.000015	1.87E−11	0.281458	−12.2	−45.7	1543	2464	3024	−0.98
684-77	0.021	0.000	0.000863	0.000007	0.281905	0.000015	1.87E−11	0.281892	−14.5	−30.7	753	1888	2575	−0.97
684-78	0.016	0.000	0.000699	0.000005	0.281947	0.000017	1.87E−11	0.281937	−12.1	−29.2	789	1821	2453	−0.98
684-80	0.015	0.000	0.000608	0.000003	0.281076	0.000017	1.87E−11	0.281044	0.8	−60.0	2757	2999	3148	−0.98
685														
685-51	0.027	0.000	0.001004	0.000004	0.281985	0.000010	1.87E−11	0.281954	7.0	−27.8	1613	1784	1886	−0.97
685-52	0.017	0.000	0.000614	0.000003	0.282367	0.000015	1.87E−11	0.282356	6.4	−14.3	954	1239	1414	−0.98
685-53	0.026	0.000	0.000978	0.000005	0.281814	0.000011	1.87E−11	0.281799	−16.6	−33.9	810	2019	2744	−0.97
685-54	0.033	0.000	0.001202	0.000011	0.281613	0.000011	1.87E−11	0.281575	−5.1	−41.0	1677	2309	2682	−0.96
685-55	0.028	0.000	0.000955	0.000012	0.282030	0.000007	1.87E−11	0.282013	−6.3	−26.2	932	1719	2192	−0.97
685-56	0.008	0.000	0.000318	0.000004	0.280699	0.000010	1.87E−11	0.280681	−6.0	−73.3	3017	3477	3765	−0.99
685-57	0.013	0.000	0.000473	0.000003	0.282361	0.000009	1.87E−11	0.282352	7.1	−14.5	993	1242	1397	−0.99
685-58	0.012	0.000	0.000405	0.000005	0.282459	0.000010	1.87E−11	0.282455	0.8	−11.1	545	1105	1454	−0.99
685-59	0.029	0.000	0.001023	0.000014	0.282522	0.000020	1.87E−11	0.282514	0.3	−8.8	429	1034	1396	−0.97

Sample	$^{176}Yb/^{177}Hf$	2σ	$^{176}Lu/^{177}Hf$	2σ	$^{176}Hf/^{177}Hf$	2σ	λ	$^{176}Hf/^{177}Hf_i$	$\varepsilon_{Hf}(t)$	εHf(0)	Age(Ma)	T_{DM}(Ma)	T_{DM2}(Ma)	$f_{Lu/Hf}$
685-60	0.016	0.000	0.000598	0.000007	0.281536	0.000010	1.87E−11	0.281513	1.6	−43.7	2066	2378	2570	−0.98
685-61	0.014	0.000	0.000501	0.000003	0.281484	0.000011	1.87E−11	0.281467	−6.6	−45.5	1777	2442	2854	−0.98
685-62	0.018	0.000	0.000645	0.000001	0.281995	0.000010	1.87E−11	0.281983	−5.7	−27.5	1007	1753	2212	−0.98
685-63	0.019	0.000	0.000633	0.000013	0.281253	0.000012	1.87E−11	0.281229	−10.9	−53.7	1961	2763	3255	−0.98
685-64	0.029	0.000	0.000945	0.000017	0.281916	0.000011	1.87E−11	0.281897	−7.6	−30.3	1056	1876	2370	−0.97
685-65	0.083	0.001	0.002883	0.000022	0.282215	0.000023	1.87E−11	0.282177	−5.4	−19.7	709	1540	1971	−0.91
685-66	0.028	0.000	0.000988	0.000004	0.282384	0.000011	1.87E−11	0.282375	−3.3	−13.7	490	1227	1669	−0.97
685-67	0.055	0.001	0.001757	0.000039	0.282289	0.000013	1.87E−11	0.282256	3.9	−17.1	1004	1388	1606	−0.95
685-68	0.029	0.001	0.001249	0.000021	0.282825	0.000009	1.87E−11	0.282813	12.5	1.9	502	610	673	−0.96
685-69	0.029	0.000	0.001136	0.000006	0.281842	0.000018	1.87E−11	0.281810	−1.4	−32.9	1471	1989	2296	−0.97
685-70	0.024	0.000	0.000803	0.000010	0.281999	0.000010	1.87E−11	0.281983	−4.1	−27.3	1075	1755	2168	−0.98
685-71	0.024	0.000	0.000767	0.000005	0.282170	0.000009	1.87E−11	0.282155	1.9	−21.3	1071	1517	1789	−0.98
685-72	0.014	0.000	0.000415	0.000002	0.282088	0.000010	1.87E−11	0.282077	6.1	−24.2	1380	1616	1763	−0.99
685-73	0.014	0.000	0.000452	0.000004	0.281254	0.000011	1.87E−11	0.281234	−1.2	−53.7	2376	2749	2980	−0.99
685-74	0.035	0.000	0.001171	0.000004	0.281794	0.000013	1.87E−11	0.281776	−17.4	−34.6	808	2057	2796	−0.96
685-75	0.007	0.000	0.000184	0.000001	0.280964	0.000007	1.87E−11	0.280956	−13.2	−63.9	2285	3115	3641	−0.99
685-76	0.021	0.000	0.000793	0.000010	0.281939	0.000009	1.87E−11	0.281926	−10.3	−29.5	890	1837	2413	−0.98
685-77	0.030	0.000	0.001136	0.000012	0.282275	0.000029	1.87E−11	0.282264	−6.9	−17.6	501	1385	1909	−0.97

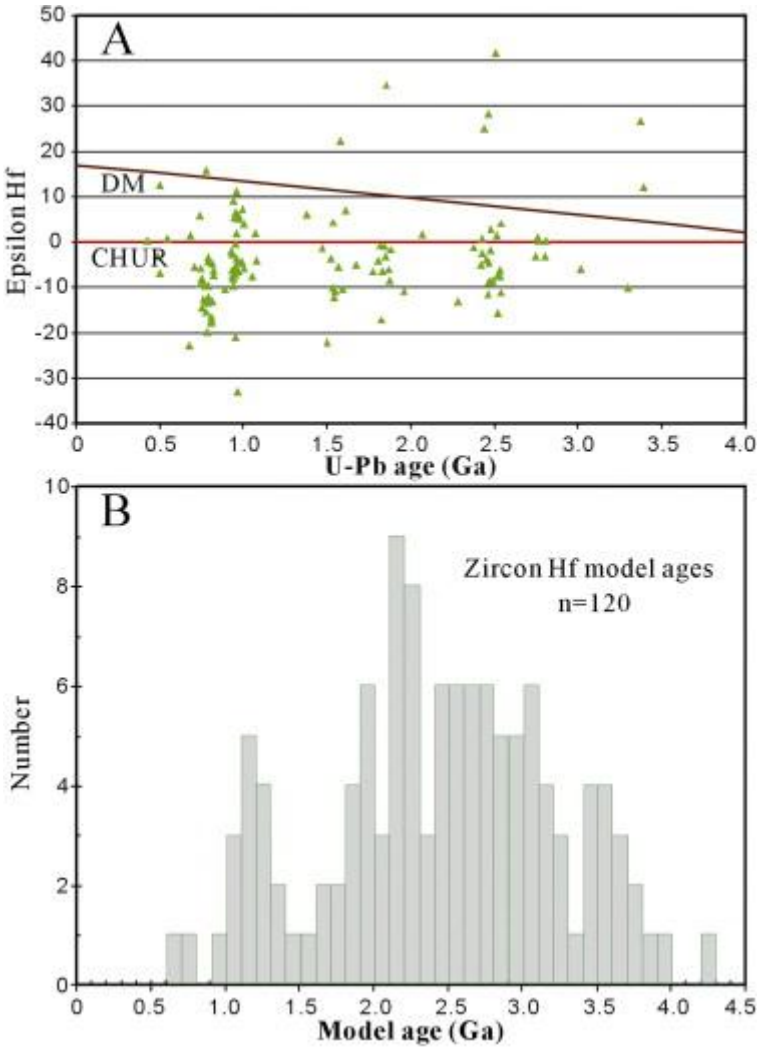

Fig. 12. : (A) Epsilon Hf vs. U–Pb age of the detrital zircons; (B) histograms of zircon Hf model age.

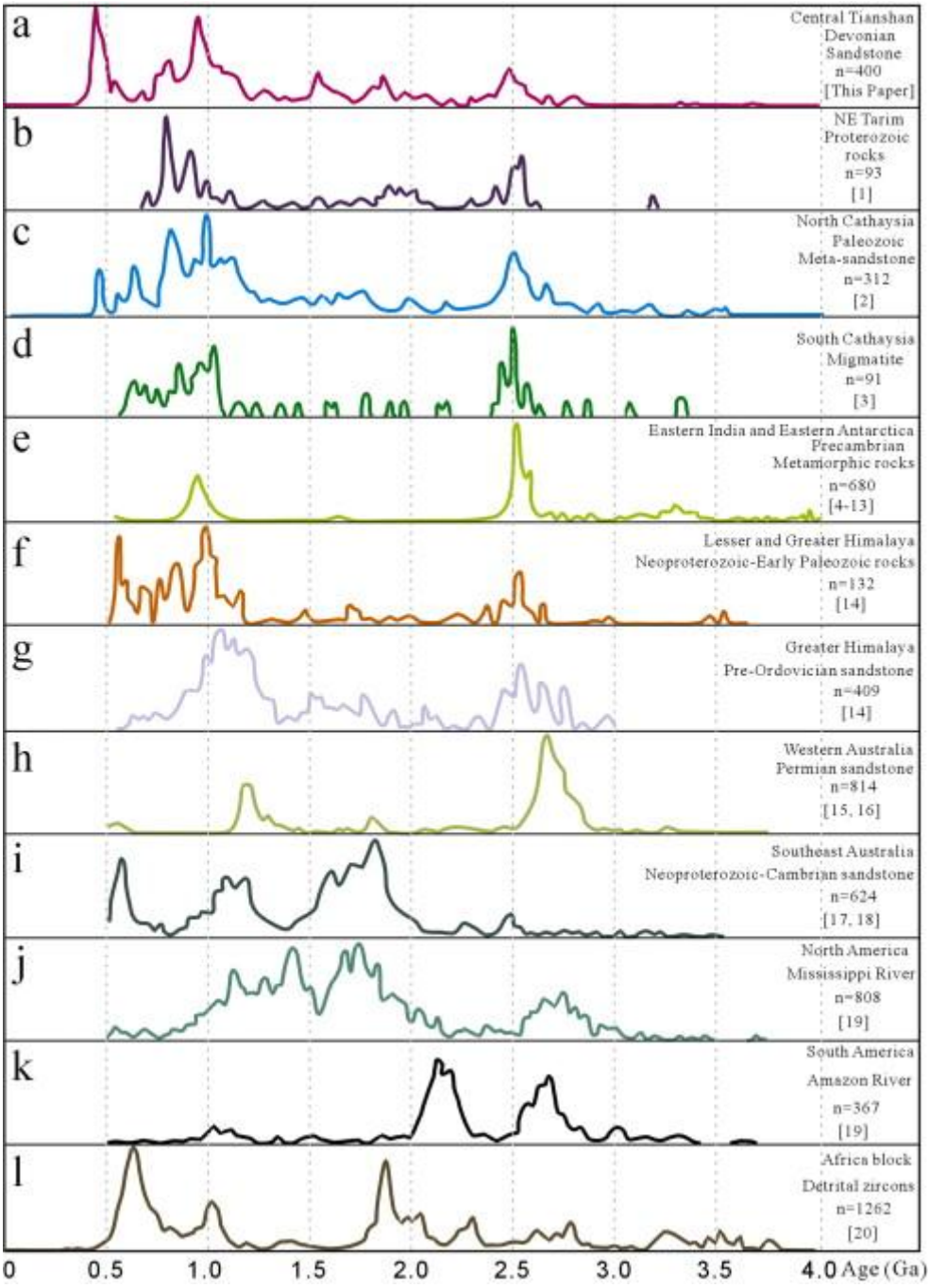

Fig. 13. : Precambrian age distributions from the Tarim and other cratons around the world. Data cited from [1–20]: [1] Shu et al. (2010); [2] Xiang and Shu (2010); [3] Yu et al. (2008); [4] Harley and Black (1997); [5] Mishra et al. (1999); [6] Boger et al. (2000); [7] Jayananda et al. (2000); [8] Fitzsimons (2000); [9] Kelly et al. (2002); [10] Carson et al. (2002); [11] Mondal et al. (2002); [12] Hokada et al. (2003); [13] Hokada et al. (2004); [14] Gehrels et al. (2003); [15] Griffin et al. (2004); [16] Veevers et al. (2005); [17] Ireland et al. (1998); [18] Berry et al., 2001 R. Berry, G.A. Jenner, S. Meffre and M.N. Tubrett, A North American provenance for Neoproterozoic to Cambrian sandstones in Tasmania?. *Earth Planet. Sci. Lett.*, **192** (2001), pp. 207–222. Berry et al. (2001); [19] Rino et al. (2004); and [20] Condie et al. (2009)